PhD Thesis

Versatile Applications of Carbon Nanoparticles

MD PALASHUDDIN SK

Department of Chemistry
Indian Institute of Technology Guwahati

April 2015

Versatile Applications of Carbon Nanoparticles

A thesis submitted by

Md Palashuddin Sk
Roll No. 09612225

to

Indian Institute of Technology Guwahati

for the award of the degree of

Doctor of Philosophy

Department of Chemistry
Indian Institute of Technology Guwahati
Guwahati – 781 039
India

April 2015

DECLARATION

The work contained in this thesis, entitled, '**Versatile Applications of Carbon Nanoparticles**' has been carried out by me under the supervision of Dr. Arun Chattopadhyay, Professor, Department of Chemistry, Indian Institute of Technology Guwahati for the award of the degree of **Doctor of Philosophy**. The contents of this thesis have not been submitted elsewhere for the award of any degree.

Md Palashuddin Sk

IIT Guwahati
April, 2015

INDIAN INSTITUTE OF TECHNOLOGY, GUWAHATI

Department of Chemistry

CERTIFICATE

It is certified that the work contained in the thesis, entitled, '**Versatile Applications of Carbon Nanoparticles**' has been carried out by Md Palashuddin Sk, a student of the Department of Chemistry, Indian Institute of Technology Guwahati, for the award of the degree of Doctor of Philosophy under my supervision. This work has not been submitted elsewhere for any degree.

Dr. Arun Chattopadhyay

Professor
Department of Chemistry
IIT Guwahati
Guwahati – 781 039, India

April, 2015

Dedicated to my beloved Parents

Mr. Md Anesuddin Sk
and
Mrs. Rowsanara Begum

Acknowledgements

I feel highly obliged to acknowledge everyone who has directly or indirectly provided their support during the course of my Ph.D. studies. It is my duty to acknowledge each and everyone but the list is too long and if I forget to mention a few, kindly understand that you all are equally important to me.

I would like to express my immense gratitude to my thesis supervisor Prof. Arun Chattopadhyay, for his guidance, continuous support, ceaseless encouragement and advice throughout my doctoral studies. He gave me freedom to pursue my own interest in the research fields that fascinated me. I am especially thankful to him for giving me the opportunities, to learn and operate various sophisticated instruments. His immense dedication to the research, simple innovative thoughts and a very high degree of discipline, sincerity and dynamic personality has always motivated me the most. I feel that I am fortunate enough to have received the opportunity of working under one of the best supervisor.

I am indebted to Prof. Siddhartha Sankar Ghosh, Prof. Anumita Paul and Dr. Chandan K. Jana for their valuable suggestions, guidance, support and significant contribution in my collaborative work. Discussions with them have always been very supportive and inspiring. I am thankful to my doctoral committee chairman Dr. Lal Mohan Kundu, and the other committee members, Dr. Bhubaneswar Mandal and Dr. Aiyagari Ramesh for their constructive criticism as well as important suggestion. Their assessment of my research work helped me in bringing my thesis to its present form. I am obliged to all the faculty members of the Department of Chemistry for their co-operation from time to time. I would like to especially thank Prof. A. T. Khan for his kind affection towards me.

I am grateful to Department of Chemistry, Centre for Nanotechnology, Central Instruments Facility, IIT Guwahati for giving me opportunity to work here. I acknowledge CSIR, New Delhi for providing financial support through JRF and SRF fellowship. I am thankful to all the non-teaching staff members of Department of Chemistry, Centre for Nanotechnology, and Central Instruments Facility. I would like to especially thank Indrajit Da, Kula da and Madhurjya da for giving me required training to operate very sophisticated instruments. I thank Department of Chemical Engineering, IIT Guwahati for AAS analysis. I am thankful to Department of Physics and Meteorology, IIT Kharagpur for allowing me to use their XPS facility.

I would like to acknowledge my teachers from my school as well as in the University for their excellent teaching which they have provided me throughout my academics. I owe

my gratitude to Swami Gwanolokananda ji Maharaj, Krishnendu Sir, Selim Sir, Dr. Aminul Islam, Dr. Suhail Sabir and Dr. Sayem Alam for their help and encouragement. Krishendu sir and Selim sir taught me the very basics of chemistry which inspired me to pursue my graduate studies in Chemical Science. I can never forget Sayem Bhai for his guidance and effort which enabled me to overcome various difficult circumstances. I thank Dr. Shaik Rafi Ahamed for his kind affection and hospitality during several occasions.

I offer my heartfelt thanks to my lab seniors Dr. Subhojit Das, Dr. Sadhucharan Mallick, Dr. Jasmini Deka, Dr. Krishna Kanti Dey, Dr. Arumugam Murugadoss, Dr. Sonit Kumar Gogoi, Dr. Biswa Ranjan Panda, Dr. Devasish Chowdhury, Dr. Gitanjali Majumdar, Dr. Shilpa Sharma and Dr. Tridib Kumar Sarma. A special thanks to Sonit Da, Subhojit Da, Sadhu Da, Jasmini Di and Murugadoss Da for their invaluable support and encouragement. I admire Subhojit Da for his punctuality, management ability, for giving me good lab training and for his valuable suggestions that boosted my confidence again and again. Definitely, I will always miss his company. I also enjoyed my hostel life as well as stay in the lab of Prof. Chattopadhyay with Krishna Da, Subhojit Da and Sadhu Da.

It is my immense pleasure to thank my collaborator Dr. Amit Jaiswal, Sunil and Upashi, for their tremendous help in my research work. I owe my gratitude to Dr. Amit Jaiswal for my thesis chapter-2, Sunil for thesis chapter-5 and Upashi for thesis chapter-6. I enjoyed working with Dr. Amaresh Kumar Sahoo, Dr. Niramala Devi, Kafeel and Ayan. Working with them was a great experience. I would also like to acknowledge the M.Sc project students Bhaswati, Prativa and Ayan and the B.Tech project student, Saurabh Soni. I developed my supervision skill helping their project work. I am really thankful to Kafeel, Ayan and Saurabh for their help at various circumstances.

The journey of my Ph.D. life has not been easy; it had its own ups and downs. But, with some good lab mates it turned out it to be a great learning experience. My acknowledgement will never be complete without the special mention of my present lab mates Dr. Pallab Sanupai, Dr. Raihana Begum, Dr. Madhulekha Gogoi, Rumi Di, Rama, Satyapriya, Anushree, Shilaj, Uday, Sabhyasachi, Srestha, Deepanjali and Bandhan. Thanks to all of my lab mates for maintaining culture of unity in diversity in our lab. My special thanks to Raihana Di and Pallab Da for their advice and help.

The most beautiful part of Ph.D. life that I met was with some good friends, seniors and juniors like Saroj, Rahul, Kiran, Murali, Chirantan, Ashif Da, Zia Bhai, Zahir Bhai, Anusuya Di, Rajes Da, Julfikar, Pankaj Da, Atul Da, Chaitanya Da, Arghya, Satavisha, Nilufa, Afsana, Ajaz Bhai, Sameer, Anisur, Humayun Basha, Siddiq Basha, Sabera, Adil, Sahnawaz, Belal, Kobirul, Wajid, Akhtar, Shaad, Nasim, Niyaz Bhai, Atiur, Akhi, Maidul, Srimanto

Guin, Debasis (DK), Mostakim, Obaidullah, Rezwan, Tausif, Nawab, Farhan, Seraj Bhai, Faizi Bhai, Musawwer Bhai, Prasanta, Krapa Shankar, Ashraful, Saugata, Ashim, Arindam, Mandar, Prasenjit. My special thanks to Zia Bhai and Ashif Da for their personal and professional suggestions and their helps. It is indeed my great pleasure to thank Somnath for his help for ICP-OES analysis at IISc Bangalore. I acknowledge Hemanta and Vikash for EPR analysis. I also take this opportunity to thank some of my best friends Murshid, Tauqueer, Monirul, Aiman, Sajid, Anisur, Alamgir, Mizanur (Sani), Fahima, Ripon, Asif. I will ever be indebted for their love, inspiration and support. I am also thankful to Wasim, Ataur, Kulsum, Anjum, Reshma, Sheerin, Moniruzzaman Bhai, Zahir Bhai, Mushir Bhai, Munendra Da, Danish, Jitendra, Ethisam, Kalam, Rajib, Saijuddin. I acknowledge Bidya Mandir, coffee shop (core-3) and Anjan Deka Ji canteen (Brahmaputra Hostel). My deepest thanks to villagers of Namoni Jola (nearby main gate of IIT Guwahati) for their kind affection.

I would like to acknowledge my parents, my sisters (Nargis Apa, Sirin Apa & Nasrin) and my younger brother Illias. I will never be able to thank my parents enough for giving me education, for teaching me moral values, for their immense sacrifices, their tireless support, encouragement and for their blessings. I am obliged to my caring and loving brother Illias for his strong support. I am also thankful to my three brother-in-law (Apel Bhai, Muktadi Bhai & Rafikul), grandmother (Nani), Phuppi, Najrul Mama, Sirajul Mama, Abu Hena Mama and relatives for their support and inspiration. I am fortunate to have Kabirun and am thankful for her friendship, love, care, encouragement and support at various points of my life. Finally, I would like to thank almighty God.

Palashuddin

Contents

CHAPTER-1

Introduction and Literature Review

1.1. INTRODUCTION

The term 'nano', which is the most dominated, influential word in discussions, publications, solution of scientific problems in research etc., in scientific community as well as in public life in this century, refers to the range between 1 to 100 nm. It is explicitly associated with any object that has at least one dimension in this range, which accomplish the common definition of nanomaterial and more precisely nanoparticle (NP). The significance of the term 'Nano' lies in properties at nanoscale level i.e. surface-to-volume ratio of a particle dramatically increases as the size decreases that spawn to change physico-chemical and optoelectronic properties of the nanomaterials. This fundamental transformation in properties engenders new properties which could be tuned with size and shape and are distinctively different from bulk materials and which are ideal for various applications in energy, the environment, food, catalysis, medicine, optics, electronics, etc. Nanomaterials can be classified based on various properties and composition, such as metal based nanomaterials, semiconductor quantum dots, and carbon based nanomaterials. However, here I present a brief review of a few nanomaterials, with special emphasis on the carbon based nanomaterials and their properties.

1.2. METAL BASED NANOMATERIALS

The structural components of metallic nanomaterial are metals, metal oxides, metal sulphides etc., possessing $\leq 10^6$ atoms bonded together resulting into intermediate state of matter [1-2]. This intermediate state provides more number of atoms at or near the surface or interface [3-4]. The dimensions of the materials results in difference from bulk materials in properties like energy levels, electronic structure and reactivity [3-8]. In coinage metals (Cu, Ag and Au), a new phenomenon emerges, which is called localized surface plasmon resonance (LSPR), originating due to the collective oscillation of free electrons at the surface of spherical NP, following interaction with electromagnetic field [8-10]. This results in fascinating optical properties, depending on the size, shape, local environment as well as dielectric properties of medium, and they display colors in visible light and have been utilized in various applications [11-14]. Another advantage of having 'nano' size is in the form of magnetic property of NPs like in magnetite (Fe_3O_4), maghemite (γ-Fe_2O_3), Fe, Co and Ni. It has been found that a finite-size effect as well as surface effect dominates the magnetic properties of the NPs and having a large magnetic moment each nanoparticle works as giant paramagnetic atom to applied magnetic fields with negligible remanence and coercivity [15-16]. These make them suitable for various applications

like catalysis, biomedicine, data storage, nano-fluids, magnetic resonance imaging, and environmental remediation.

1.3. QUANTUM DOTS

Quantum dots (Qdots) are an intriguing class of semiconducting nanomaterials having sizes below 10 nm and smaller radii than the bulk exciton Bohr radius [17]. The interesting size-dependent opto-electronic properties of Qdots have been attracting researcher from various disciplines to work on a new class of materials since last 26 years [18]. The reasons behind the exceptional properties of Qdots are the number of surface atoms/ions which are a large fraction of the total atoms and quantum confinement of the electronic motion arises when size of the particle is as small as the de Broglie wavelength of the electron wave function [17]. The photoluminescence property of Qdot has been exploited in various biological applications and they are often portrayed as alternative to organic dyes, due to their excellent resistance to photo-bleaching, size tunable absorption and emission spectra and broad excitation spectrum with narrow emission [19-21].

The use of Qdot as alternative of organic fluorophore started with successful cell labeling, using CdSe-CdS core-shell, zinc sulfide–capped cadmium selenide Qdots by Alivisatos and Nie groups in the year 1998 [19, 21]. Further, Alivisatos groups demonstrated the antigen detection in fixed cellular monolayers using Qdots. After that, the implication of Qdots or Qdot-bioconjugates as cell markers has been widely explored by different groups *in vivo* as well as *in vitro* and in real-time tracking of molecules inside the cells [22-23]. They have emerged as a potential imaging candidate for labeling plasma membrane proteins, cytoplasmic proteins, nuclear proteins and cellular antigens in fixed cells [24-29]. In an elegant study, Akerman *et al.* practically manifested the animal imaging *in vivo* using ZnS-capped CdSe Qdots [30]. However, the unique photophysical and photochemical properties of Qdots were not restricted as imaging agents; they have been also applied for optical biosensing applications such as immunoassays, nucleic acid detection, biomolecule sensing, and catalysis monitoring [31-32]. On the other hand, Qdots have become popular due to their promising applications as efficient and cheaper photovoltaic cells, light emitting devices and photo-detectors [33-39].

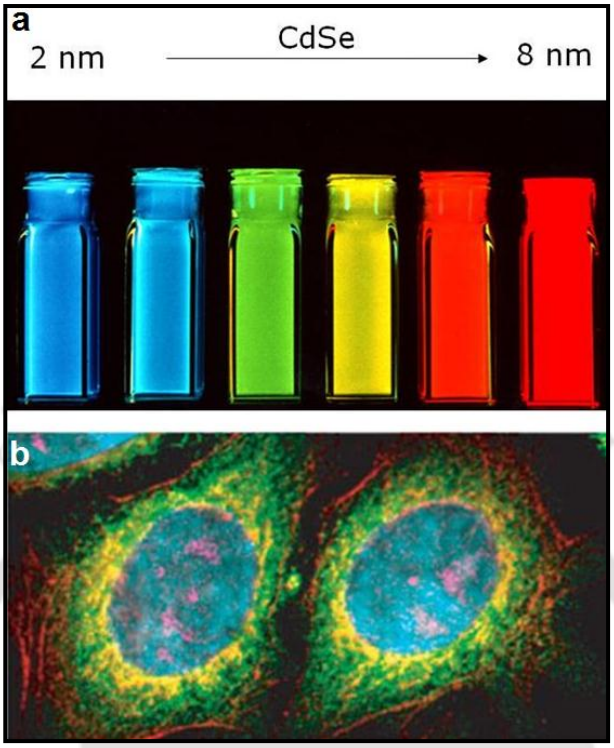

Figure 1.1. (a) The size dependent fluorescence properties of CdSe Qdots. (Reproduced with permission from *J. Phys. Chem. B*, **1997**, *101*, 9463.) **(b)** Five-color QD staining of fixed human epithelial cells. Cyan corresponds to 655 nm Qdots labeling the nucleus, magenta- 605 nm Qdots labelling Ki-67 protein, orange-525 nm Qdots labeling mitochondria, green- 565nm Qdots labeling microtubules and red- 705nm Qdots labeling actin filaments. (Reproduced with permission from *Nature Materials,* **2005**, *4*, 435.)

1.3.1. Quantum Dots Toxicity

In spite of tremendous success of Qdots in biomedical applications, there is also concerned about the toxicity of Qdots and it became a critical question on the use of Qdots in living cells. Currently, alleviation of toxicity of Qdots has been turned into an emerging research field for clinical applications. Generally, chemical compositions (heavy metals like Cd, Hg, Pb, As, Pb) of most of the Qdots are known to cause toxicities in vertebrates. However, Qdot toxicity assessment is still an enigma and is complicated. Although, various reports suggested that the toxicity originated from multiple reasons like surface capping agent specifically functional groups of capping agents, Qdot size, surfactant molecule on surface of Qdots, leaching of metals ions, chemical stability, oxidative and photolytic stability, bioaccumulation, abnormal local concentration, and nanoscale effects of the particles and free radical generation [40-48]. As a

result, various strategies have been developed to reduce the toxicity of Qdots, like coating strategy which improved the biocompatibility and cadmium free Qdots synthesis such as III–V (for example InP), Mn or Cu doped zinc chalcogenide, others material based QDots (for example $CuInS_2$, $CuInSe_2$) [49-52].

1.4. CARBON BASED NANOMATERIALS

Nanostructured carbon materials are versatile, promising and popular nanomaterials used in the modern interdisciplinary research. The Noble Prizes, in Chemistry for discovering buckminsterfullerene C_{60} (1996) and in Physics for graphene (2010) signify the importance as well as potential of the nanostructured carbon materials or nanocarbons. The journey of nanostructure carbon materials started with the discovery of buckminsterfullerene C_{60} which led to a new field of nanoscale carbon chemistry, other than naturally occurring three allotropes of carbon- amorphous carbon, graphite, and diamond. The discovery of carbon nanotubes has also generated a new era in nanotechnology. Nanostructured carbon materials could be classified as zero-dimensional (fullerenes), one-dimensional (carbon nanotubes), and two-dimensional (graphene) carbon materials [53, 54]. Fullerene possesses soccer ball like structure consisting of 12 pentagons and 20 hexagons. On the other hand, pure carbon nanotubes can be envisaged as a single sheet of graphite rolled up into a nanoscale tube form, which is known as single-walled carbon nanotube (SWCNT). If more than one SWCNT stacked one inside the other, it is called multiwalled carbon nanotube (MWCNT). Generally, structure of graphene comprises of a single layer of graphite with sp^2 hybridized carbon atoms that are densely packed in a honeycomb crystal lattice. The beauty of graphene reflects as mother of all graphitic form as well as building block for carbon nanomaterials. They possess excellent mechanical strength, electrical and thermal conductivity, and optical properties, which make them suitable materials for various applications like renewable energy conversion system such as solar cells and fuel cells, energy storage devices like super capacitors and batteries, and in catalysis, biomedical applications, drug delivery etc. [53-57]. Recently, one more carbon based member is included to this family which is known as carbon nanoparticles (CNPs).

1.4.1. Carbon Nanoparticles

The unique optical properties, photo-stability and resistant to metabolic degradation in bio-applications of semiconducting Qdots have branded them as promising and potential candidates for imaging and other biomedical applications and often depicted as alternatives of organic

fluorophore [58-63]. In spite of several advantageous properties, conventional Qdots also have some drawbacks since most of the Qdots are synthesized from heavy metals and thus are known to be toxic to the environment as well as mammalian cells, at even relatively low concentrations. In this regard, extensive efforts have been made to explore benign fluorescent nanomaterials to replace Qdots. Recently, the discovery of a new type of carbon based potentially valuable fluorescent nanomaterials, called as CNPs have generated enormous interest due to their low toxicity, environmental adaptability and bio friendliness [58-63].

CNPs could be defined as discrete, quasi-spherical amorphous or crystalline fascinating class of carbon based excitation tunable fluorescent nanomaterials [58, 62]. Generally; the particles with size less than 10 nm of CNPs are called as carbon dots (Cdots). They possess excellent water solubility, chemical inertness, low toxicity, eco-friendliness, ease of functionalization and outstanding photo-stability [58-63, 214]. Thus, Cdots are emerging as future 'nanolight' with potential applications in bioimaging, biolabeling, sensing, and development of optoelectronic devices. Along with emission based applications, they have been also exploited in nanomedicine, chemical sensing, photocatalysis and electrocatalysis.

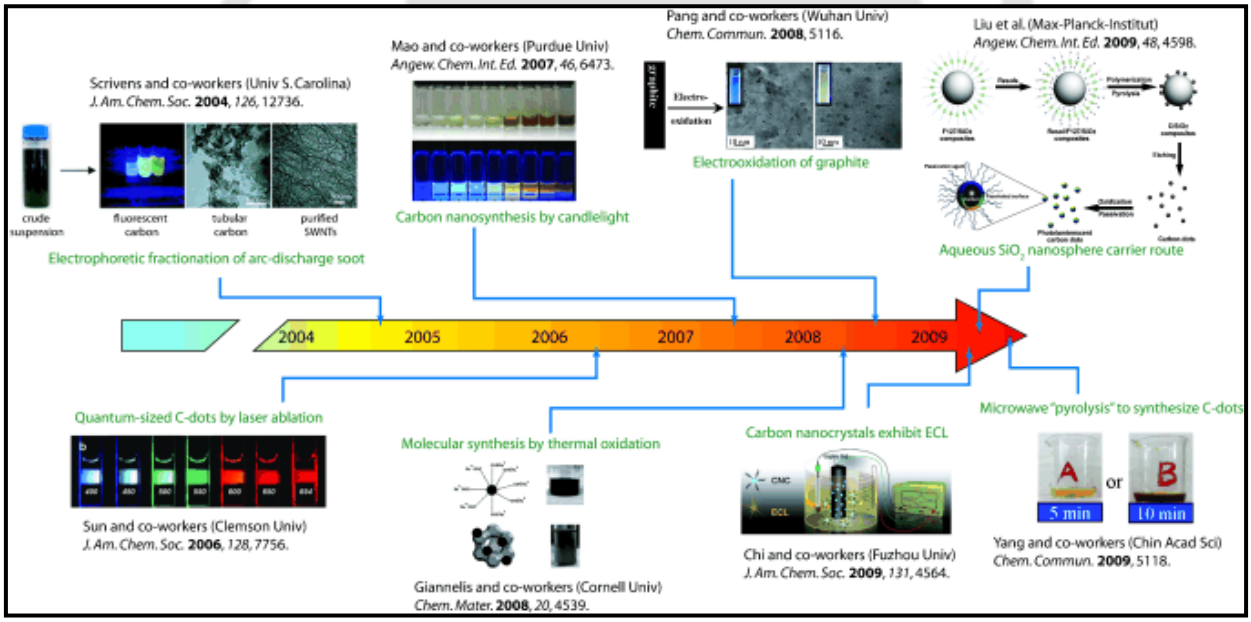

Figure 1.2. Timeline covering the activity of Cdots found in literature till 2009. (Reproduced with permission from *Angew. Chem. Int. Ed.* **2010**, *49*, 6726.)

1.4.1.1. Brief History

Cdots were first discovered unexpectedly by Scrivens *et al.* at the time of purification of single-walled carbon nanotubes (SWNTs) in 2004 [64]. They isolated a fluorescent component through preparative electrophoresis during purifying single-walled carbon nanotubes, derived from arc-discharge soot and then this component had appeared and to be known as Cdots. This observation inspired to search for nontoxic nanomaterials of similar optical properties and thus first physical synthesis method of Cdots through laser ablation was reported by Sun and Co-workers in 2006 [65]. Then Liu *et al.* demonstrated the preparation of Cdots using combustion oxidation method in 2007 [66]. In the same year, Sun and his team successfully employed Cdots for multiphoton bioimaging in the human breast cancer cells [67]. In the year of 2008, two new synthesis methods of Cdots were developed, namely, by electrooxidation of graphite in aqueous solution and thermal oxidation using citric acid as a precursor [68-69]. In an elegant study by Sun group, they depicted the potential application of Cdots for the first time by using them in optical imaging *in vivo* [70]. Further, microwave pyrolysis approach using carbohydrate as precursor (2009) has opened new synthetic route of Cdots, which is a simpler, safer, eco-friendly and cheap, encouraging interest in this emerging field [71]. After 2009, the field has become more popular.

1.4.1.2. Synthetic Methods

The synthetic methods for preparing Cdots could be generalized in two categories- top-down and bottom-up [58-63]. Normally, top-down methods are associated with breaking down of larger carbon structure through arc discharge [64], laser ablation [65, 72] and electrochemical oxidation process [68, 73-75]. On the other hand, bottom-up methods pertain to synthesis of Cdots from molecular precursor via combustion/thermal treatments [66, 69, 76-77, 82-84], supported synthesis [69, 78] and microwave/ultrasonic [71, 79-81] methods. Usually, a variety of molecular precursors such as citric acid [69, 82-83], carbohydrates [71, 80, 84-85], amino acid [86] polyethylene glycol [79] ethylenediaminetetraacetic acid [87], ethanol [88], glucosamine [89] and ascorbic acid [90] has been used for the preparation of Cdots.

However, another scope for the Cdot synthesis is to develop large scale, greener and cost-effective method and is free from complex instrumental set-ups or post-treatments [60, 62]. In this regards, Cdots were prepared from biomass and bio-waste such as watermelon peels [91], pomelo peels [92], paper ash [99], plant leaves [98] and also from orange juice [93], strawberry juice [94], sugar cane juice [95], banana juice [100], egg shell membrane ash [101], organogel

[96], gelatin [97], meat products [102], natural silk [103], bovine serum albumin [104], hair fiber [105] and chitosan [106].

1.4.1.3. Composition

Generally, the fundamental compositions of Cdots are carbon, oxygen and nitrogen, depending on the synthetic methods as well as precursors [58-59, 63, 213]. The ratios of these three elements are not consistent; they may vary from synthetic route to route. However, to tune the optical properties, doping has been done occasionally with several elements like boron, phosphorus or chlorine. Unlike graphene, Cdots may contain sp^2, sp^3 hybridized carbon and also they may or may not be structured like graphene. Also, they may be amorphous or crystalline in nature. The surface of the Cdots is enriched with various functional groups like oxygenated groups (C–O, C=O and O–C=O), amide, C–N–C and –NH and this depends on the precursor as well as synthetic methods.

1.4.1.4. Fluorescence Property

The beauty as well as popularity of these fascinating light emitting materials lay on their wavelength tunable photoluminescence property, which is one of the most attractive fundamental features of Cdots. However, the origin of their luminescence is not clearly understood yet and needs further clarification [58-59]. It is believed that the cause of emission of Cdots might be as a result of the quantum effect or emissive traps or radiative recombination of excitons [58-59]. Very recently, Wang *et al.* unraveled the origin of green luminescence in Cdots [107]. They claimed that the formations of special molecule-like states consisting of several carbon atoms on the edge of carbon backbone and functional groups with C═O (carbonyl and carboxyl groups) in Cdots are mainly responsible for their green fluorescence. Zhao *et al.* and Vinci *et al.* clarified the reason for the excitation tunable fluorescence and they found in their separate investigations that the mixture of different sizes Cdots produced excitation-dependent emission [108-109]. In this regard, it is also observed that the optical behavior of Cdots can be associated with different emissive sites on each Cdot, irrespective of different sizes in the sample [65].

In the perspective of potential applications of Cdots, higher quantum yields as well as emissions at red and near-IR special regions are essential [59-60]. In this regard, various strategies like precursors, synthetic methods, surface passivation, doping in the core and on the surface have been adopted to improve the optical property of the Cdots. Sun and coworkers had manipulated the brightness of the photoluminescence of Cdots using passivating agent with

quantum yield from 4% to 10% [65]. Further, Liu *et al.* enhanced the quantum yield of Cdots up to 14.7% using the same surface passivation technique of Sun and coworkers [66]. In doping technique, Cdot cores were doped with nitrogen, sulfur, phosphorus, boron/nitrogen and also the surfaces were doped with inorganic salts like ZnO, ZnS, or TiO_2 to get higher quantum yield [110, 213]. However, synthetic strategies and precursor play significant role to tune the optical property. For instance, Giannelis and coworker had succeeded to achieve 53% quantum yield for hydrophobic Cdots by thermal pyrolysis and Zheng *et al.* reported 88.6% for water soluble Cdots [61]. In both cases, carbon source precursor is citric acid but the synthesis methods are different and higher quantum yield was obtained in comparison to previously reported methods with averaged quantum yield at around 6% obtained using carbon source precursor other than citric acid. Although, Cdots display fluorescence in the wide range of spectrum but emission of most of the Cdots dominate the blue-green region [60-61]. Therefore, a few efforts also have been taken to develop red and near-IR fluorescent Cdots, which is desirable for bioimaging.

It has been widely established that the luminescent property of Cdots remains unchanged and stable in presence of a high salt concentration and in the wide range of pH [111]. They show high photostability on continuous irradiation of UV-light as compared to any popular dye molecule [58-63, 214].

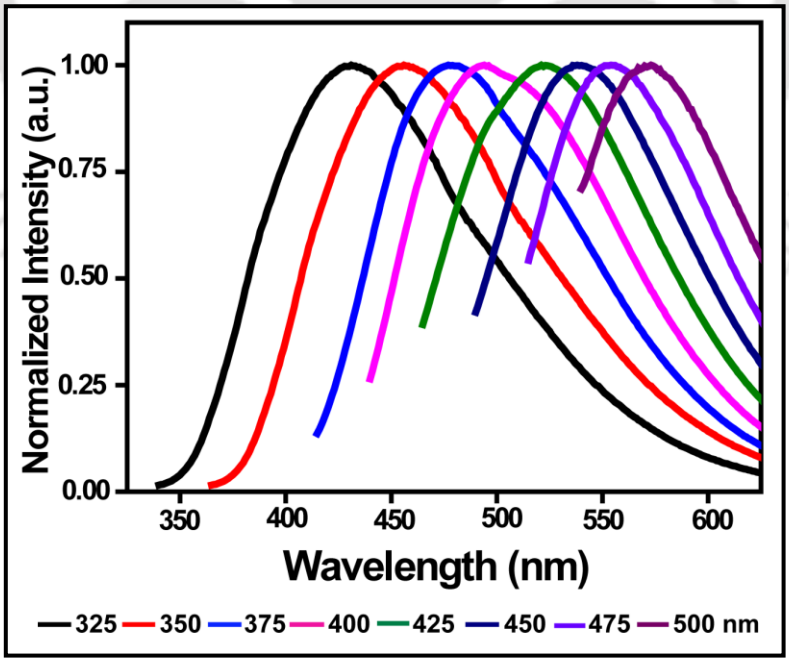

Figure 1.3. Excitation dependent photoluminescence properties of Cdots. Reproduced with permission from *Sci. Rep.* **2012**, *2*, 383.)

1.4.1.5. Cytotoxicity

For the bio-applications of nanomaterials, a matter of concern is related to their toxicity and biocompatibility. Therefore, there are many reports available on toxicity and biocompatibility studies *in vitro*, but few *in vivo* and it has been reported that Cdots are lowly cytotoxic and biocompatible [58-63]. Thus, Cdots have been accepted as non-toxic or lowly toxic nanomaterials. In this regard, our laboratory has demonstrated the non-cytotoxicity of Cdots synthesized from microwave heating of polyethylene glycol in mammalian cells (HT 29 cells) *in vitro* [79].

1.*4.1.6. Applications*

Bioimaging, Drug delivery and therapy

The advantage of Cdots over semiconducting Qdots includes ease of synthesis, low or no toxicity, biocompatibility, water solubility, chemical inertness, photochemical stability and ease of modification. The properties make them viable alternatives to Qdots and ideal candidates for bioimaging *in vitro* and *in vivo* [58-63]. Cdots are also exploited in drug delivery, photodynamic therapy and photothermal therapy applications [60-63].

Sensor

Intrinsic luminescent property of Cdots has been employed for versatile applications i.e. in chemical sensing and biosensing [62-63]. Cdots are able to detect various metal ions like Hg^{2+}, Cu^{2+},Fe^{3+},Pb^{2+},Cr(VI) and Ag^{+}, anions like $C_2O_4^{2-}$, PO_4^{3-}, CN^{-}, F^{-}, S^{2-}, ClO^{-} and I^{-}, organic molecules like ascorbic acid, 4-nitrophenol, quercetin, 2,4-dinitrophenol and 2-amino-3,4,8-trimethyl-3H-imidazo[4,5-f]quinoxalin, and sense pH and NO_2 gas. As biosensors, Cdots are efficient to sense biomolecules like nucleic acid, thrombin, bacteria cells in sewage water, small bioanalytes like anti-bacterial drugs amoxicillin, dopamine, ascorbic acid and glucose.

Apart from fluorescence based sensing, Cdots are capable of sensing NO_2^{-} and Co^{2+}, utilizing chemiluminescence property, pentachlorophenol and Cu^{2+}, using electrochemiluminescence property [63].

Photocatalysis

Cdots have been used as photocatalysts in organic transformations as they have the ability to harvest long wavelength light [62]. Therefore, they have been applied in various photocatalytic reactions such as selective oxidation of alcohols to benzaldehydes using NIR light, green

oxidation of cyclohexane to cyclohexanone, removal of organic pollutants, selective hydrocarbon oxidation and photochemical production of H_2 from water by irradiation of visible light.

Electrocatalysis

Cdots are also emerging as electrocatalytic materials for oxygen reduction reaction, as an alternative to platinum-based electrocatalysts because of their high stability and good electrical conductivity [62].

Optoelectronics

Cdots are now becoming an alternative to Qdots in the field of optoelectronics [60]. They have been used in electroluminescent devices resulting as light emitting diodes, based on electrically exciting the Cdots and optical down-conversion based device resulting into color-conversion light emitting diodes through their optical excitation.

1.5. MOTIVATION

In the introduction section of this thesis, various aspects of CNP are illustrated by identifying the key areas of this field. CNP has been portrayed as an alternative of Qdots since its discovery. But the question still remains - 'Should CNPs be considered as safe-NPs?' There is debate prevalent among the researchers, regarding the immediate and long-term implications of nanomaterials with regard to human health as well as the environment. So, the best solution is to search for naturally occurring nanoparticles, especially those which have been either consumed by human beings from long time or the ones which have been in contact with human body and have not caused any major health concerns. We understood from the literature that only heating of starting material at proper temperature is required to synthesize CNPs, which inspired us to search CNP in various food and food products.

Charcoal has been extensively used as a supporting material for catalysts like Pd, Pt etc. and has great impact on catalysis. In view of this, CNP can also be used to enhance the catalytic activity of catalysts as both have the same basic element - carbon. This analysis prompted us to check the catalytic activity of gold NPs supported by CNP as an effective catalyst.

It has been found that most of the applications of Cdots are due to their optical properties, especially photoluminescence. In this regard, bright emission is one of the most significant parameters, and still most of the synthetic methods of Cdots are restricted to be performed inside specialized laboratories with certain conditions like harsh reaction conditions, time consuming, as well as lack of ease of large scale high quantum yield Cdot production. So there is

a clear need to devise a simple synthesis method for highly luminescent Cdots. These bright emissive Cdots could be employed in various applications as markers, sensors, etc. Also, the logic operations of Cdots have still been unexplored, and the robust photo-physical properties of Cdots could be exploited to construct various logic gates in multiphase like liquid and solid phases.

Further, CNPs are also becoming popular because of their biological applications, as they possess very low toxicity and the surface of CNP is enriched with various polar functionalities. All these advantages have manifested into CNP being a suitable delivery vehicle in drug delivery applications. However, there is still a scope of delivering metal ions into the cancerous cells using the surface of CNP which is capable of forming complexes with metals, like various anticancer metal-complexes.

1.6. OUTLINE OF THE THESIS

The thesis contains seven chapters. The first chapter (the current chapter) of this thesis is an introductory chapter on nanomaterials especifically CNPs. It reviews the emergence of CNPs, their general importance and key developments of various aspects such as advancement of synthetic methods, composition, photoluminescence property, cytotoxicity, diverse applications etc.

In **Chapter 2**, the finding of the presence of CNPs in different carbohydrate based food caramels, *viz.* bread, *jaggery*, sugar caramel, corn flakes and biscuits, where the preparation involves heating of the starting material is illustrated. The CNPs were amorphous in nature; the particles were spherical having sizes in the range of 4-30 nm, depending upon the source of extraction. The results also indicated that particles formed at higher temperature were smaller than those formed at lower temperature. Excitation tunable photoluminescence was observed for all the samples with quantum yield (QY) 1.2, 0.55 and 0.63%, for CNPs from bread, *jaggery* and sugar caramels, respectively. The present discovery suggests possible usefulness of CNPs for various biological applications as the sources of extraction are regular food items, some of which have been consumed by humans for centuries, and thus they can be considered as safe.

Chapter 3 delineates synthesis of CNP supported Au NP starting with Au NP-chitosan composite and its catalytic activity. The formation of the composite was established using UV-visible spectroscopy, fluorescence spectroscopy, powder X-ray diffraction (XRD), X-ray photoelectron spectroscopy (XPS) and transmission electron microscopy (TEM) studies. In the composite, the size of Au NPs was 4.9 ±1.4 nm, while that of CNPs varied from 50 nm to 350

nm. Then the catalytic activity was examined. The composite NPs efficiently converted phehylboronic acid to biphenyl through homocoupling. In addition, a plausible mechanism relying on the role of Au-NPs as the active site was proposed which rationalizes the solvent dependent reactivity and selectivity of the reaction. The catalyst was stable and could be recycled are important for its practical application.

Chapter 4 describes a new and facile method of synthesis of highly fluorescent Cdots using a commercially available induction coil heater. The Cdots were produced when an aqueous solution of citric acid and a diamine compound was heated at 100 ^{o}C for 12-15 min. The Cdots, with an average size of less than 5 nm (being produced when ethylenediamine was used), emitted blue light with high quantum yield, when excited by UV light. The quantum yield was dependent on the nature of diamine and was as high as 73.5% for ethylenediamine. The as-prepared Cdots could easily be converted into gel by mixing with chitosan biopolymer. The gel could be used for filling up the refill of a ball-point pen and be used for UV-active marking, for sensing of explosive compounds (such as picric acid and 2,4 –dinitrophenol) with high efficiency and for other fluorescence based applications. The use of commercial induction coil heater, scalability and high chance of commercial viability make the method especially appealing.

Chapter 5 also deals with luminescent Cdots (as mentioned in chapter 4), which could be used to pursue cascade logic operations in two different phases. Basic and higher integrated logic operations were achieved based on the changes of photoluminescence of Cdots through interactions with metal ions and organic molecules in liquid dispersion as well as in the solid phase. For example, in the presence of Fe^{3+} ions, quenching of emission of Cdots was observed. The emission could be recovered following treatment with ascorbic acid or cysteine. On the other hand, emission quenched by picric acid could be recovered by using a phase transfer process. We have also established a logic system using Fe^{2+} and H_2O_2 which could distinguish Fe^{3+} from Fe^{2+} ions. Overall, the simple and complex logic systems, being capable of operating in dual phases, offer applications in various analytical purposes as well as detection of important elements in diverse environment.

Chapter 6 demonstrates that Cu^{2+} embedded CNP (Cu-CNP) acts as an anticancer agent. The fluorescent Cu-CNP was synthesized by using CNPs and copper salt at 50 ^{o}C (pH=9-11). The formation of Cu-CNP was established using UV-visible spectroscopy, fluorescence spectroscopy, IR spectroscopy, powder X-ray diffraction (XRD) and transmission electron microscopy (TEM) studies. The average size of the Cu-CNP was found to be 92.7 ± 49.8 nm. Then the anticancer activity of Cu-CNP was carried out by standard MTT assay followed by cell cycle analysis and caspase3 assay where it has been found to undergo apoptosis. In this regard, the inherent blue

emission of Cu-CNP could be used to monitor the cellular uptake by confocal microscopy. Overall, good biocompatibility, bright emission, cellular imaging application, and anticancer effect of Cu-CNP will make it a promising candidate for future theranostic applications.

The last chapter (**Chapter 7**) deals with the future prospects of the key findings of the research works carried out in this thesis.

CHAPTER-2

Presence of Amorphous Carbon Nanoparticles in Food Caramels

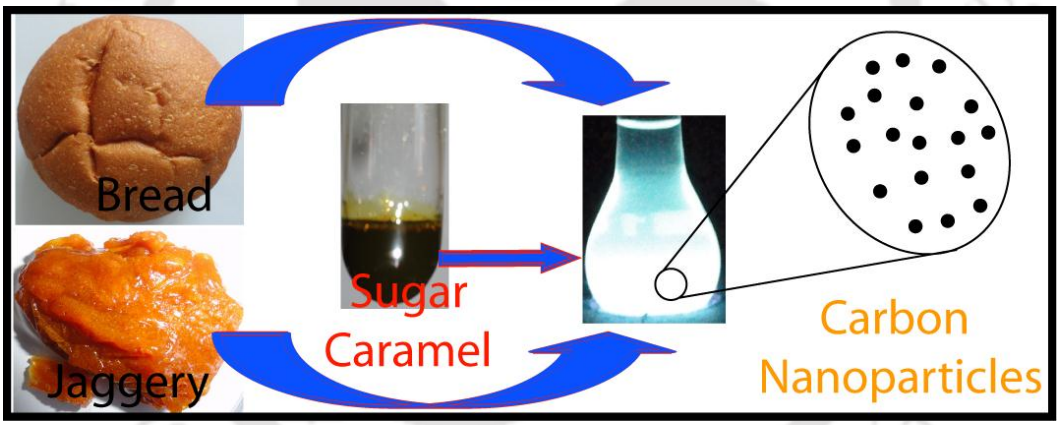

Highlights:

- *Cytotoxicity of nanomaterials; safe nanomaterials for biological applications.*
- *Revelation of 'nanolight' CNPs in caramelized food items.*

2.1. INTRODUCTION

The use as well as presence of nanoparticles (NPs) in food is a hotly debated area, owing to their short and long term effects on human health and the environment [112–115]. The promise of targeted and/or sustained release of drug, food colourants and flavours, while incorporated with NP, makes the pursuit of understanding of their functioning and fate a worthy exercise [116–118]. Although, substantial development in the engineering of consumable NPs [116–118] and their effects *in vitro* and *in vivo* have taken place [119]; few biodegradable NPs have entered clinical trials and have been marketed [120–121]. While NP formulations for topical applications are accepted by majority of population [122], the idea of the consumption of these particles, either for curing a disease or for having nutritional or flavouring benefit, creates an alarm for the public. The reason behind this seems to be their potential effect on human health following consumption, which has received little attention; and the lack of awareness, which has raised concerns regarding the safety of nanomaterials in biological and food applications [112–115]. A way around this problem, could originate out of direct derivation of nanomaterials from food products, especially from traditional food items. These materials could be considered safe for biological applications when there is no known toxicity and thus may possibly alleviate the misapprehension that all NPs are toxic.

History of nanotechnology is replete with examples of use of nanomaterials dating back to millennia [123–125]. The dye used in colouring hair to black, during the Greco-Roman period, is now known to have been consisted of PbS nanocrystals (NCs) [123]. Romans exhibited their mastery in technology in the Lycurgus cup by harnessing the optical properties of gold (Au) NPs [124]. The extraordinary mechanical strength and a sharp cutting edge in Damascus sabre have recently been attributed to the presence of carbon nanotubes (CNTs) and cementite nanowires [125]. In all the cases mentioned above, while the technology based on nanomaterials were known to different civilizations, the nanoscale nature of their functional constituents have only been revealed recently. The 'nano' dimensionality is not only confined to engineered materials or technology; nature also creates NPs or nanostructures which are present as functional components in an organism; either in the form of enzymes which catalyze most of the biological reactions or as ribosomes which act as the sites for protein synthesis. It was the invention of

sophisticated microscopic and analytical techniques which has led to the discovery of these nanostructures. In this regard, the idea of searching for nanomaterials within regular food items cannot be inexplicit. This motivated us to search for NPs in food items, which can potentially be used for biological application, where the concern of the origin and toxicity of the nanomaterials can easily be waived off. In this chapter, I have described the presence of carbon nanoparticles (CNPs) in regular carbohydrate based food caramels, such as in bread, jaggery, corn flakes and biscuits. The CNPs have been found to be present in those samples, where the preparation of food mainly involves heating of the starting ingredients in absence of water, leading to formation of caramels. Arguably; this discovery revealed that human consumption of nanomaterials in the form of food caramels has its history possibly from the period when human for the first time started eating bread.

2.2. EXPERIMENTAL

Materials. Bread buns (Homa Bread, Guwahati, India), *jaggery*, cornflakes (Real Crunch Corn flakes, India), biscuits (Britannia Marie Gold, India) and sugar (*Daurala* Sugar Works, India) were purchased from the local market. Bis (2-methoxy-4-nitro-5-sulfophenyl)-2H-tetrazolium-5-carboxanilide was received from Sigma-Aldrich, USA. Milli-Q grade water with a resistivity of 18.2 $M\Omega.cm^{-1}$ was used in all the experiments.

Preparation and Extraction of CNPs. Bread buns were analysed to check the presence of CNPs within it. The top brown layer of bread was carefully excised and 1 g of it was dissolved in 20 mL methanol by sonicating it at 35 kHz in a bath sonicator (Elmasonic TI-H-5 Elma, Germany) for 10 min. Following sonication, the volume of the methanol was reduced to 3 mL in a rotary evaporator before further purification. *Jaggery* (prepared from sugarcane juice) purchased from the market was heated following a traditional procedure which is as follows. Initially, *jaggery* (say 50 g) was mixed with water (about 10-15 mL) to make it sufficiently moist. The entire amount was then placed on a hot pan, which was being heated in the medium flame of a commercial gas stove. The mixture was constantly stirred using a kitchen spatula. In about 5 min, when the color of the mixture turned dark brown, the entire amount was transferred to a pan containing a thin layer of oil and brought to room temperature. The oil layer helped in preventing aggregation of the mass and also in spreading the content over the pan. The *jaggery* caramel, which was ready for use then, was dissolved in methanol and allowed to stand for a few minutes to remove larger impurities. The sedimented particles from both the samples were

removed by filtration. Centrifugation of the supernatant at 5000 rpm was performed further to remove impurities of smaller size. The yellow coloured supernatant thus obtained was further purified by column chromatography (using silica 60-120 mesh) with methanol: dichloromethane (2:3) mixture and finally dialysis (using 1 KDa membrane) was carried out to remove salts and other ions, if any. Similar procedures were followed for the extraction of CNPs from commercially purchased cornflakes and biscuits. Caramel was also prepared in laboratory by heating commercially available sugar. Sugar was taken in a glass vial and heated in an oil bath at 200 ^{o}C for 10 min till the solid turned brown. The brown colored sticky mass was cooled down to room temperature and was then dissolved in methanol, followed by purification using column chromatography. The sample was then concentrated by evaporating the solvent in rotary-evaporator and then it was dissolved in water and finally dialysed before further analysis.

Analytical Measurements. The extracted CNPs were characterized using TEM (JEOL 2100 UHR-TEM), UV-vis (Perkin Elmer Lambda 25) and fluorescence spectrophotometers (FluoroMax-4, *Jobin Yvon*). The TEM analysis was performed at an accelerating voltage of 80 kV, unless otherwise mentioned, and the sample was prepared by drop casting 5 μL of the respective sample on a 300 mesh carbon coated copper grids and subsequent air drying before analysis. ^{13}C nuclear magnetic resonance (^{13}C NMR, 100 MHz) of the dispersion was carried out in a Varian 400 MHz FT-NMR using D_2O as the solvent. Thermogravimetric analysis (TGA) was performed in Q600 SDT Simultaneous DSC-TGA heat flow analyzer and powder XRD study was done using a Brucker D8 Advanced X-ray diffraction measurement system, with Cu Ka source (λ =1.54 Å). Sonication was done by Elmasonic TI-H-5 Elma, Germany.

Quantum Yield Calculation. The quantum yield (QY) was calculated using quinine sulphate in 0.10 M H_2SO_4 solution as a standard, at an excitation wavelength of 365 nm, and the absorbance was kept below 0.15. The QY of the samples were determined according to the following formula:

$$QY_S = QY_R \left(\frac{m_S}{m_R}\right)\left(\frac{\eta_S}{\eta_R}\right)^2$$

Where, QY is the quantum yield, m is the slope of the plot of integrated fluorescence intensity *vs* absorbance and h is the refractive index of the solvent. For the aqueous solutions η_S/η_R=1. The subscript R refers to the reference fluorophore *i.e.* quinine sulphate solution and S for the sample. The values obtained are given in Table 2.1.

Table 2.1. Quantum yield calculation

SN	Sample	Slope	QY	QY (%)
1	Quinine sulphate	1,87,63,45,623.23	0.54 (standard)	54 (standard)
2	CNPs from bread	4,23,31,851.73	0.01218283	1.21
3	CNPs from *jaggery*	1,91,15,656.68	0.005501361	0.55
4	CNPs from sugar caramel	2,21,22,160.83	0.006366613	0.63

In Vitro Cytotoxicity Assays. HeLa cells were obtained from National Center for Cell Sciences (NCCS), Pune, India and were cultured in Dulbecco's modified Eagle's medium supplemented with penicillin (50 units mL^{-1}), streptomycin (50 mg mL^{-1}), and 10% (v/v) fetal bovine serum. Cells were maintained in 5% CO_2 humidified incubator at 37 ^oC. The cells were seeded in a 96 well culture plates at a density of 5000 cells/well and were allowed to grow overnight. The CNPs were then added into the wells in a concentration range of 50 ng/mL to 2 µg/mL and incubated in a humidified incubator for 24 h at 37 ^oC and 5% CO_2. XTT (Bis(2-methoxy-4-nitro-5-sulfophenyl)-2H-tetrazolium-5-carboxanilide) based cell viability assay was carried out according to the manufacturer's protocol, to determine the percentage of viable cells. The assay is based on the metabolic activity of the cells to reduce the tetrazolium salt XTT to orange colored compounds of formazan and the intensity of the dye is proportional to the number of metabolically active cells. The percentage cell viability of the untreated cells (control) was taken as 100%. All measurements were collected in triplicate and the values are expressed as mean ± standard error (SE). Statistical analysis for ANOVA was performed using Sigma Plot.

2.3. RESULTS & DISCUSSION

The CNPs isolated from the outer brown part of the bread bun and the caramels obtained from commercially purchased sugar (following caramelization) and *jaggery* were analysed by UV-vis and fluorescence spectroscopy. The UV-vis spectrum of each of the dispersions consisted of a peak (marked with star) and a shoulder (marked with arrow) between 240 nm and 400 nm and

is shown in Figure 2.1. In addition, there is the presence of a strong background till 540 nm. The peaks and the background extinction are known to occur for CNPs and they are consistent with the literature reports [58]. The exact assignment of the peaks is still not known and hence the difference among the individual samples could not be explained.

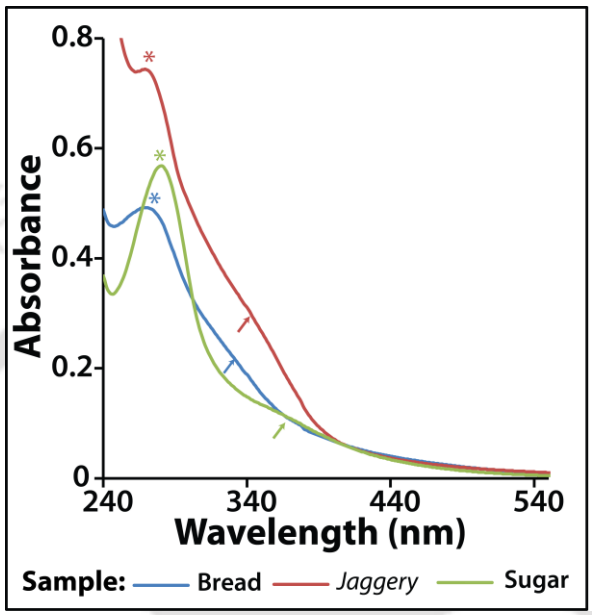

Figure 2.1. UV-vis spectra of CNPs extracted from bread, jaggery and sugar caramel.

Photographs of the original samples (bread, *jaggery* and sugar) which served as the preparatory ingredients are shown in Figures 2.2A, 2.2B and 2.2C. The photoluminescence spectra corresponding to the above dispersions (and other samples) are shown in Figures 2.2D-2.2I. The pictures of the dispersions in the presence of white light and UV light are represented in Figures 2J-2O. Under normal white light the dispersions have the characteristic caramel colour whereas, under UV light (λ_{ex}=365 nm) it showed blue luminescence. All of the dispersions exhibited excitation dependent emission spectra as shown in Figures 2G-2I, which were similar to Cdots reported previously [58]. It was also observed that with increase in the wavelength of excitation from 325 to 375 nm the luminescence intensity increased, the maximum emission intensity being observed for the excitation wavelength of 375 nm, whereas, further increase of the excitation wavelength resulted in the decrease of emission intensity. Additionally, along with decrease in the fluorescence intensity with increasing excitation wavelength the emission maxima showed red-shift, displaying the property of excitation tuneable emission. The

excitation dependent emission is an intrinsic property of CNPs, which has been widely reported by several research groups including us [79, 58, 64-66, 68, 71, 81]. The quantum yields (QYs) of the CNPs obtained from different food sources were calculated using quinine sulphate as the standard [71]. At an excitation wavelength of 365 nm, the QYs of the CNPs are summarized in Table 2.1. The results indicated that these samples had QY typical of Cdots, which is on the order of 1%; with the highest being observed for samples from bread (1.2%) and that from *jaggery* had the lowest value (0.55%).

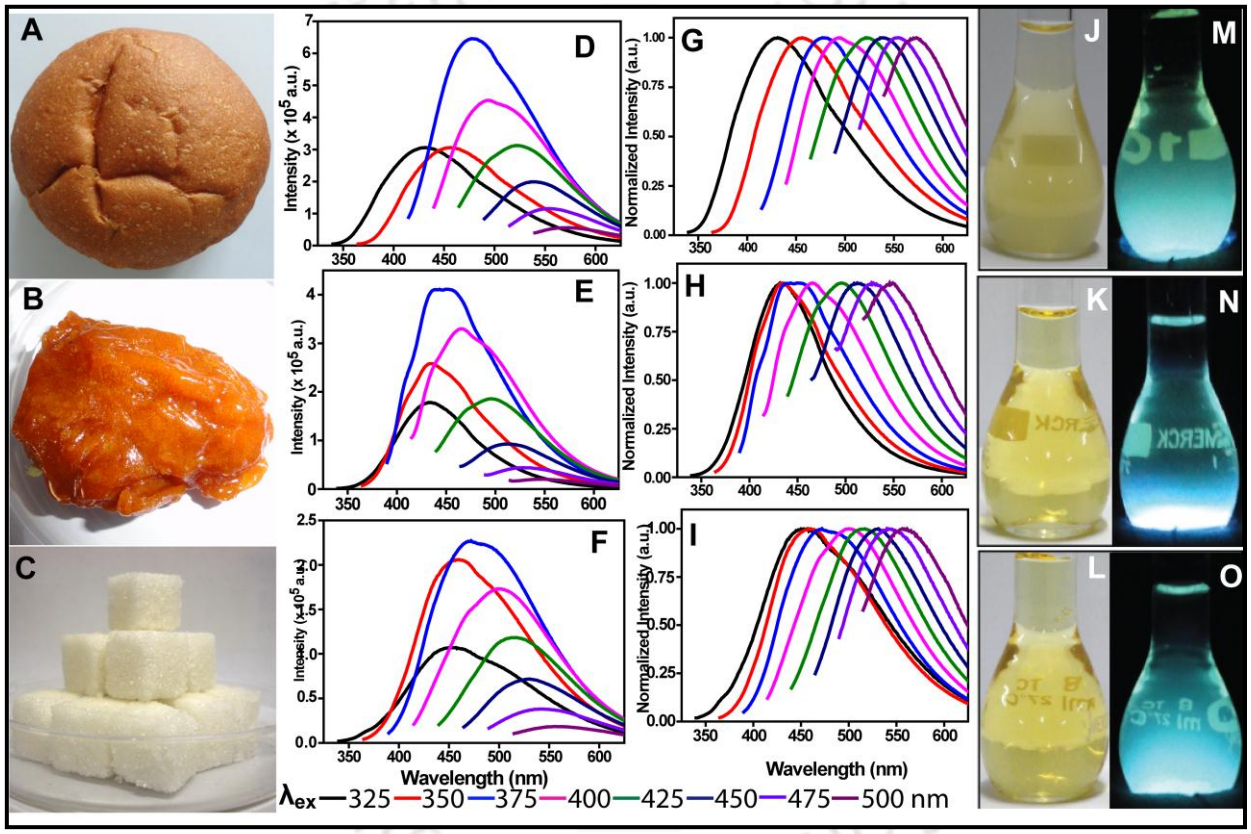

Figure 2.2. (**A**, **B**, **C**) Photographs of commercial bread, *jaggery* and sugar. (**D-I**) Excitation wavelength dependent emission spectra of CNPs from bread, *jaggery* and sugar caramel. (**J-L**) Photographs of dispersions of CNPs from bread, *jaggery* and sugar caramel observed under white light and (**M-O**) the same under UV light.

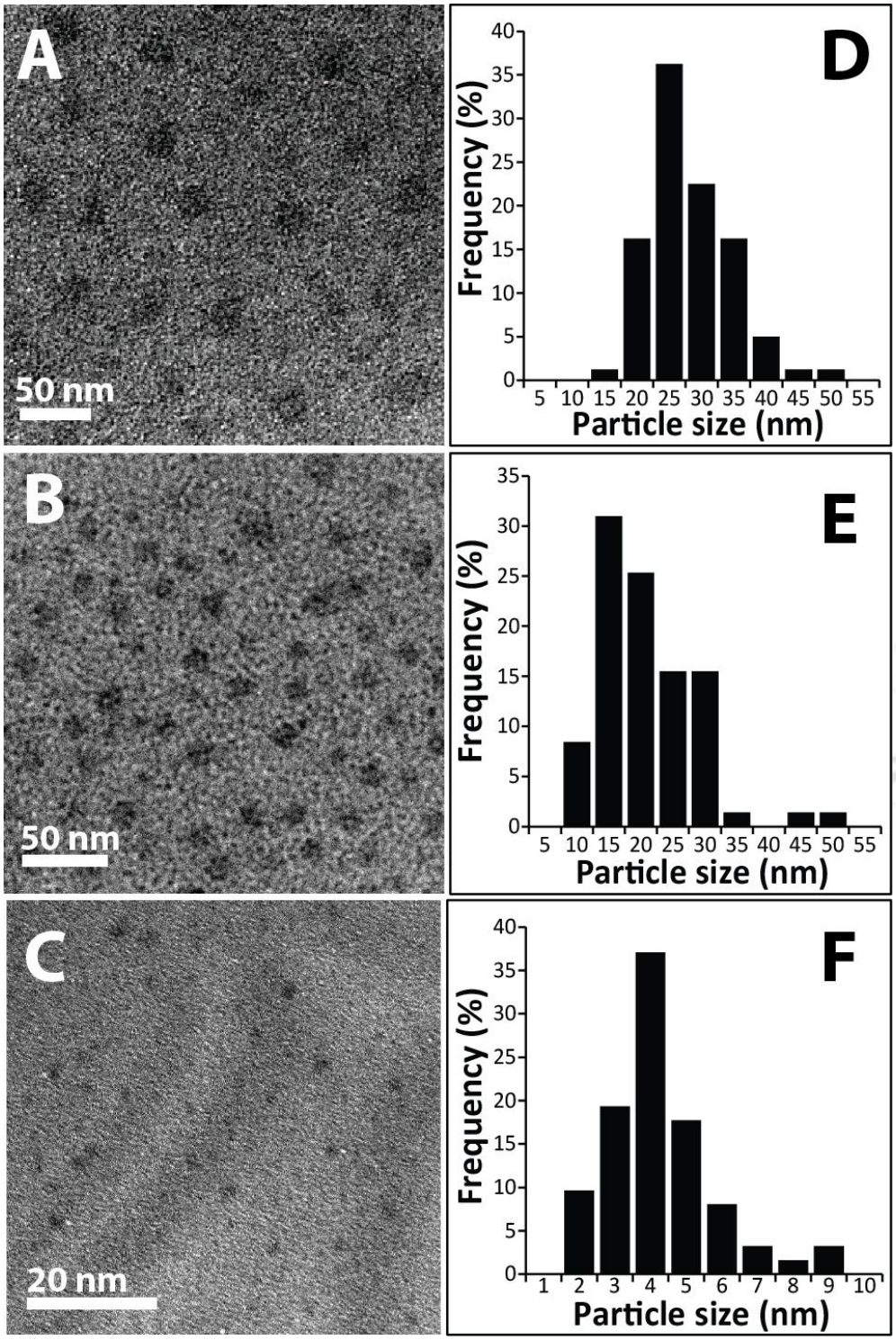

Figure 2.3. (**A**, **B**, **C**) TEM images of CNPs extracted from bread, *jaggery* and sugar caramel and (**D**, **E**, **F**) Corresponding particle size distributions of samples in that order.

Transmission electron microscopy (TEM) images of the samples obtained from the dispersions of different caramel sources (bread, *jaggery* and sugar) are represented in Figures 2.3A-2.3C, which showed the presence of uniform spherical NPs. The particle distributions calculated from the images are shown in Figures 2.3D-2.3F. The average particle sizes as calculated from the TEM images for samples from bread, *jaggery* and sugar caramel, were determined to be 27.5 ± 6.1, 20.3 ± 7.5, 4.3 ± 1.5 nm respectively. The results clearly indicated that NPs were present in the dispersions extracted from bread, *jaggery*, and caramel of sugar. While the sample from bread had the highest particle size, the particles from sugar caramel produced at 200 ^{o}C had the lowest size and the particle sizes of the sample from *jaggery* were in between the two. In addition, caramels from sugar, produced by heating at 180 ^{o}C for 10 min, had particles of size 25.8 ± 12.4 nm (Figure 2.4).

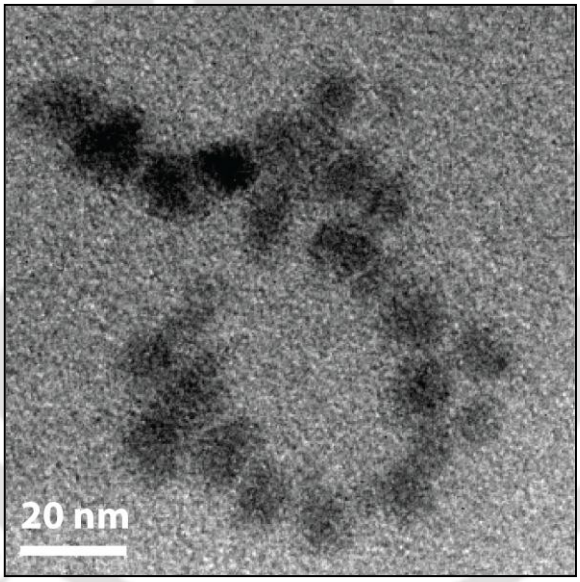

Figure 2.4. TEM image of CNPs prepared by heating sugar at 180 ^{o}C for 10 min.

CNPs were also extracted from commercially procured biscuits and corn flakes and the corresponding spectroscopic data are shown in Figure 2.5. They also showed excitation tunable emission like CNPs from bread, jaggery and sugar caramel. The samples from corn flakes and biscuits indicated the presence of NPs having sizes of 10.5 ± 2.8 nm and 3.9 ± 1.3 nm respectively (Figure 2.5).

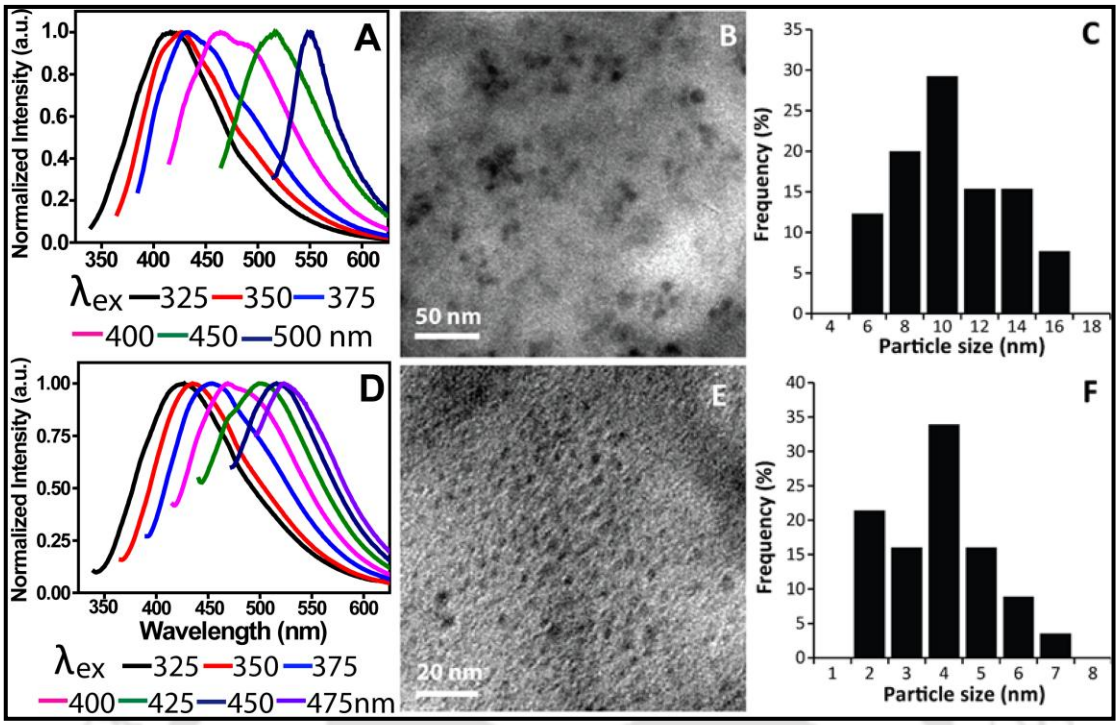

Figure 2.5. (**A**) Excitation wavelength dependent emission spectra, (**B**) TEM image and (**C**) particle size distribution of CNPs extracted from corn flakes. (**D**) Excitation wavelength dependent emission spectra, (**E**) TEM image and **(F)** particle size distribution of CNPs extracted from biscuits.

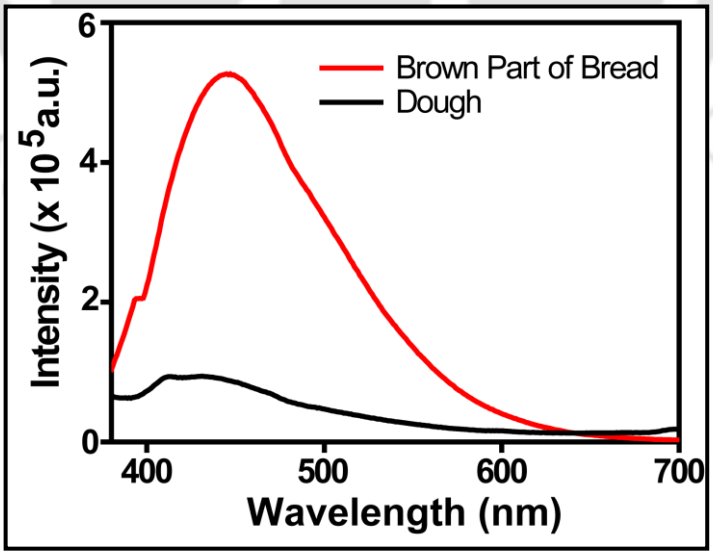

Figure 2.6. Fluorescence spectra of CNPs isolated from the brown part of the bread and the dough used for bread preparation.

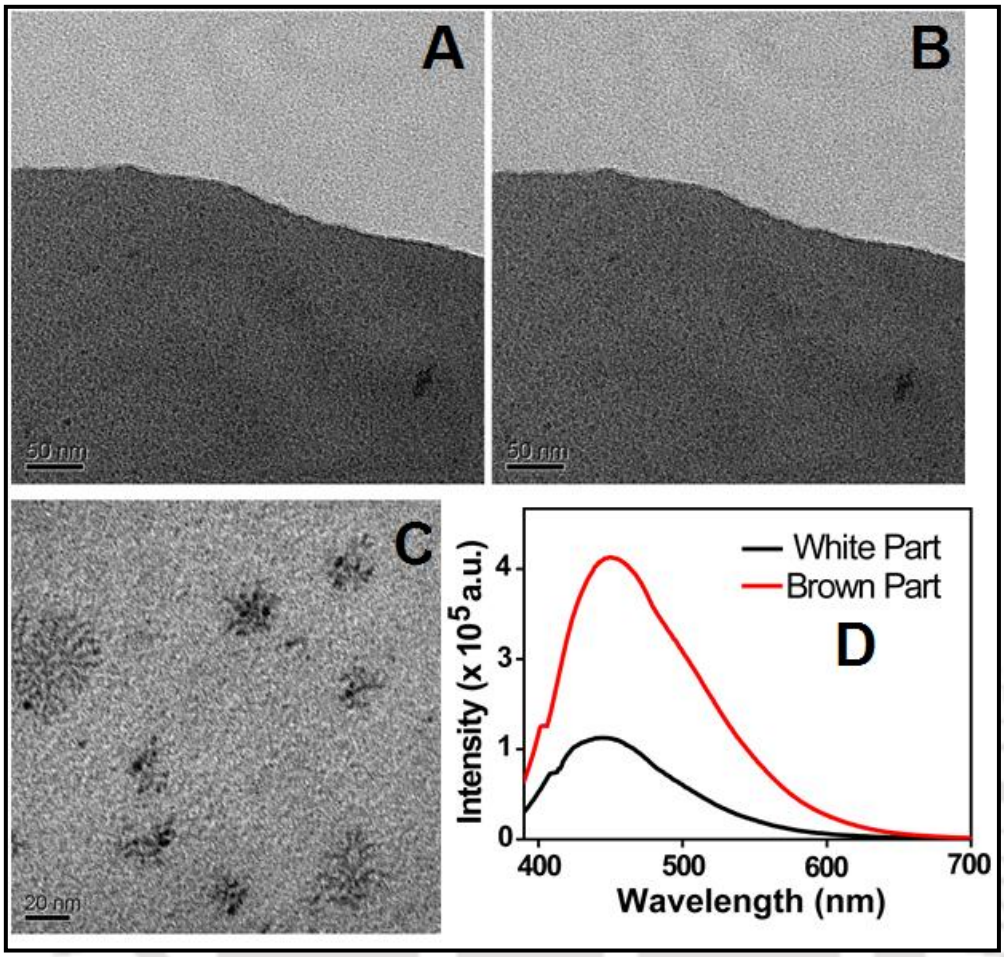

Figure 2.7. Effect of electron beam irradiation on the sample prepared from sugar solution. (**A**) TEM image of sample from sugar solution drop cast on a TEM grid as observed under 200 KV electron beam. (**B**) TEM image of the same portion of the sample observed after 5 min of irradiation of the beam at 200 kV. (**C**) TEM image of the dispersion obtained from the white part of the bread. (**D**) Fluorescence spectra of dispersions obtained from white and brown parts of the bread having identical absorption at the wavelength of 375 nm. The excitation wavelength was set at 375 nm.

The UV-visible and fluorescence spectra of the dispersion of CNPs extracted from different food sources displayed features similar to those of Cdots synthesized chemically and thereby suggesting the presence of CNPs in the samples. The fundamental mechanism of photoluminescence of CNPs is still a major question; however, it is thought that the presence of different surface trap sites could be one of the factors for the luminescence [58, 65]. The origin of fluorescence from the obtained dispersion could only be attributed to the presence of CNPs

because the analysis of the starting material for preparation of bread did not show any significant fluorescence (Figure 2.6). Sugar is known to be a nonfluorescent material, but the caramel prepared upon heating sugar showed the emergence of excitation tuneable luminescence, further confirming the formation of CNPs. Additionally, it was observed that the heating temperature for preparing the caramel had significant effect on the size of NPs formed. Caramels prepared at 180 ^{o}C and 200 ^{o}C had the sizes of 25.8 ± 12.4 and 4.3 ± 1.5 respectively. This indicated that smaller particles were possibly formed at the higher temperature. In other words, the larger particle sizes of NPs obtained from bread and *jaggery* could be due to their low heating temperatures whereas the smaller particles sizes of NPs obtained from sugar caramel, corn flakes and biscuits could be due to higher heating temperatures. It may also be mentioned here that there could be other factors, such as the rate and duration of heating and chemical constituents of the samples, determining the sizes of the produced CNPs. The possibility of the formation of CNPs while preparing and analysing the sample in electron microscopy can be ruled out because when drop cast sample from sugar solution was observed in TEM no such particle formation was detected, even under the exposure of a 200 kV electron beam for several minutes. The images obtained at different time of irradiation, of the sample from sugar solution, in the electron beam of TEM are shown in Figure 2.7 (A & B). It is worth noting that similar extraction process was also used for determining the presence of CNPs, if any, in the interior white part of bread. TEM analysis revealed the presence of inhomogeneous particles (Figure 2.7C) which could be due to the suboptimal temperature in the inner zone. The fluorescence intensity of this dispersion was significantly low compared to that obtained from the brown part of the bread (Figure 2.7D). The sizes of the CNPs produced varied from sample to sample, indicating the possibility of heating temperature as the primary factor determining their sizes. However, it was interesting to observe that for all samples the particles produced were nearly uniform and spherical. To have an idea of the amount of CNPs which can be extracted from a food source, I analysed the amount of particles obtained from 1 g each of *jaggery* and the brown layer of bread. It was observed that about 3 and 2 % w/w of CNPs, in the respective samples were present. The calculation is based on the amount of the starting ingredient taken for the isolation of CNPs and the sample recovered after purification. However, the amount recovered from these materials cannot solely be attributed to CNPs as polymeric layer will always remain surrounding these particles. Isolation of nude CNPs without the polymeric layer has not been possible in the present condition; even then it can give an approximate value about the fraction of particles extracted.

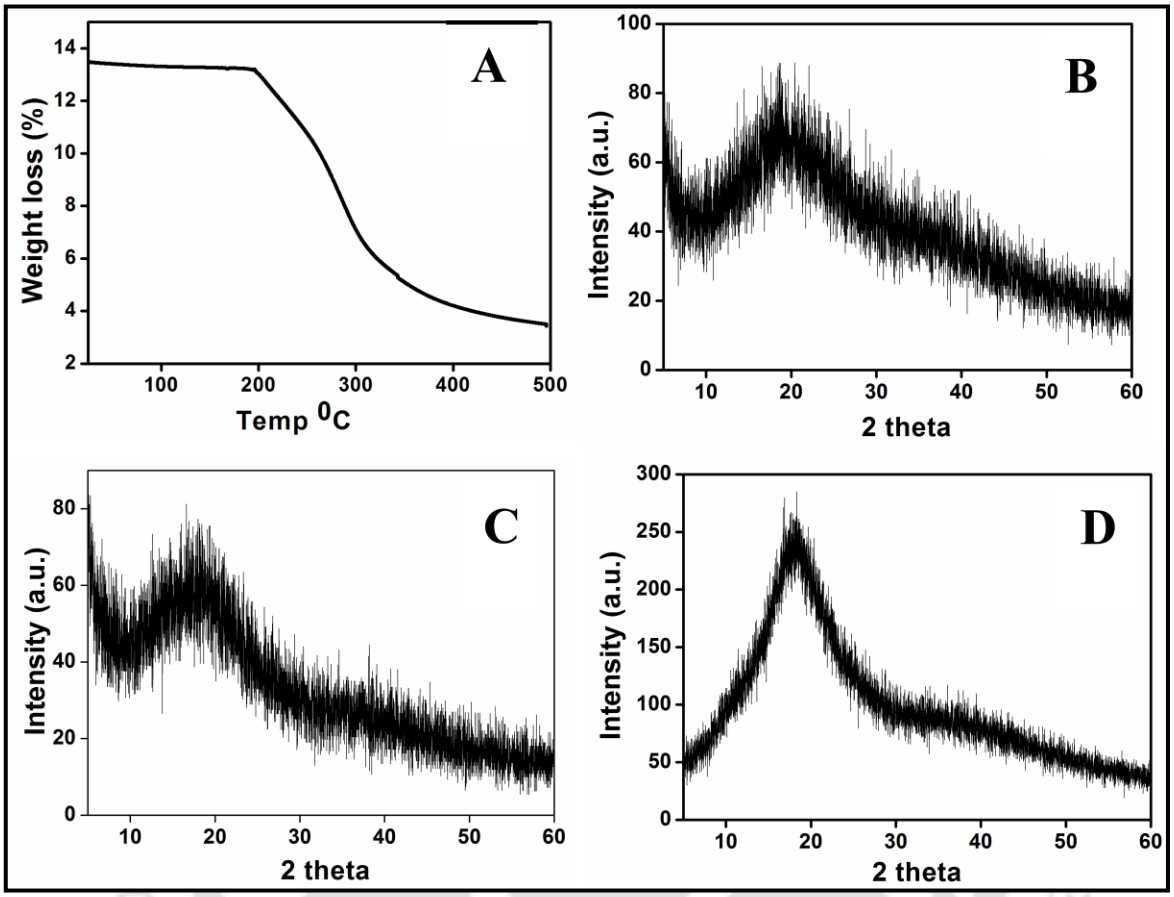

Figure 2.8. (A) Thermogravimetric analysis of sugar. Powder XRD pattern of CNPs extracted from (**B**) bread, (**C**) *jaggery* and (**D**) sugar caramel.

Thermogravimetric analysis of sugar indicated decomposition starting at below 200 ^oC with steady decrease in weight till 350 ^oC (Figure 2.8A). Loss of weight signifies the dehydration process of carbohydrate or formation of CO_2 [126]. Thus the NPs could possibly be produced at a temperature even lower than 200 ^oC. Samples from bread, *jaggery* and sugar showed broad X-ray diffraction (XRD) peak at about $2\theta = 18^o$ (Figure 2.8B-D), with no clear signature for crystalline nature of any of the samples. The above results indicated that NPs present in the caramels of bread, *jaggery*, corn flakes, biscuits and sugar caramel possibly consisted of amorphous carbon.

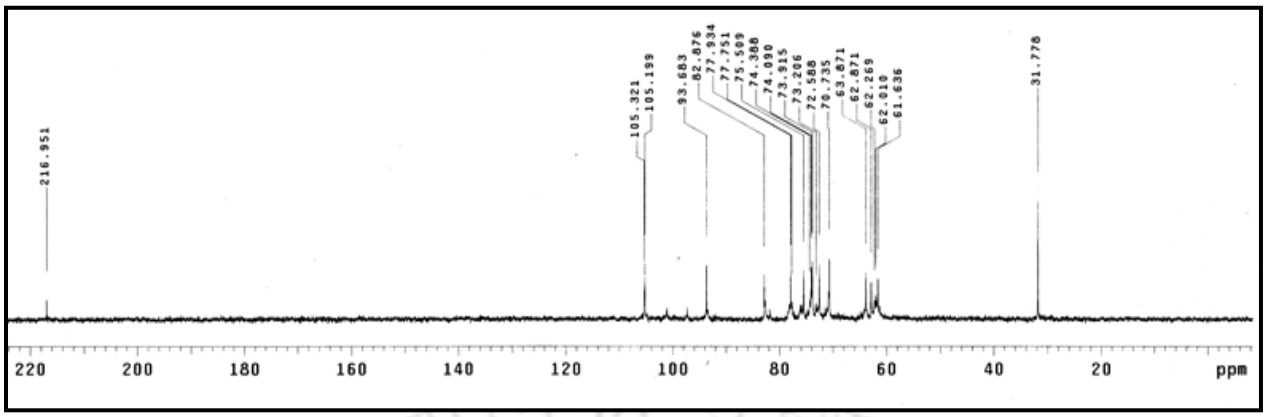

Figure 2.9. ^{13}C NMR spectrum of CNPs extracted from bread

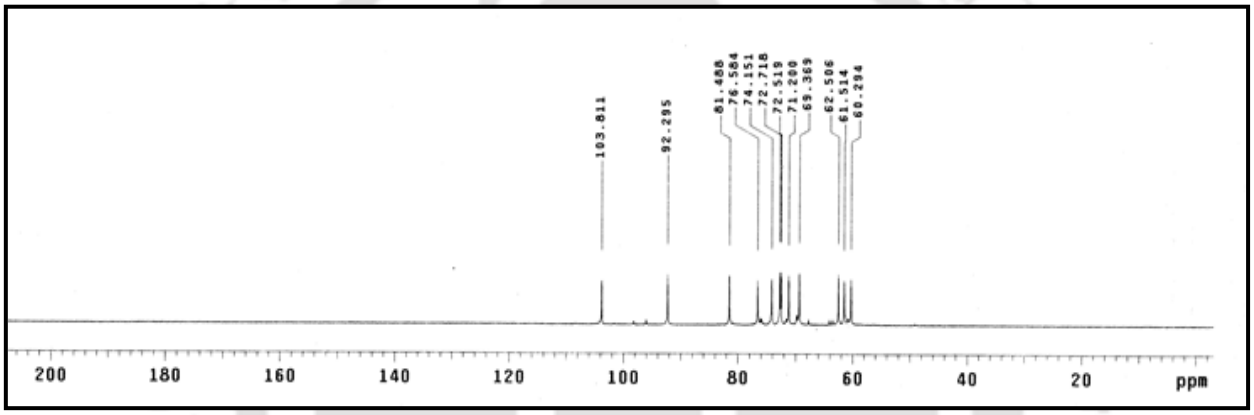

Figure 2.10. ^{13}C NMR spectrum of CNPs extracted from *jaggery*.

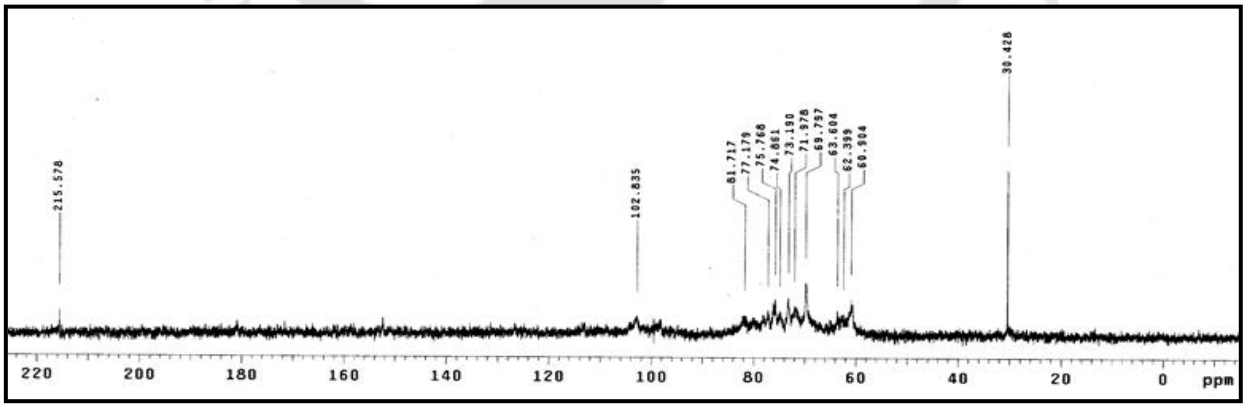

Figure 2.11. ^{13}C NMR spectrum of CNPs from sugar.

Further, ^{13}C NMR (nuclear magnetic resonance) spectra of samples from bread, *jaggery* and sugar (Figures 2.9, 2.10 and 2.11) revealed the presence of peaks between δ = 60 ppm and δ = 105 ppm. The peaks clearly indicated the presence of carbohydrate unit in the extracted CNPs. There were two additional ^{13}C peaks observed in case of CNPs extracted from bread (δ = 216.951 ppm, δ = 31.778ppm) and sugar (δ = 215.578 ppm, δ = 30.428 ppm), depicting the presence of keto (-C=O) and methyl groups in the surface functional moieties. The NMR studies revealed that the CNPs were coated with hydrophilic carbohydrate units. No peaks corresponding to the aromatic region was observed, which again supported the luminescence to be originating from the CNPs present in the dispersion.

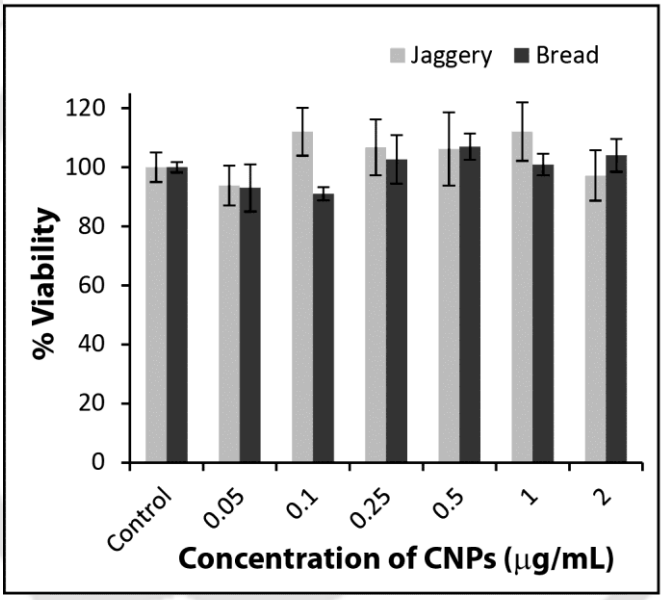

Figure 2.12. Cytotoxicity analysis of the CNPs extracted from *jaggery* and bread (24 h post-treatment) by XTT based cell viability assay. Results are presented as mean ± standard error.

Further, in order to probe the extent of cytotoxicity of the extracted CNPs, we performed XTT based cell viability assay at varying concentrations of CNPs. The plot of percentage viability of cells to that of varying concentration of CNPs (0.05 mg/mL to 2.0 mg/mL) is shown in Figure 2.12. As is clear from the figure, no cytotoxicity was apparent even at the highest concentration of CNPs (2.0 mg/mL) used. In addition, one way ANOVA showed that the difference in the mean percentage viability of cells at different concentration of CNPs extracted from *jaggery* (F= 0.652, P= 0.689) and bread (F = 1.152, P = 0.384) were not statistically significant.

2.4. CONCLUSIONS

In summary, my current work revealed the presence of CNPs in carbohydrate based regular food caramels from bread, *jaggery*, corn flakes and biscuit. The excitation wavelength dependent emission characteristics of the CNPs from food caramels were similar to those generated from sugar; however, the particle sizes varied indicating temperature - dependent formation of CNPs of different sizes. NMR spectroscopy revealed that the CNPs were coated with carbohydrate units. It is interesting to note that for centuries these caramels containing CNPs have been consumed by human beings with no known toxicity and thus it can be considered to have no or minimum risk on human health and may be used as a safe nanomaterial. Our finding of the presence of fluorescent CNPs in food caramels may also help their use in tracking and imaging conjugated biomolecules and drugs *in vivo* without being imperilled.

CHAPTER-3

A Gold-Carbon Nanoparticle Composite as an Efficient Catalyst for Homocoupling Reaction

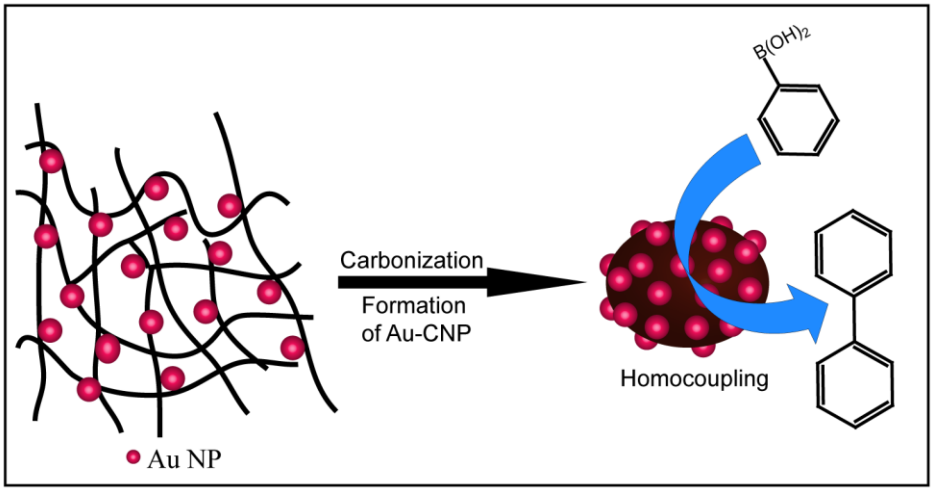

Highlights:

- *Design of CNP-based composite nanomaterial catalyst.*
- *Enhanced reactivity and selectivity in homocoupling reaction of phenylboronic acid and plausible mechanism.*

3.1. INTRODUCTION

Progress in catalytic chemical reactions – the mainstay of chemistry of new molecules or pathways of reactions – depends on development of efficient, environmentally friendly and cost-effective catalysts [127]. Although the tremendous growth that has taken place in this regard for the last one hundred years or so seems to overwhelm any new attempt in this regard, there is still plenty of opportunity for finding new catalysts, relook at old catalysts in a modified form or for developing combination of catalysts in order to have the best of all worlds.

For example, charcoal-supported Pd or Pt metal catalysts have contributed greatly in catalytic organic transformations [127-128]. Recent reports suggest that carbon nanoparticles (CNPs) could provide better option, owing to their stability, sizes, ease of dispersion in liquid medium and facile formation of composites – especially with catalytic metal nanoparticles (NPs) [58, 79, 132]. In addition, CNP supported metal NPs have been used for photocatalysis [132] and surface enhanced Raman spectroscopy (SERS) [130]. Further, porous carbon supported metal NPs have been used extensively for reduction of nitroaromarotics [131-132].

Among the metal NPs, catalytic activity of Au NP, supported on the surfaces of various organic and inorganic substrates, has made Au an alternative choice [133, 138-140]. For example, carbon supported Au NPs have been used for performing reduction and oxidation reactions [134-135]. However, it is also important to develop newer methods for pursuing coupling reactions on supported Au NPs. A case could be the production of biaryls, which are an important class of compounds being present as active moiety in pharmaceutically important molecules, natural products and in advanced functional materials [136-137]. Transition metal catalysed oxidative homocoupling of the arylboronic acid is a major pathway to achieve the homomeric biaryls synthetically [138-146]. In this context, palladium based catalysis has dominated the field [145-146]. However, several other metal catalysts as well as the reaction conditions were varied to minimize the limitation and increase the efficiency of the parent palladium catalysed coupling reaction. In one such case, cationic Au either supported on metal oxides and polysaccharides or complexed with organic ligands is shown to serve as efficient catalyst for self-coupling of arylboronic acid [138, 141, 147]. However, higher loading of 2.25 to 30 mole percent of the catalyst was required for high conversion and selectivity. It has also been

The work contained herein is published in the peer reviewed journal [Sk *et al.* ***Chem. Commun.*** 2013, *49*, 8235.]
Reproduced with permission of The Royal Society of Chemistry.

demonstrated - although only in two instances - that Au NPs are efficient in catalyzing oxidative coupling of aryl boronic acid. For example, PVP-stabilized Au NP catalyzes homocoupling reaction under aerial condition [140]. Even though high conversion of starting material was achieved, poor selectivity towards desired biaryl was observed. On the other hand, Mg-Al mixed oxide supported Au NPs require high pressure of oxygen and higher temperature for higher conversion and better selectivity [139]. Therefore, developing novel catalyst, in order to bridge the gap between ambient reaction conditions and reactivity-selectivity, is desirable so that the application potential of the reaction could be expanded further.

In this chapter I have demonstrated an easy and bio-friendly method of preparation of composite of Au NPs and CNPs, which was used for carrying out facile homocoupling reaction of phenylboronic acid to provide excellent conversion with high selectivity under aerial reaction conditions. In the composite, the size of Au NPs was 4.9±1.4 nm, while that of CNPs varied from 50 nm to 350 nm. In addition, a mechanistic proposal relying on the role of Au NP as the active site is described, which rationalizes the solvent dependent reactivity and selectivity of the reaction.

3.2. EXPERIMENTAL

Materials. Phenylboronic acid, hydrogen tetrachloroaurate ($HAuCl_4$, 17% Au in HCl) were purchased from Sigma-Aldrich. Sodium borohydride (95%) and glacial acetic acid (99-100%) were purchased from Merck. Chitosan was procured from Marine Chemicals, India. All were used as received without further purification. Elix grade water from a MilliQ purification system was used in all the experiments.

Preparation of the Gold-Carbon Nanoparticle (Au-CNP) Composite. First, 100 mg chitosan was taken in a round-bottom (RB) flask and then 20 mL of water was added followed by addition of 100 μL acetic acid. The mixture was stirred until chitosan was dissolved. After that 500 μL of 17.2 mM $HAuCl_4$ was added to the mixture and stirred vigorously for 30 min at below 25 ^oC. Freshly prepared 0.25 M $NaBH_4$ (1 mL) was quickly added at room temperature. Then color of the solution changed from pale yellow to dark red, indicating the formation of gold nanoparticles and stirring was continued for another 30 min.

In second step, freshly prepared chitosan-stabilized Au NP was heated at 200 ^oC so that all the water was evaporated and the mixture became dry. Then it was cooled to room temperature and 10 mL of 0.15 M HCl was added to it. Again, it was heated at 200 ^oC for 2 h and at this point the condenser (of the setup) was removed to evaporate all the water. To ensure the

carbonization process, I waited for a minute and after that quickly removed it from oil bath and cooled it to room temperature following addition of 5 mL of water. This was followed by centrifugation of the above mixture at 5300 rpm and the supernatant was separated. The supernatant was centrifuged at 5300 rpm following addition of acetone (5:1 V/V). The pellet obtained from centrifugation was dried at 40 ^{o}C for 12 h before further use. The gold loading was at 1.95 wt% as measured from ICP analysis.

Preparation of CNP. CNPs were prepared by the same process as the preparation of Au-CNP. Here, 100 mg chitosan was taken in a 100 mL RB flask with 20 mL in it and then 100 µL acetic acid was added to the mixture. It was stirred until chitosan was dissolved. The rest of the procedure was same as the 2nd step of the Au-CNP preparation. It was purified by centrifugation with acetone/water mixture (5:1) and keeping the centrifuged pellet at 40 ^{o}C for 12 h to dry.

Preparation of Au-Chitosan. Chitosan stabilized gold nanoparticle (Au-Chitosan) was prepared by following the first step of the preparation of Au-CNP and the product was purified by centrifugation at 5300 rpm followed by washing with acetone/water mixture (5:1). Then the sample was kept for drying at 40 ^{o}C for 12 h. The Au loading was 1.86 wt% as measured using ICP analysis.

General Procedure for Homocoupling Reaction. The aerobic homocoupling of phenyl boronic acid was carried out in a 10 mL RB flask at 70 ^{o}C. Phenylboronic acid (0.3 mmol, 36.6 mg), K_2CO_3 (0.425 mmol, 58.7 mg), Au-CNP (10 mg) were taken in a RB and then 0.5 mL water and 1 mL toluene were added to the mixture. The mixture was heated at 70 ^{o}C with constant stirring for 7 h, under open flask condition. The progress of the reaction was monitored by TLC. After 7 h, the reaction mixture was extracted by ethyl acetate (3 x 15 mL). The combined organic layer was concentrated and the crude product was purified by column chromatography, using hexane as eluent to obtain biphenyl (19.8 mg, 86%) and phenol (3.4 mg, 12%).

Protocol to make Deoxygenated Condition. The concentration of dissolved oxygen in water was reduced by the freeze - pump – thaw cycles which was performed for three times. Then the reaction was performed under inert atmospheric condition with deoxygenated toluene. The procedure was same as mentioned in the general procedure. The conversion of starting material was 19% and 24% respectively for two different batches of experiments.

Recycling of Catalyst. After completion of reaction, catalyst was recycled by centrifugation, followed by washing with acetone/water mixture in a ratio of 5:1. In all cases, the reaction condition was same as mentioned in the general procedure above.

Analytical Measurements. The Au-CNP composite was characterized using transmission electron microscopy (JEOL 2100 UHR-TEM) operating at 200KV, UV-vis spectroscopy (Hitachi U 2900spectrophotometer), photoluminescence spectroscopy (Horiba Fluoromax-4 spectrofluorometer), powder XRD (Brucker D8 Advanced X-ray diffraction measurement system) with Cu Kα source (λ =1.54 Å), particle size analysis (Malvern zeta size; Nano ZS 90). Raman spectra were recorded by Horiba LabRAM HR800. Also, X-ray photoelectron spectroscopy (XPS) and inductive coupled plasma-optical emission spectrometer (ICP) measurements were performed with PHI 500 Versa Probe II (ULVAC-PHI, INC, Japan) and Thermo-iCAP 6000 Series, respectively.

Quantum Yield Calculation with respect to Quinine sulphate (QS) in 0.1 M H_2SO_4. I have calculated Quantum yield with respect to quinine sulphate using the formula:

$$Q_S = Q_R \times \frac{I_S}{I_R} \times \frac{A_R}{A_S} \times \frac{\eta_S^2}{\eta_R^2}$$

Where, Q_S = quantum yield of sample; Q_R = quantum yield of reference; I_S = area under PL curve of sample; I_R = area under PL curve of reference; A_R = absorbance of the reference; A_S = absorbance of the sample; η_S = refractive index of sample; η_R = refractive index of reference.

Q.Y. of quinine sulphate = 0.54, Refractive Index: water = 1.33

(The concentration of all samples and the reference quinine sulphate were adjusted so that the optical densities of all samples were 0.10 ± 0.03 at the excitation wavelength (350 nm)).

Turn Over Frequency (TOF)

$$TOF = \frac{\text{mmol of product formed}}{\text{mmol of catalyst} \times \text{time(h)}}$$

The result from experiment was as follows. Product = 0.129 mmol, catalyst = 0.000992 mmol and time = 7 h.

3.3. RESULTS & DISCUSSION

Chitosan-stabilized Au NPs were synthesized by reduction of $HAuCl_4$ in the presence of $NaBH_4$ and chitosan at room temperature. This was followed by heating the mixture at 200 ^oC for 2 h which led to formation of a paste. The mixture was heated additionally for 1 min, during which carbonization took place. The final dried powder was black in colour, which could easily be dispersed in water by mild sonication. Photographs of the powder and the dispersion are shown in Figure. 3.1 (A and B). UV-vis spectrum of the dispersion (Figure. 3.1C) consisted of three peaks at 267 nm, 345 nm and at 522 nm. The peak at 267 nm and 345 nm are characteristic of CNPs (imputed to the $\pi-\pi^*$ transition), whereas that at 522 nm is due to Au NPs [58, 79]. On the other hand, as prepared chitosan –Au NP composite exhibited a single peak at 510 nm, indicating the presence of Au NPs only. Further, photoluminescence property of the composite resembled that of carbon dots. For example, as shown in Figure.3.1D. & 3.3B, the excitation-tuneable emission peaks in the range of 325 nm to 500 nm of the composite resembled those of CNPs. However, the quantum yield of luminescence was higher for the composite (0.54%) in comparison to that of the CNPs (0.36%). Transmission electron microscopy (TEM) measurements indicated the presence of distinct particles of average size 4.9 ± 1.4 nm, embedded in larger particles of sizes in the range of 50 nm to 350 nm (Figure. 3.1E, 3.1G, 3.2, 3.4). Also, a large number of Au NPs were embedded in each of the larger particles, as is evident from TEM measurements. That the smaller particles were due to Au was confirmed from selected area electron diffraction (SAED) measurement (Figure. 3.1F). Further, high resolution TEM (HRTEM) measurements indicated the presence of planes owing to lattice spacing of 0.224 nm, which is due to (111) planes of metallic Au. On the other hand, the larger particles could be CNPs. X-ray diffraction (XRD) measurements indicated the presence of four planes of Au, namely, (111), (200), (220) and (311) leading to diffractions at 38.3^o, 44.6^o, 64.8^o, and 77.8^o (JCPDS 4-0783), respectively (Figure.3.1H). A broad peak at 24.8 ^{o} is assigned to amorphous CNPs.

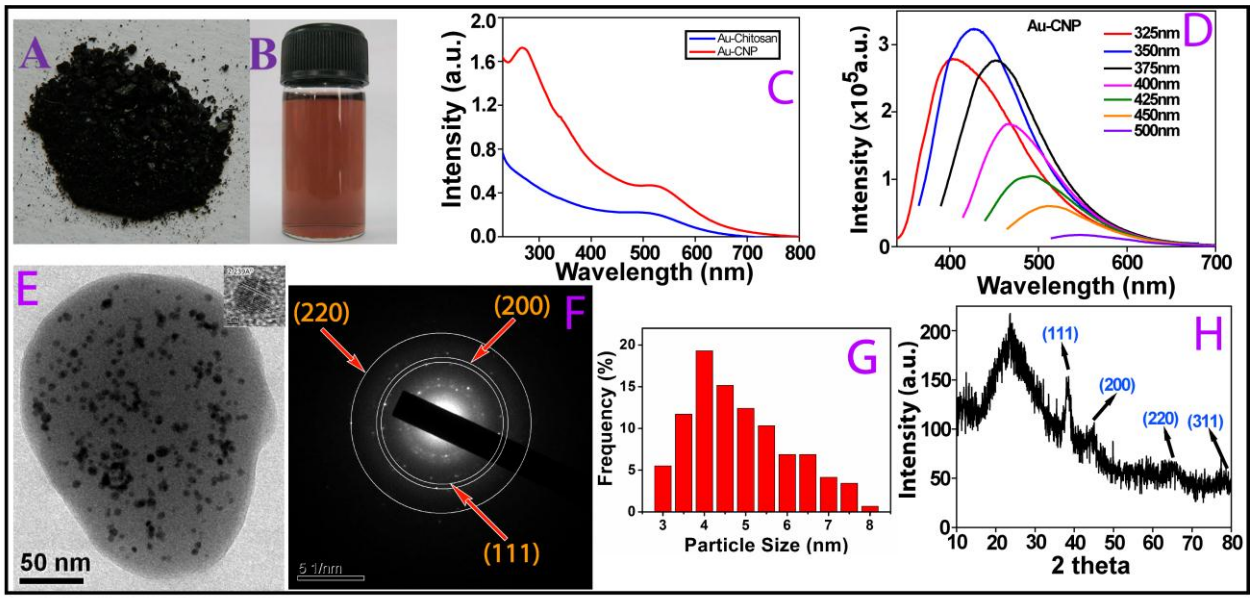

Figure. 3.1. Photographs of **(A)** dry composite and **(B)** that of the composite dispersed in water. **(C)** Absorption spectra of Au-CNP composite and Au NP-chitosan. **(D)** Fluorescence spectra of Au-CNP composite. **(E)** TEM image of Au-CNP composite with HRTEM image in the inset. **(F)** SAED pattern of Au-CNP composite **(G)** Size distribution of Au NP present in the composite as calculated from TEM. **(H)** Powder XRD data of Au-CNP composite images.

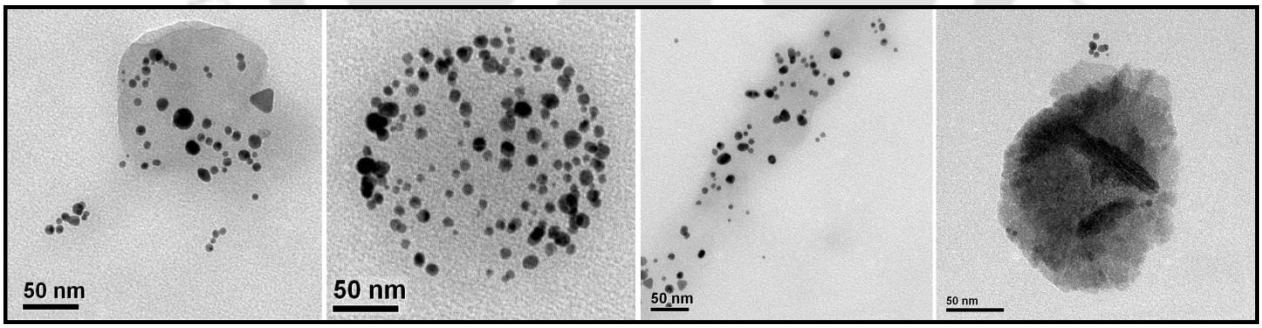

Figure.3.2. Representative additional TEM images of the Au-CNP composite nanoparticles.

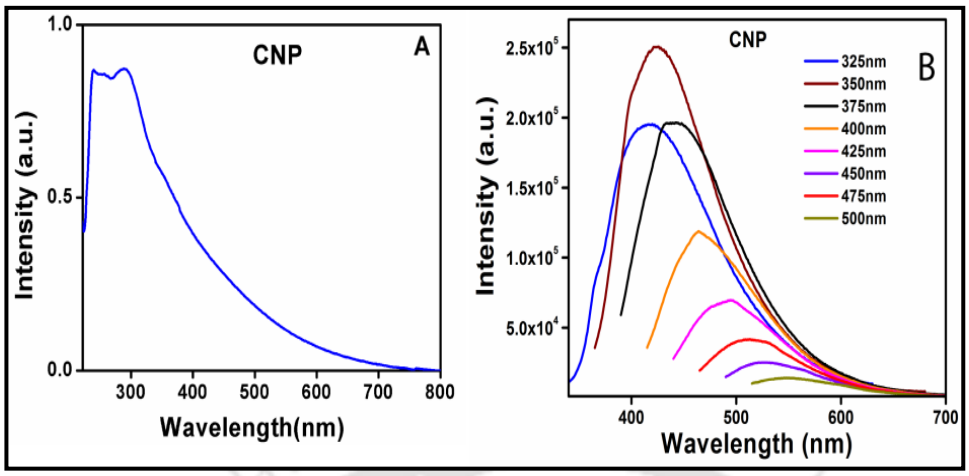

Figure.3.3. (A) Absorption spectrum of CNPs produced following the process of preparation of Au-CNP. **(B)** Fluorescence spectra of CNP.

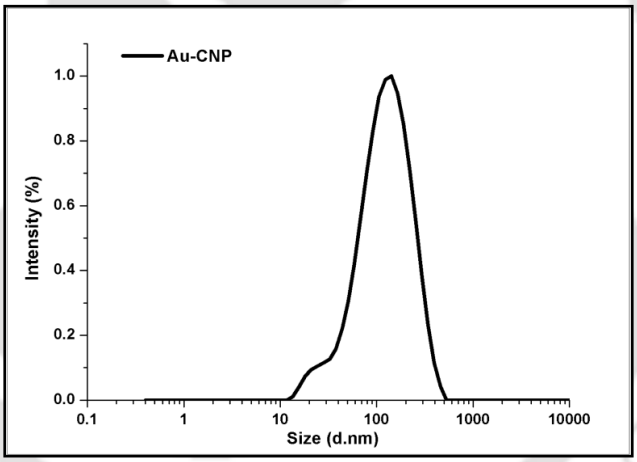

Figure. 3.4. Dynamic light scattering based particle size analysis of Au-CNP composite.

X-ray photoelectron spectroscopy analysis of the composite evidenced the presence of peaks at 84.1 eV and 87.8 eV (Figure. 3.5), where the binding energies correspond to the $4f_{7/2}$ and $4f_{5/2}$ states of metallic gold i.e. Au^{o}. Thus the presence of Au^{+} or Au^{3+} species could be ruled out. Further, analysis of peaks due to carbon species indicated the presence of C-C (284.9 ev), C-OH or C-O-C (286.5 ev) and C=O (287.9 ev) functional groups. On the other hand, inductive coupled plasma (ICP) spectroscopy indicated 1.95% of Au loading in the composite. Additionally, Raman

spectroscopy measurements indicated the presence of broad peaks at 1341 cm^{-1} and 1581 cm^{-1}, corresponding to D and G bands of sp^2 carbon, signifying the formation of CNPs (Figure. 3.6).

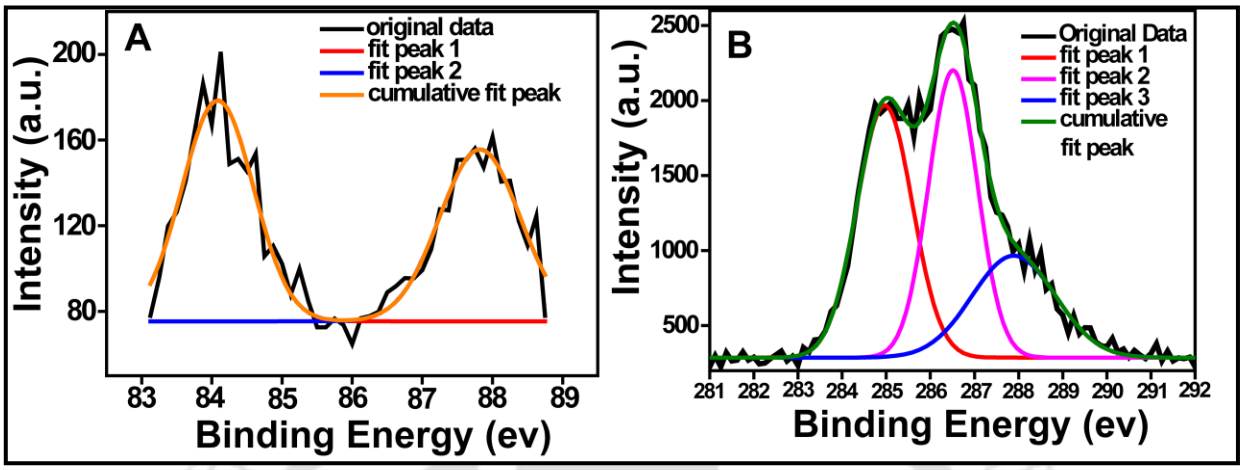

Figure. 3.5. X-ray photoelectron spectra of Au-CNP composite. **(A)** is for Au 4f and **(B)** is for C 1s.

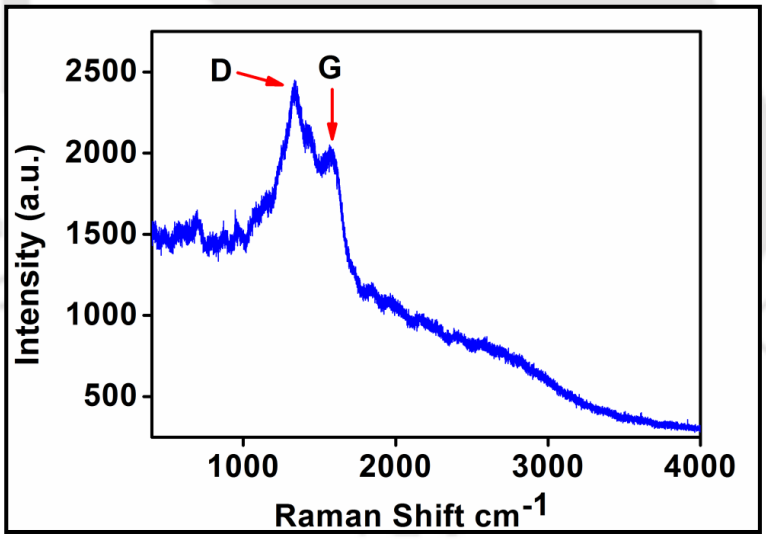

Figure. 3.6. Raman spectrum of the Au-CNP composite.

The above results indicated the formation of smaller Au NPs embedded in the larger amorphous CNPs. Also, the absence of any oxidation states other than Au^0 makes the Au-CNP composite ideal for studying the efficacy of Au NP catalyzed coupling reactions. It may be

mentioned here that the smallness of the sizes of the CNPs (in the composite), as compared to traditional charcoal support makes, the composite an ideal platform for microheterogeneous reactions. It is important to mention here that catalytic reactions in microheterogeneous medium is inherently advantageous over its heterogeneous counterpart, owing to the ease of product diffusion, in addition to availability of large surface area for reactions.

Table 3.1. Au-CNP catalysed homocoupling of phenylboronic acid[a]

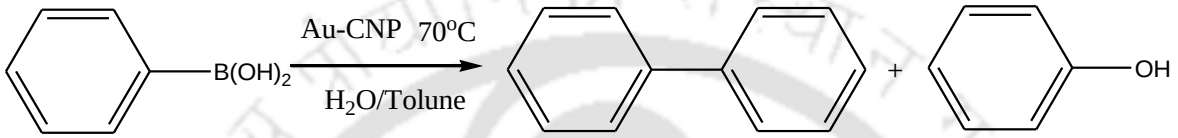

Entry	Solvent	Catalyst	Oxygen	Ph-Ph[b]	Ph-OH[b]	Conversion
1[c]	Toluene/H_2O	Au-CNP	atm.	86%	12%	98%
2	Toluene/H_2O	---------	atm.	--------	--------	--------
3	Toluene/H_2O	Chitosan	atm.	--------	--------	--------
4	Toluene/H_2O	CNP	atm.	--------	--------	--------
5	Toluene	Au-CNP	atm.	--------	--------	--------
6	Toluene	Au-CNP	balloon	--------	--------	--------
7	H_2O	Au-CNP	atm.	68%	18.3%	86.3%
8	Toluene/H_2O	Au-CNP	free	--------	--------	19% (24%)
9	Toluene/H_2O	Au-CNP	balloon	74%	26%	100%

[a]Reaction Condition: 0.3 mmol phenylboronic acid, 1mL toluene, 0.5 mL water, 10 mg catalyst (Au loading 0.66 mol%), 70 °C in open flask and 7h. [b]Isolated yields. [c]Gas-chromatographic analysis showed the yield to be 88% (refer to page no. 51-57). From the GC data, internal response factor (IRF) was found 0.94 and also I calculated amount of biphenyl present in the reaction mixture. I found 20.4 mg biphenyl i.e. 88.4%. I have added 19.8 mg naphthalene as internal standard in the reaction.

Table. 3.2. Additional control experiments

1	MeOH	Au-CNP	atmospheric	--------	--------	--------
2	MeOH/H_2O	Au-CNP	atmospheric	20.3%	4.6%	25%
3	Toluene/H_2O	Au-Chitosan	atmospheric	49.3%	14.5%	64%
4	Toluene/2eq H_2O	Au-CNP	atmospheric	--------	--------	--------
5	Toluene/2eq H_2O	Au-CNP	balloon	--------	--------	--------
6	Toluene/H_2O	Au-CNP	Closed flask	84.8%	10.6%	95.4%

In order to investigate the catalytic activity of the composite, the well-known C-C bond forming homocoupling reaction of phenylboronic acid was pursued. Thus, phenylboronic acid in a binary solvent mixture (2:1 V/V ratio of toluene and water) was allowed to react in the presence of catalytic amount of the composite, under the aerial conditions at 70 ^oC, which was found to be the best reaction temperature (Table 3.3.). A conversion of 98% of the phenylboronic acid in 7 h, in the presence of only 0.66 mol% of the gold leading to the TOF (turn over frequency) of 19 was observed. Biphenyl was isolated with yield of 86%, along with 12% of phenol, a by-product of oxidation of phenylboronic acid, presumably by the H_2O_2 generated in the reaction. Control experiments (Table 3.1.) carried out in absence of catalyst and in the presence of CNP or chitosan did not result in the product formation. Thus Au NPs in the composite played key role in the catalytic conversion of phenylboronic acid to biphenyl. Further, reaction involving chitosan-stabilized Au NPs lacked selectivity and had lower conversion efficiency (Table 3.2, entry 3). Interestingly, when the reaction was carried out in toluene only medium there was no product formation (Table 3.1. entry 5), even when gaseous O_2 was passed through the reaction mixture. On the other hand, in the water (only) medium 86% conversion – although with reduced selectivity – was observed. Interestingly, the extent of conversion was reduced when deaerated water was used instead. Additionally, externally added oxygen facilitated the reaction (Table 3.1. entry 9), where the reaction was completed in 3.5 h with a TOF of 32. However, more amount of phenol was formed reducing the biphenyl to phenol selectivity to ~3:1 from 7:1 (Table 3.1. entry 1).

Table 3.3. Temperature-dependent experiments

Entry	Solvent	Catalyst	Temperature	Ph-Ph	Ph-OH	Conversion
1	Toluene/H_2O	Au-CNP	RT (35 °C)	--------	--------	11%
2	Toluene/H_2O	Au-CNP	50 °C	14%	24%	38%
3*	Toluene/H_2O	Au-CNP	100 °C	54%	14%	68%

* I observed removal of water (co-solvent necessary for the reaction) via evaporation. After 2.5h, 0.5 mL water was added further into the reaction mixture. The reaction was stopped after 6.5h.

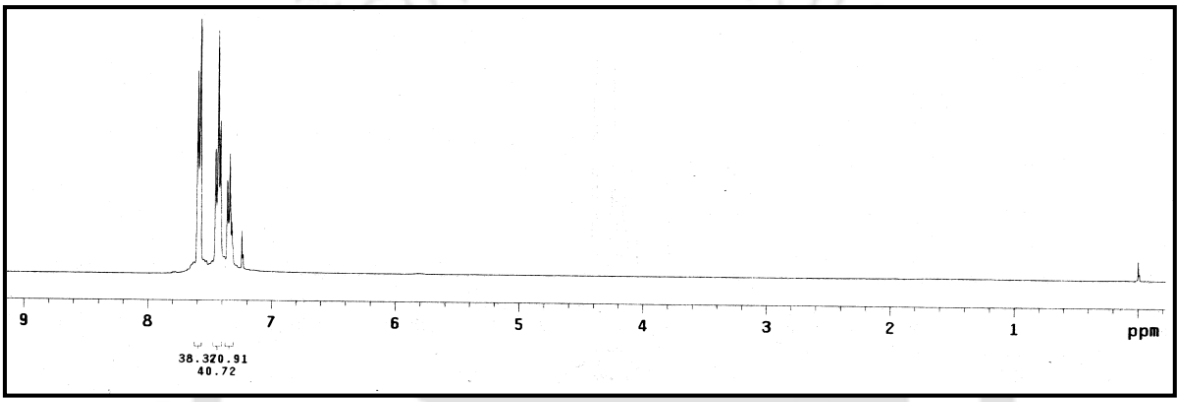

Figure.3.7. ^{1}H NMR of isolated product.

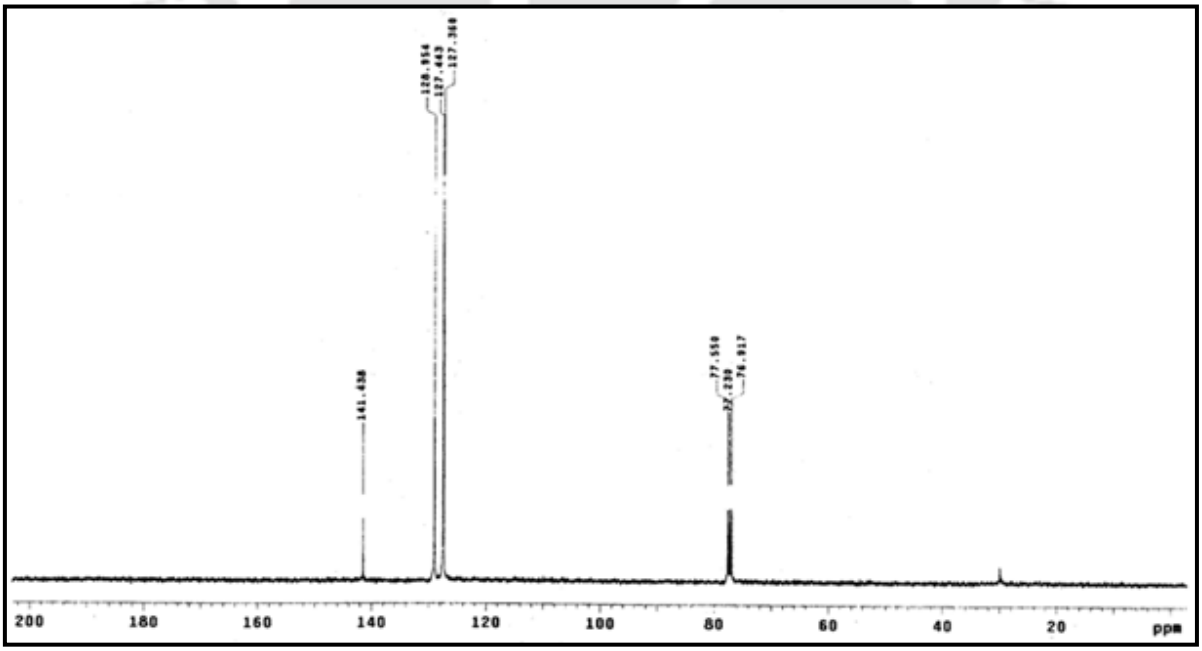

Figure.3.8. ^{13}C NMR of isolated product.

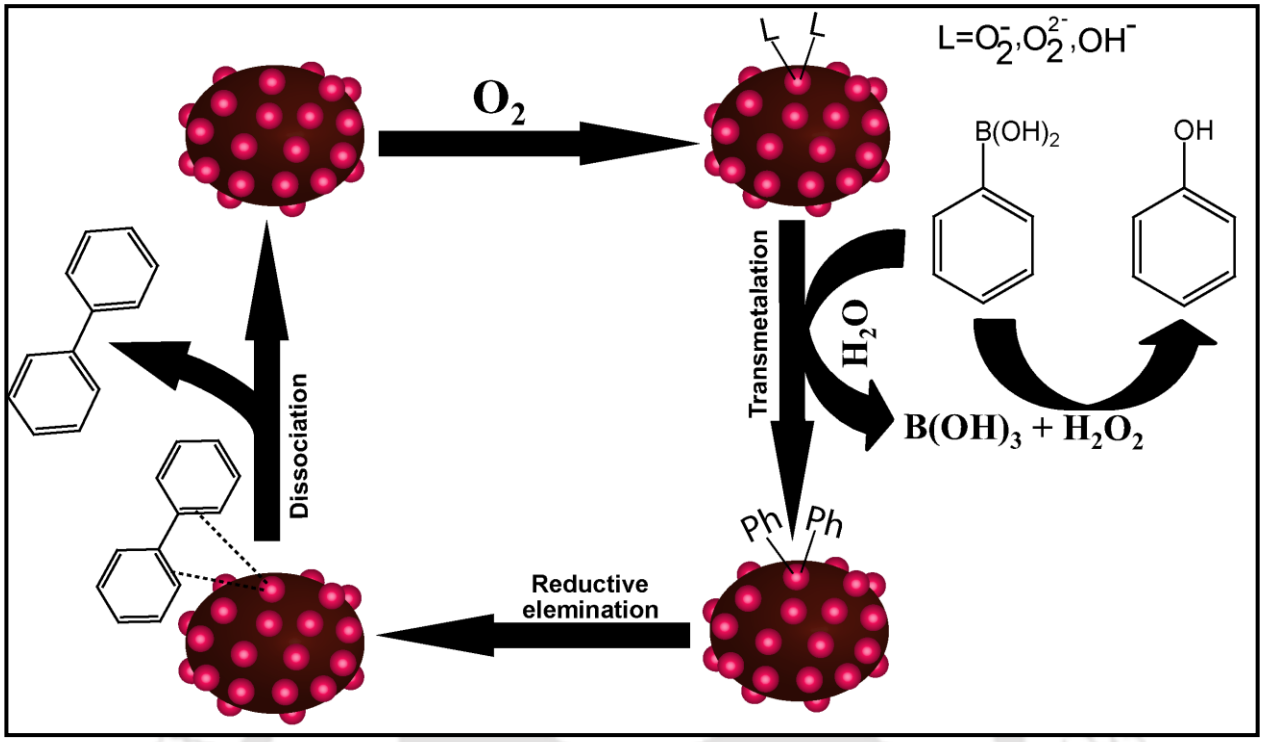

Scheme 3.1. Proposed mechanism of aerobic homocoupling reaction of phenylboronic acid catalyzed by Au-CNP composite.

Based on these experimental findings and the literature reports, a plausible mechanism of Au-CNP catalyzed homocoupling reaction is depicted in scheme 3.1 [138-140, 147]. The surface of the Au-NP is oxidized, by dissolved molecular oxygen [139-140, 148-150], to positively charged species being associated with oxygenated ligands (e.g. O_2^{2-}, O_2^- or OH^-), in the first step of the catalytic cycle. The electron rich nature of CNP probably facilitates the aerial oxidation of Au NP, which is reflected in the enhanced catalytic activity of Au-CNP compared to Au-chitosan [151-152]. The base-mediated activation of phenylboronic acid occurred, prior to the double transmetallation on the charged Au surface. However, the ligand (coordinated to Au) induced transmetallation could also be possible. In parallel, H_2O_2 generated in situ from reduced oxygen (super oxide and/or peroxide) could have oxidized phenylboronic acid to phenol [149]. Finally, the reductive elimination with consequent product dissociation provided desired biphenyl, returning the Au-nanoparticle in to the catalytic cycle for the next turn over.

The increase in the percentage of the phenol in the reaction in only water compared to that in toluene-water mixture can be rationalized with the help of proposed mechanism, by considering the comparative rate of transmetallation and oxidation of starting material. In

contrast to the reaction in water, for the case of toluene-water mixture, biphenyl being hydrophobic diffuses immediately after its formation to toluene and thus the catalytic sites become ready for another cycle. However, due to higher amount of dissolved O_2 in only water or in toluene-water medium with externally added oxygen, the formation of higher amount of oxidizing species may lead to the larger amount of phenol formation. In contrast to the mechanism proposed by Carrettin *et al.* using Au-CeO_2 [138], our mechanistic proposal relies on the positively charged Au NP as the active catalyst for the homocoupling reaction of phenylboronic acid. Furthermore, solvent dependent reactivity and the selectivity observed experimentally are in accordance with the proposed mechanism.

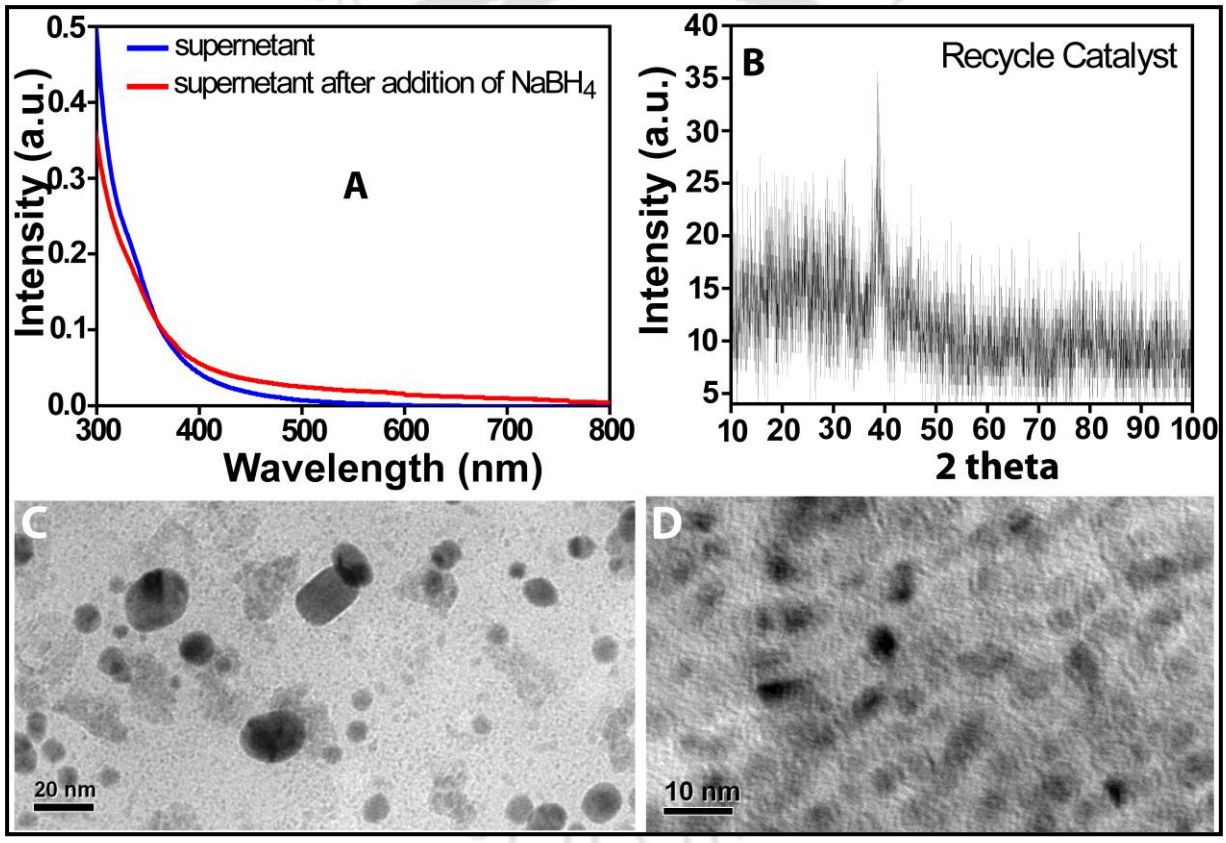

Figure.3.9. (A) Absorption spectra of supernatant of the reaction mixture collected following isolation of the product. **(B)** Powder XRD pattern of the recycled catalyst (after first recycled). **(C, D)** TEM images of recycled Au-CNP catalyst (of two different recycled samples). (**C**) The sample was prepared following completion of the first cycle of reaction; (**D**) the sample was from the completion of the second cycle.

The stability and the ability to recycle the catalyst were also investigated. Firstly, the supernatant of the reaction mixture showed no significant absorbance above 300 nm (Figure. 3.9A.), thus excluding the presence of ionic Au species in the medium and at the same time indicating the stability of the NPs. Moreover, TEM and XRD studies of the recovered catalyst indicated the stability of the Au NPs in terms of their shape and size (Figure. 3.9). Accordingly, the catalyst was successfully recycled twice without compromising the conversion (98%) of the starting material as well as the yield (89%) of the desired product.

Table 3.4. Performance of Recycled Catalyst

Time	%yields	Conversion (%)
1st	89	99.5
2nd	89	99

3.4. CONCLUSIONS

In summary, I have developed a simple method to synthesize Au-CNP composite, which was used for homocoupling reaction of phenylboronic acid. Importantly, selectivity of the reaction in the presence of H_2O and dissolved oxygen indicated the exceptional role played by Au NPs being supported on CNP. That the catalyst was stable and could be recycled is important for its practical application. This reaction may open new doors of metal-CNP composite towards coupling reaction and production of fine chemicals and pharmaceuticals of industrial importance.

Gas-Chromatographic Analysis

a) GC of pure Biphenyl

Qualitative/Quantitative Report

File: C:\TURBOMASS\OFN.PRO\Data\BP.raw
Acquired: 05-Jul-13 06:22:30 PM Printed: 06-Jul-13 11:08 AM
Description: GBPIC
GC/MS Method: GC: RAMP 10 METAHNOL.mth MS: RAMP10 METHANOL.EXP Page 1 of 2
Sample ID: GCMS-0355-MeOH-APL Vial Number: 2

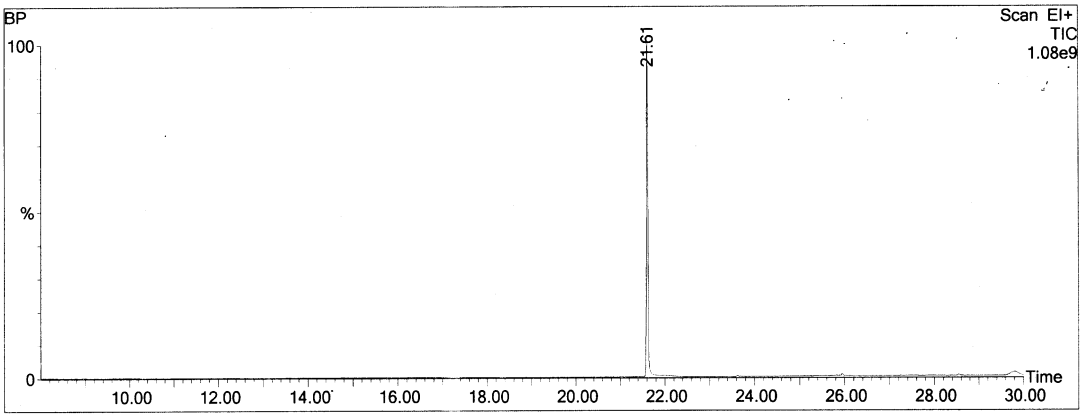

#	RT	Scan	Height	Area	Area %	Norm %	Name	
1	8.949	190	2,150,250	67,410.7	0.125	0.16		
2	9.854	371	625,540	44,032.1	0.082	0.10		
3	14.006	1201	619,916	48,760.2	0.091	0.12		
4	14.741	1348	873,098	47,434.8	0.088	0.11		
5	14.781	1356	1,244,000	55,140.6	0.102	0.13		
6	15.762	1552	813,776	40,939.8	0.076	0.10		
7	16.247	1649	1,190,831	81,260.0	0.151	0.19		
8	16.332	1666	1,436,381	87,517.7	0.162	0.21		
9	16.432	1686	1,197,350	47,817.0	0.089	0.11		
10	16.622	1724	1,064,588	58,029.8	0.108	0.14		
11	16.737	1747	1,226,305	82,042.2	0.152	0.19		
12	16.837	1767	1,094,482	42,921.9	0.080	0.10		
13	21.039	2607	1,495,648	48,317.2	0.090	0.11		
14	21.384	2676	1,129,492	52,639.4	0.098	0.12		
15	21.439	2687	1,104,545	90,786.5	0.169	0.21		
16	21.614	2722	1,076,733,440	42,262,072.0	78.453	100.00		
17	21.959	2791	5,826,133	1,692,026.2	3.141	4.00		
18	23.620	3123	3,621,632	151,488.8	0.281	0.36		
19	23.685	3136	1,501,677	44,189.4	0.082	0.10		
20	23.740	3147	1,135,920	50,930.7	0.095	0.12		
21	24.665	3332	1,040,209	44,959.2	0.083	0.11		
22	24.710	3341	995,932	58,055.6	0.108	0.14		

Inst() ACQUISITION
Oven: Initial temp 50°C for 2 min, ramp 10°C/min to 280°C, hold 5 min, InjAauto=290°C, Volume=1 µL, Split=50:1, Carrier Gas=He, Solvent Delay=8.00 min, Transfer Temp=200°C, Source Temp=180°C, Scan: 50 to 600Da, Column 60.0m x 250µm

b) GC of pure Phenol

Qualitative/Quantitative Report

File: C:\TURBOMASS\OFN.PRO\Data\PHoh.raw
Acquired: 05-Jul-13 06:56:45 PM
Description: GBPIC
GC/MS Method: GC: RAMP 10 METAHNOL.mth MS: RAMP10 METHANOL.EXP
Sample ID: GCMS-0356-MeOH-APL

Printed: 06-Jul-13 11:08 AM
Page 1 of 2
Vial Number: 3

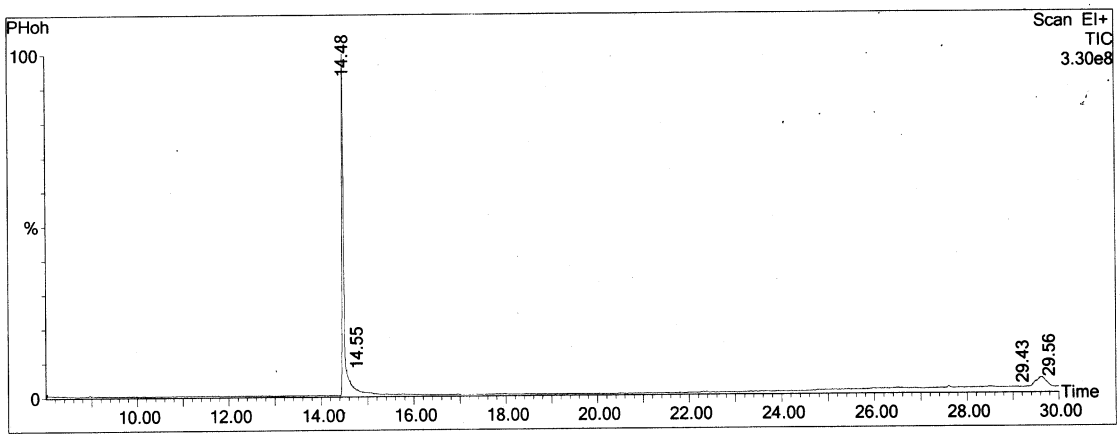

#	RT	Scan	Height	Area	Area %	Norm %	Name	
1	8.959	192	1,612,792	75,871.1	0.253	0.48		
2	11.630	726	912,914	48,668.2	0.162	0.30		
3	14.481	1296	328,981,632	15,965,426.0	53.229	100.00		
4	14.906	1381	3,453,720	355,920.3	1.187	2.23		
5	15.046	1409	2,864,162	99,778.9	0.333	0.62		
6	15.076	1415	2,845,654	364,637.0	1.216	2.28		
7	15.396	1479	1,376,706	50,756.9	0.169	0.32		
8	15.421	1484	1,231,610	56,213.0	0.187	0.35		
9	15.496	1499	1,022,989	62,669.3	0.209	0.39		
10	15.737	1547	1,248,302	85,963.1	0.287	0.54		
11	15.857	1571	947,092	52,607.8	0.175	0.33		
12	15.912	1582	918,519	63,365.3	0.211	0.40		
13	17.972	1994	849,631	69,939.2	0.233	0.44		
14	22.309	2861	1,460,278	70,107.0	0.234	0.44		
15	22.379	2875	1,227,275	78,819.1	0.263	0.49		
16	23.570	3113	1,022,833	59,783.2	0.199	0.37		
17	23.645	3128	1,063,529	48,489.4	0.162	0.30		
18	24.775	3354	1,444,880	70,167.7	0.234	0.44		
19	24.815	3362	1,463,069	59,439.9	0.198	0.37		
20	24.940	3387	1,451,284	101,937.8	0.340	0.64		
21	25.045	3408	1,410,054	81,087.3	0.270	0.51		
22	25.130	3425	1,403,078	115,087.9	0.384	0.72		

Inst() ACQUISITION
Oven: Initial temp 50°C for 2 min, ramp 10°C/min to 280°C, hold 5 min, InjAauto=290°C, Volume=1 µL, Split=50:1, Carrier Gas=He, Solvent Delay=8.00 min, Transfer Temp=200°C, Source Temp=180°C, Scan: 50 to 600Da, Column 60.0m x 250µm

c) GC of pure Naphthalene (Internal Standard)

Qualitative/Quantitative Report

File: C:\TURBOMASS\OFN.PRO\Data\NP.raw
Acquired: 05-Jul-13 05:33:59 PM
Description: GBPIC
GC/MS Method: GC: RAMP 10 METAHNOL.mth MS: RAMP10 METHANOL.EXP
Sample ID: GCMS-0353-MeOH-APL

Printed: 06-Jul-13 11:06 AM
Page 1 of 2
Vial Number: 1

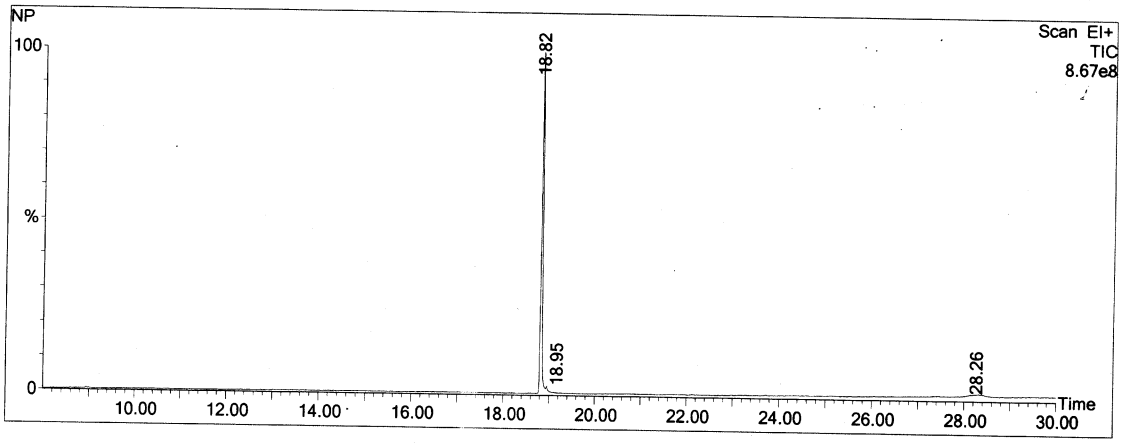

#	RT	Scan	Height	Area	Area %	Norm %	Name	
1	8.944	189	3,282,364	131,405.9	0.232	0.39		
2	10.259	452	1,331,204	83,138.0	0.147	0.25		
3	10.379	476	1,388,476	85,572.1	0.151	0.25		
4	10.664	533	1,415,016	77,868.2	0.137	0.23		
5	12.325	865	1,295,374	88,123.0	0.156	0.26		
6	12.995	999	1,447,451	85,629.6	0.151	0.26		
7	13.260	1052	1,984,392	110,347.6	0.195	0.33		
8	13.436	1087	1,868,089	202,267.1	0.357	0.60		
9	13.546	1109	1,851,910	114,201.4	0.202	0.34		
10	13.691	1138	1,787,582	148,476.1	0.262	0.44		
11	14.226	1245	1,385,752	129,567.1	0.229	0.39		
12	14.586	1317	1,393,417	77,040.9	0.136	0.23		
13	14.801	1360	1,611,823	103,431.1	0.183	0.31		
14	15.031	1406	1,492,629	87,618.9	0.155	0.26		
15	15.316	1463	1,649,913	88,861.8	0.157	0.26		
16	15.962	1592	1,561,350	79,205.2	0.140	0.24		
17	16.287	1657	1,941,880	193,185.0	0.341	0.58		
18	16.492	1698	1,625,465	102,442.5	0.181	0.31		
19	16.692	1738	2,182,852	120,954.0	0.213	0.36		
20	16.777	1755	1,926,358	111,017.3	0.196	0.33		
21	17.037	1807	2,123,106	197,787.5	0.349	0.59		
22	17.132	1826	2,339,996	149,298.8	0.263	0.44		

Inst() ACQUISITION
Oven: Initial temp 50°C for 2 min, ramp 10°C/min to 280°C, hold 5 min, InjAauto=290°C, Volume=1 µL, Split=50:1, Carrier Gas=He, Solvent Delay=2.00 min, Transfer Temp=200°C, Source Temp=180°C, Scan: 50 to 600Da, Column 60.0m x 250µm

Qualitative/Quantitative Report

File: C:\TURBOMASS\OFN.PRO\Data\NP.raw
Acquired: 05-Jul-13 05:33:59 PM
Description: GBPIC
GC/MS Method: GC: RAMP 10 METAHNOL.mth MS: RAMP10 METHANOL.EXP
Sample ID: GCMS-0353-MeOH-APL

Printed: 06-Jul-13 11:06 AM
Page 2 of 2
Vial Number: 1

#	RT	Scan	Height	Area	Area %	Norm %	Name	
23	17.357	1871	1,988,865	74,903.3	0.132	0.22		
24	17.777	1955	1,561,179	96,165.8	0.170	0.29		
25	18.823	2164	863,561,728	33,578,664.0	59.261	100.00		
26	18.948	2189	16,306,575	1,144,395.9	2.020	3.41		
27	19.088	2217	3,286,100	352,718.0	0.622	1.05		
28	20.233	2446	1,582,686	121,052.9	0.214	0.36		
29	20.703	2540	1,947,480	75,164.7	0.133	0.22		
30	20.764	2552	1,828,210	107,767.6	0.190	0.32		
31	21.144	2628	1,695,966	78,197.6	0.138	0.23		
32	21.604	2720	1,734,812	101,224.5	0.179	0.30		
33	21.889	2777	2,091,191	111,688.9	0.197	0.33		
34	21.979	2795	1,852,552	88,872.0	0.157	0.26		
35	22.139	2827	1,844,442	119,135.6	0.210	0.35		
36	22.284	2856	1,599,120	81,614.6	0.144	0.24		
37	22.969	2993	1,442,264	86,609.2	0.153	0.26		
38	23.730	3145	2,259,611	117,106.6	0.207	0.35		
39	25.130	3425	1,773,386	123,087.1	0.217	0.37		
40	25.525	3504	1,809,522	86,305.4	0.152	0.26		
41	27.086	3816	1,603,168	95,973.4	0.169	0.29		
42	27.326	3864	2,991,741	95,853.8	0.169	0.29		
43	27.376	3874	2,562,157	75,663.7	0.134	0.23		
44	27.416	3882	3,024,851	137,024.9	0.242	0.41		
45	27.461	3891	3,162,228	90,663.3	0.160	0.27		
46	27.551	3909	2,037,596	79,579.1	0.140	0.24		
47	27.771	3953	1,806,066	142,558.2	0.252	0.42		
48	27.861	3971	2,744,068	110,520.1	0.195	0.33		
49	28.272	4053	7,652,229	3,012,434.8	5.316	8.97		
50	28.617	4122	1,988,032	92,666.7	0.164	0.28		

Inst() ACQUISITION
Oven: Initial temp 50°C for 2 min, ramp 10°C/min to 280°C, hold 5 min, InjAauto=290°C, Volume=1 µL, Split=50:1, Carrier Gas=He, Solvent Delay=2.00 min, Transfer Temp=200°C, Source Temp=180°C, Scan: 50 to 600Da, Column 60.0m x 250µm

d) GC of 1:1 mixture of Biphenyl and Naphthalene

Qualitative/Quantitative Report

File: C:\TURBOMASS\OFN.PRO\Data\BNP.raw
Acquired: 05-Jul-13 07:30:59 PM Printed: 06-Jul-13 11:08 AM
Description: GBPIC
GC/MS Method: GC: RAMP 10 METAHNOL.mth MS: RAMP10 METHANOL.EXP Page 1 of 2
Sample ID: GCMS-0357-MeOH-APL Vial Number: 4

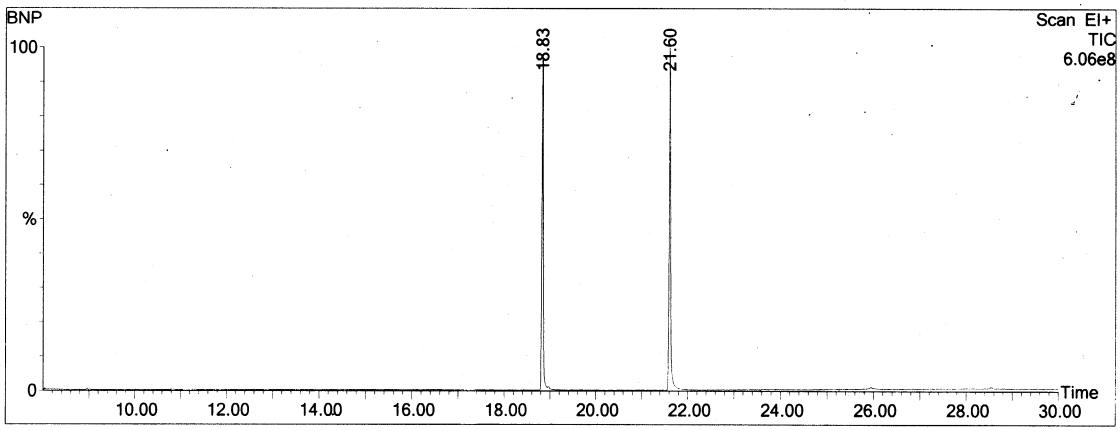

#	RT	Scan	Height	Area	Area %	Norm %	Name	
1	8.959	192	2,074,527	65,956.2	0.121	0.28		
2	9.014	203	1,111,343	36,188.6	0.066	0.15		
3	10.805	561	699,364	33,464.6	0.061	0.14		
4	10.850	570	636,025	38,016.6	0.070	0.16		
5	11.120	624	799,560	36,720.2	0.067	0.16		
6	14.771	1354	696,082	33,891.2	0.062	0.14		
7	15.122	1424	746,510	39,872.8	0.073	0.17		
8	15.472	1494	667,800	38,647.4	0.071	0.16		
9	16.542	1708	813,366	41,891.9	0.077	0.18		
10	18.828	2165	584,523,264	22,135,654.0	40.518	94.37		
11	18.963	2192	7,017,682	493,279.0	0.903	2.10		
12	19.148	2229	666,632	34,978.0	0.064	0.15		
13	20.909	2581	699,414	33,397.7	0.061	0.14		
14	21.039	2607	952,033	44,249.2	0.081	0.19		
15	21.604	2720	605,363,584	23,456,716.0	42.936	100.00		
16	21.914	2782	1,527,879	52,968.6	0.097	0.23		
17	21.989	2797	1,028,576	41,430.6	0.076	0.18		
18	22.085	2816	688,347	37,317.6	0.068	0.16		
19	23.210	3041	828,050	35,417.8	0.065	0.15		
20	23.630	3125	1,956,983	131,663.7	0.241	0.56		
21	23.785	3156	962,191	45,584.9	0.083	0.19		
22	23.855	3170	1,042,600	51,462.2	0.094	0.22		

Inst() ACQUISITION
Oven: Initial temp 50°C for 2 min, ramp 10°C/min to 280°C, hold 5 min, InjAauto=290°C, Volume=1 µL, Split=50:1, Carrier Gas=He, Solvent Delay=8.00 min, Transfer Temp=200°C, Source Temp=180°C, Scan: 50 to 600Da, Column 60.0m x 250µm

e) GC of Reaction Mixture

Qualitative/Quantitative Report

File: C:\TURBOMASS\OFN.PRO\Data\RXN-1.raw
Acquired: 05-Jul-13 08:39:21 PM Printed: 06-Jul-13 11:09 AM
Description: GBPIC
GC/MS Method: GC: RAMP 10 METAHNOL.mth MS: RAMP10 METHANOL.EXP
Sample ID: GCMS-0359-MeOH-APL Vial Number: 6

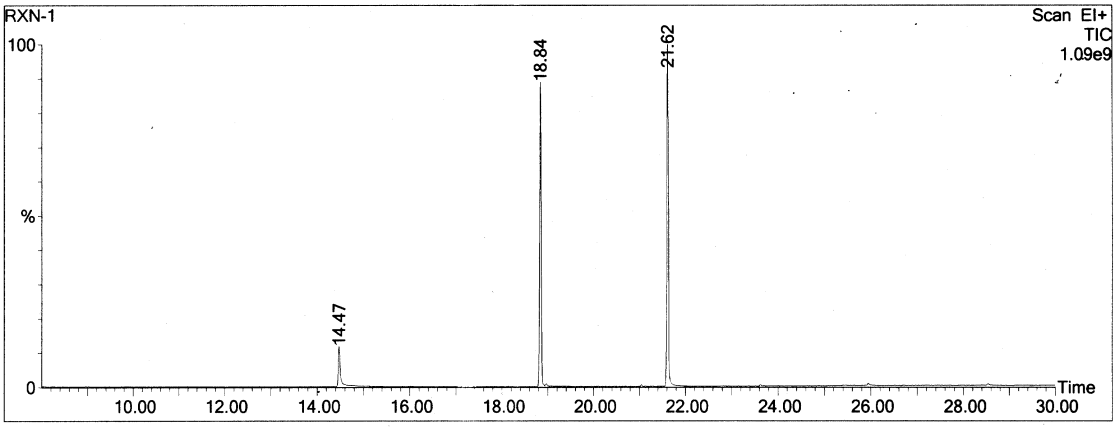

#	RT	Scan	Height	Area	Area %	Norm %	Name	
1	8.959	192	1,779,218	62,193.5	0.064	0.15		
2	9.014	203	954,004	47,707.0	0.049	0.12		
3	14.471	1294	127,828,688	7,424,364.5	7.608	18.01		
4	14.891	1378	2,590,840	67,258.8	0.069	0.16		
5	14.921	1384	1,927,404	57,874.9	0.059	0.14		
6	14.961	1392	1,768,154	91,769.8	0.094	0.22		
7	15.036	1407	1,620,464	48,638.2	0.050	0.12		
8	15.066	1413	1,580,716	48,218.6	0.049	0.12		
9	15.091	1418	1,605,584	73,684.9	0.076	0.18		
10	15.141	1428	1,078,758	43,115.1	0.044	0.10		
11	15.201	1440	1,238,295	54,169.9	0.056	0.13		
12	15.286	1457	1,051,482	47,280.3	0.048	0.11		
13	15.326	1465	917,108	47,797.7	0.049	0.12		
14	15.977	1595	942,965	45,582.6	0.047	0.11		
15	16.512	1702	973,785	42,871.8	0.044	0.10		
16	18.112	2022	1,459,168	51,941.6	0.053	0.13		
17	18.843	2168	968,315,136	37,540,484.0	38.470	91.05		
18	18.968	2193	9,252,244	441,920.6	0.453	1.07		
19	19.078	2215	1,603,049	113,546.2	0.116	0.28		
20	19.323	2264	1,285,585	45,511.4	0.047	0.11		
21	19.453	2290	1,127,537	43,259.7	0.044	0.10		
22	21.049	2609	5,281,171	155,725.3	0.160	0.38		

Inst() ACQUISITION
Oven: Initial temp 50°C for 2 min, ramp 10°C/min to 280°C, hold 5 min, InjAauto=290°C, Volume=1 µL, Split=50:1, Carrier Gas=He, Solvent Delay=8.00 min, Transfer Temp=200°C, Source Temp=180°C, Scan: 50 to 600Da, Column 60.0m x 250µm

Qualitative/Quantitative Report

File: C:\TURBOMASS\OFN.PRO\Data\RXN-1.raw
Acquired: 05-Jul-13 08:39:21 PM Printed: 06-Jul-13 11:09 AM
Description: GBPIC
GC/MS Method: GC: RAMP 10 METAHNOL.mth MS: RAMP10 METHANOL.EXP
Sample ID: GCMS-0359-MeOH-APL Vial Number: 6

#	RT	Scan	Height	Area	Area %	Norm %	Name	
23	21.619	2723	1,087,373,824	41,231,036.0	42.252	100.00		
24	21.974	2794	1,220,029	64,314.5	0.066	0.16		
25	23.620	3123	5,124,658	201,344.3	0.206	0.49		
26	23.705	3140	1,280,878	56,538.7	0.058	0.14		
27	24.450	3289	805,167	51,006.9	0.052	0.12		
28	25.240	3447	985,181	43,599.2	0.045	0.11		
29	25.405	3480	2,082,067	103,255.0	0.106	0.25		
30	25.470	3493	1,910,820	103,109.1	0.106	0.25		
31	25.545	3508	1,759,299	90,186.6	0.092	0.22		
32	25.590	3517	1,585,263	71,806.1	0.074	0.17		
33	25.640	3527	1,498,001	43,030.1	0.044	0.10		
34	25.881	3575	1,681,034	50,199.5	0.051	0.12		
35	25.941	3587	7,254,811	446,605.5	0.458	1.08		
36	26.516	3702	1,059,926	48,709.2	0.050	0.12		
37	26.716	3742	1,022,255	66,495.3	0.068	0.16		
38	26.956	3790	869,194	49,348.6	0.051	0.12		
39	27.166	3832	1,463,915	64,733.0	0.066	0.16		
40	27.261	3851	1,108,254	46,353.4	0.048	0.11		
41	27.446	3888	1,363,652	47,380.1	0.049	0.11		
42	27.981	3995	1,355,401	91,043.2	0.093	0.22		
43	28.126	4024	1,220,337	42,128.9	0.043	0.10		
44	28.297	4058	1,573,857	69,090.6	0.071	0.17		
45	28.402	4079	1,994,600	86,911.4	0.089	0.21		
46	28.437	4086	1,480,823	57,810.7	0.059	0.14		
47	28.527	4104	5,507,447	328,098.3	0.336	0.80		
48	28.612	4121	2,228,513	87,757.0	0.090	0.21		
49	28.667	4132	1,219,610	54,057.4	0.055	0.13		
50	29.162	4231	1,374,702	63,370.8	0.065	0.15		

Inst() ACQUISITION
Oven: Initial temp 50°C for 2 min, ramp 10°C/min to 280°C, hold 5 min, InjAauto=290°C, Volume=1 µL, Split=50:1, Carrier Gas=He, Solvent Delay=8.00 min, Transfer Temp=200°C, Source Temp=180°C, Scan: 50 to 600Da, Column 60.0m x 250µm

CHAPTER-4

Highly Fluorescent Carbon Dots as Invisible Ink and Explosive Sensor

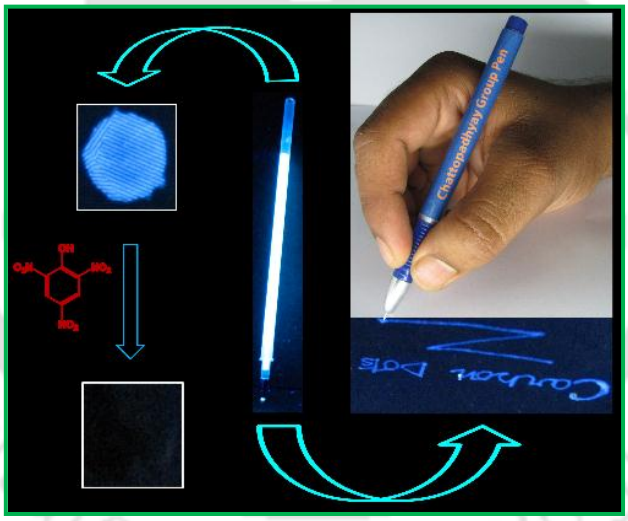

Highlights:

- *Facile, large scale and environment friendly synthesis of high quantum yield Cdots.*
- *Applications based on bright photoluminescence of Cdots: Invisible ink & Explosive sensor*

4.1. INTRODUCTION

Maturity of a technology is not only expressed by the extent of development in the field and in applications but also by the degree of accessibility of the methods for fabrication and consequent usage for a larger populace. In this regard, notwithstanding the recent rapid development of the field of nanoscale science and technology, there is plenty of opportunity for new and fundamentally different approaches in synthetic methodology. This is especially true for colloidal nanomaterials where methods can be made simpler and easier for production at larger scale, using commonly accessible materials and machines. In other words, synthesis of nanomaterials is still the prerogative of specialized laboratories and is yet to reach the public domain. Thus there is a need for development of synthetic methods which will be amenable to commercial production. The method could also be based on traditional knowledge.

Synthesis of carbon nanoparticles (CNPs) in a large-scale is still challenging and requires investigation, especially particles with important optical and chemical properties. The key issue is to produce large quantities of CNPs with high quantum yield (QY) for photoluminescence which demands newer methods could bring novelty and ease of production of CNPs.

Although carbohydrate and other polymer based molecules are known to produce fluorescent smaller CNPs, more popularly known as carbon dots (Cdots), there are recent reports which suggest that smaller molecules such as citric acid could be potential candidates for producing Cdots with high fluorescent quantum yield (QY) [111, 153-155, 172-173]. In addition, introduction of microwave-based methods of synthesis of Cdots has brought new results in terms of tuning of wavelength of emission and also photoluminescence QY. However, production of Cdots using these methods generally requires either harsh reaction conditions or the process is time-consuming, with not necessarily resulting in products with high QY. Further, lack of opportunity for use of solvent other than water, loss of materials during heating and energy efficiency become major hurdles for commercial scale production. In this chapter I have introduced a new method of synthesis of highly fluorescent Cdots from a mixture of citric acid and nitrogen containing passivating agent such as ethylenediamine, using commercially available induction coil heater. Induction heating is faster, safer and energy efficient in

The work contained herein is published in the peer reviewed journal [Sk *et al.* *RSC Adv.* **2014**, *4*, 31994.] Reproduced with permission of The Royal Society of Chemistry.

comparison to other commonly used heating techniques for performing chemical reactions [156]. The current method produced small Cdots with high fluorescent QY. In addition, the Cdots were coupled with chitosan polymer to produce a gel which could be used for UV-active marking. Further, the fluorescence property of the Cdots was used for sensing nitroaromatic phenol explosive with high sensitivity.

4.2. EXPERIMENTAL

Materials. Citric acid, ethylenediamine, and other chemicals were purchased from Merck India. Chitosan was procured from Marine Chemicals, India. Dialysis membrane (dialysis tubing, benzoylated) was purchased from Sigma-Aldrich. All were used as received without further purification. Elix grade water was used in all the experiments. Induction cooker and non-stick frying pan were procured from Philips (model no- HD4908, 220-240V AC, 50/60 Hz) and Prestige respectively.

Preparation of Cdots. Firstly, 3 mM (630 mg) citric acid was taken in a non-stick frying pan and then 50 mL water was added to the pan. The mixture was shaken until citric acid was dissolved. After that 2 mM (134 µL) ethylenediamine was added to it and the mixture was again shaken till a clear solution was obtained. The mixture was then placed on an induction coil heater and temperature was set at 100 ^{o}C (500 W) and reaction time was kept for 12 min. After completion of the reaction, the hot pan was cooled to room temperature either by placing on water bath or was air-cooled. The final product was dark brown syrup. The product was dissolved in 10 mL water followed by dialysis using 1 KDa (dialysis tubing, benzoylated) dialysis membrane for 24 h. The weight percentage of yield was c.a. 63% with respect to the citric acid, calculated following purification of product by dialysis. The sample was used for further analyses.

For large scale synthesis, 5.040 gm (24 mM) citric acid, 1.064 mL (16 mM) ethylenediamine and 50 mL water were taken in the frying pan. The rest of the procedure was same as above; however, the heating time was kept at 15 min. The weight percentage of yield was c.a. 86 % with respect to the citric acid as calculated before purification. Also, the weight percentage of yield was c.a. 70% with respect to the citric acid and ethylenediamine as calculated prior to purification.

I also performed the reaction at 130 ^{o}C (800 W) with 3 mM (630 mg) citric acid and 2 mM (134 µL) ethylenediamine. But heating time was set at 8-9 min. It was observed that if heating

was performed at 130 °C or higher temperature relatively lesser time was required for the formation of Cdots than that at 100 °C.

Preparation of Cdot Gel Ink. 100 mg chitosan was taken in a beaker and 10 mL water was added to it followed by the addition of 100 µL acetic acid. The mixture was stirred until chitosan was dissolved i.e. a clear solution was obtained. Then desired amount of Cdot dispersion was added to it and the mixture was stirred for 5 min. This led to the formation of gel, which was ready for use as ink for gel pen.

For the sensing applications, Cdot ink (gel) was prepared by dissolving 100 mg chitosan in 20 mL water with further addition of 100 µL acetic acid and the concentration of Cdot was kept at 0.01 mg/mL. Only 4 µL of Cdot ink was used for making spot on non-fluorescent paper and then the spot was dried for sensing or other applications.

Preparation of Cdot Film. As-prepared carbon dot ink was spread on a watch glass or polypropylene plate and was dried for 24 h at 50 °C. This led to the formation of a film which could be easily lifted using forceps.

Optical Measurements. The titration of the Cdots with different molecules in DMF solution (measured using fluorescence spectroscopy) were carried out by directly adding small aliquots (10 µL) to the 3 mL of the DMF solution (containing 0.1 mg/mL carbon dots) in a quartz cuvette (1 cm x 1 cm). Fluorescence was recorded at room temperature.

Analytical Measurements. Cdots were characterized using transmission electron microscopy (JEOL 2100 UHR-TEM, operating at 200 KV), UV-vis spectroscopy (Hitachi U 2900 spectrophotometer), photoluminescence spectroscopy (Horiba Fluoromax-4 spectrofluorometer), powder X-ray diffraction (Brucker D8 Advanced X-ray diffraction measurement system) with Cu Kα source (λ =1.54 Å), nuclear magnetic resonance spectroscopy (Bruker, 600 MHz), Fourier transform infrared spectroscopy (Perkin Elmer IR spectrometer), electron paramagnetic resonance (JEOL, Model: JES-FA200) spectrometry, time-resolved photoluminescence spectroscopy (Eddinburg Instruments, Model: FSP920) and X-ray photoelectron spectroscopy (PHI 500 Versa Probe II , ULVAC-PHI, INC, Japan).

Quantum Yield Calculation. I have calculated Quantum yield with respect to quinine sulphate (QS) in 0.1 M H_2SO4, using the following formula.

$$Q_S = Q_R \times \frac{I_S}{I_R} \times \frac{A_R}{A_S} \times \frac{\eta_S^2}{\eta_R^2}$$

Where, Q_S = quantum yield of sample; Q_R = quantum yield of reference; I_S = area under PL curve of sample; I_R = area under PL curve of reference; A_R = absorbance of the reference; A_S = absorbance of the sample; η_S = refractive index of sample; η_R = refractive index of reference.

Q.Y. of quinine sulphate = 0.54; Refractive Index: water = 1.33

(The concentration of all samples and the reference quinine sulphate were adjusted so that the optical densities of all samples were 0.020 ± 0.003 at the excitation wavelength (365 nm)).

It is important to mention here that quantum yield results reported in Table 4.1 and 4.2 were obtained from single absorbance measurements. This was done to get the best sample result. On the other hand, the quantum yield reported below for Cdots synthesized from citric acid and ethylenediamine was calculated from the integrated fluorescence intensity versus absorbance plot. Hence the difference would be due to methods used.

Quantum Yield Calculation of Cdots synthesized from Citric acid and Ethylenediamine. Quantum yield was measured according to established procedure by using quinine sulfate in 0.10 M H_2SO_4 solution as the standard. Absolute values were calculated according to the following equation:

$$Q_S = Q_R \text{ x } (m_S / m_R) \text{ x } (n_S / n_R)^2$$

Where, Q is the quantum yield, m is the slope of the plot of integrated fluorescence intensity *vs* absorbance and n is the refractive index (taken here as 1.33, the refractive index of distilled water). The subscript R refers to the reference fluorophore, quinine sulphate solution. In order

to minimize re-absorption effects, absorbance was kept below 0.15 at the excitation wavelength of 365 nm. The values m_S = 5.19 and m_R = 3.81 were obtained from the plot of integrated fluorescence intensity *vs* absorbance. The quantum yield of Cdots (obtained from reaction of citric acid with ethylenediamine) was calculated to be 73.5 %.

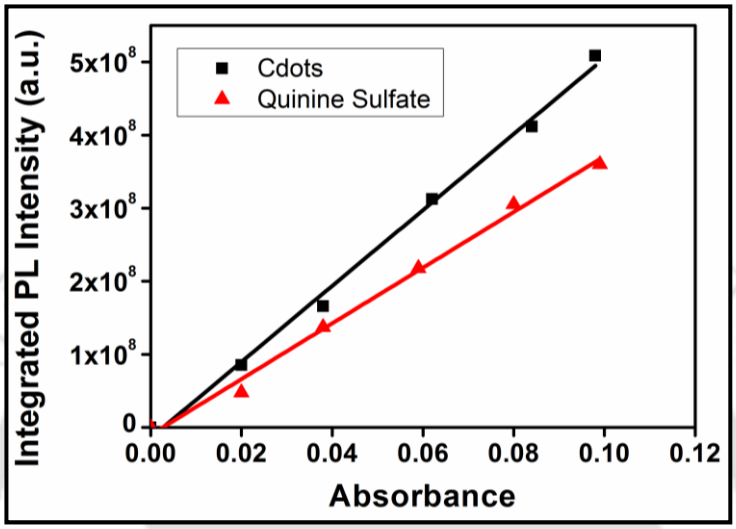

Figure. 4.1. Integrated fluorescence intensity versus absorbance of Cdots and quinine sulfate. The sample was synthesized from the reaction of citric acid with ethylenediamine.

Table 4.1. Optimization of citric acid and ethylenediamine ratio for Cdots synthesis

SN	Carbon Source	Surface Passivation Agent	Quantum Yield (%)
1	3 mM Citric Acid	No	1.6
2	3 mM Citric Acid	1 mM Ethylenediamine	12
3	3 mM Citric Acid	2 mM Ethylenediamine	70.1
4	3 mM Citric Acid	3 mM Ethylenediamine	71.4
5	3 mM Citric Acid	4 mM Ethylenediamine	72.6

Table 4.2. Quantum Yield of Cdots prepared under different reagent conditions

SN	Carbon Source	Surface Passivation Agent	QY (%)
1	Citric Acid	No	1.34 ± 0.37
2	Citric Acid	Ethylenediamine	75.9 ± 7.3
3	Citric Acid	1,3- Diaminopropane	77.3 ± 5.6
4	Citric Acid	N-(2-Aminoethyl)-1,2-ethandiamin	55.5
5	Citric Acid	o-Phenylenediamine	38.25
6	Citric Acid	p-Phenylenediamine	2.38
7	Citric Acid	N,N-Bis(2-aminoethyl)-1,2-ethandiamin	56.7
8	Citric Acid	Urea	12.90
9	Citric Acid	Thiourea	6.50
10	Citric Acid	4,7,10-Trioxa-1,13-tridecane diamine	12.8
11	Alginate	Ethylenediamine	1.63
12	Glucose	Ethylenediamine	0.41
13	Glutamic Acid	Ethylenediamine	11.56
14	Aspartic Acid	Ethylenediamine	17.16

4.3. RESULTS & DISCUSSION

Experimentally, when a mixture of citric acid and diamine (a reactant and passivating agent) in water was heated at 100 ^{o}C, in a sauce pan placed on a commercial induction coil (500 W), for 12-15 min (depending on the nature of the passivating agent), a brown paste was obtained (Figure 4.2a). The paste could easily be transferred to a vial for further analysis. The brown paste could also be dried which appeared as black powder and several such samples could be accumulated (Figure 4.2b). The powder when redispersed in water appeared brown in the visible light; however, the dispersion appeared intense blue upon excitation by UV light (Figure 4.2c). It may be mentioned here that the images in Figure 4.2 are from the product of reaction of citric acid with ethylenediamine, which was found to yield product with high fluorescence QY with an optimum molar ratio of 3:2, respectively (Table 4.1). In the subsequent sections, results will be presented for the same sample unless mentioned otherwise.

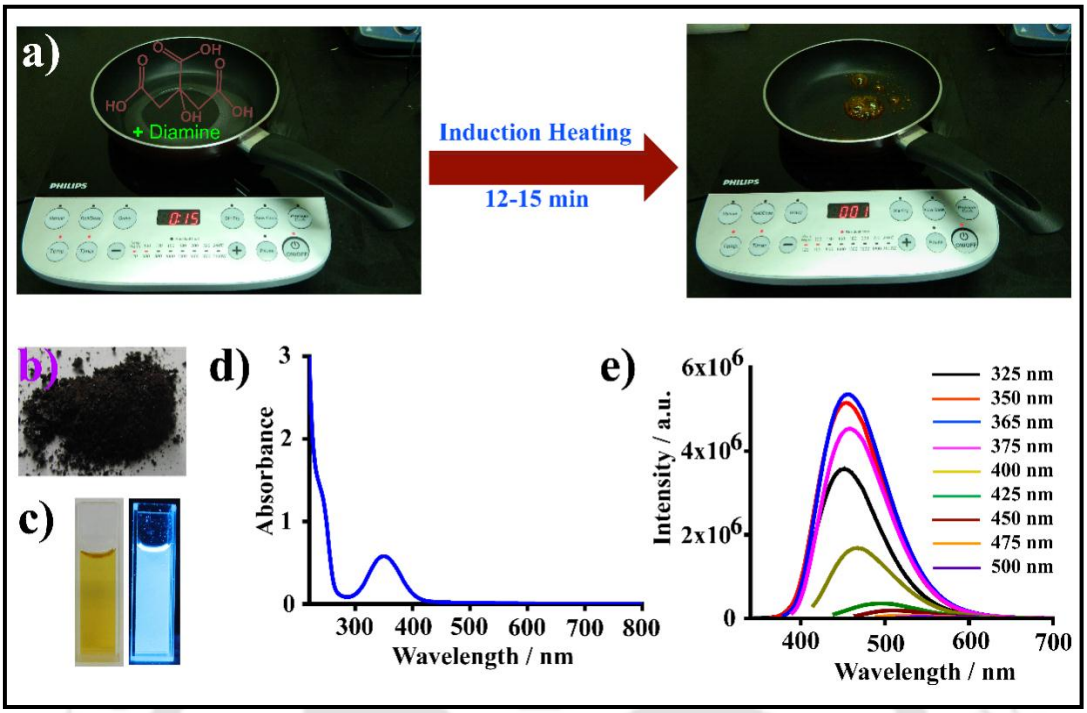

Figure. 4.2. (a) Photographs representing synthetic method for highly fluorescent Cdots. **(b)** Photogaph of dried Cdots. **(c)** Dispersion of Cdots in visible light and UV light (365 nm). **(d)** UV-Vis spectrum of Cdots in water. **(e)** Wavelength-dependent emission spectra of Cdots in water.

The UV-vis spectrum of the dispersion consisted of two peaks – one at 242 nm, while the other one appeared at 350 nm (Figure 4.2d). The peak at 242 is assigned to π-π* transition, which could be due to a product having c-c π bonds [154]. On the other hand, the peak at 350 nm is typical of Cdots, which upon excitation with the light resulted in strong blue emission at 454 nm (Figure 4.2e). The emission is assigned to surface states of Cdots [108, 111]. However, the presence of defect states cannot be ruled out [157]. Since Cdots are known to have wavelength tuneable emission, this was also pursued. It was observed that although the emission did have wavelength tuneability, however, the extent was weak. For example, when the dispersion was excited by light of wavelengths from 325 – 400 nm, there was considerable change in intensity of emission and no discernible change in emission wavelength. On the other hand, excitation beyond 400 nm resulted in weaker emission with no significant change in wavelength of emission. One reason for this could be due to the production of uniformed sized Cdots [110]. Further, QY for sample prepared from different passivating agents (in addition to citric acid as the precursor) indicated that presence of ethylenediamine provided Cdots with QY

as high as 73.5%. It may be mentioned here that QY of Cdots as high as 83 % has been reported earlier [173]. The large QY resulted in easy observation of fluorescence from Cdots using an ordinary chromatographic UV-lamp, at concentration as low as 1.0 μg/mL. All other compounds resulted in products with lower or much lower QY. The details are available in Table 4.2.

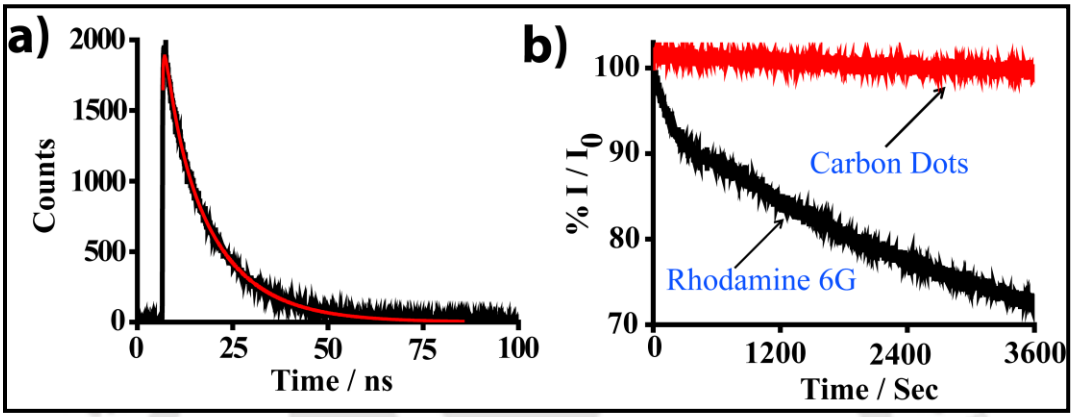

Figure 4.3. **(a)** Time-resolved fluorescence decay profile of Cdots in water. The excitation wavelength was set at 375 nm and emission was probed at 450 nm. **(b)** The effect of photo-irradiation time on the fluorescence intensity of Cdots and the organic fluorophore rhodamine 6G in water.

Time-resolved fluorescence decay profile of the Cdots dispersed in water could be fitted with bi-exponential function. The average life time was calculated to be 13.3 ns (Figure 4.3a). Interestingly, when Cdots were dispersed in dimethylformamide (DMF), average life time was 9.3 ns, again calculated using a bi-exponential function (Figure 4.11d and Table 4.3), and indicating possible solvent dependence. Further, photoluminescence studies indicated that the Cdots were stable and remained highly luminescent in the presence of high salt (KCl) concentration (Figure 4.4), rendering them useful for versatile applications, especially in the presence of high ionic strength. Studies of pH-dependent fluorescence of the Cdots revealed that the emission intensity was nearly constant in the pH range of 4 to 11 (Figure 4.4), signifying their potential utility in a wide pH range. Photostability experiments revealed that Cdots were more stable (with a decay rate of 0.022%) in comparison to a popular dye such as rhodamine 6G (having a decay rate of 0.45%, Figure 4.3b).

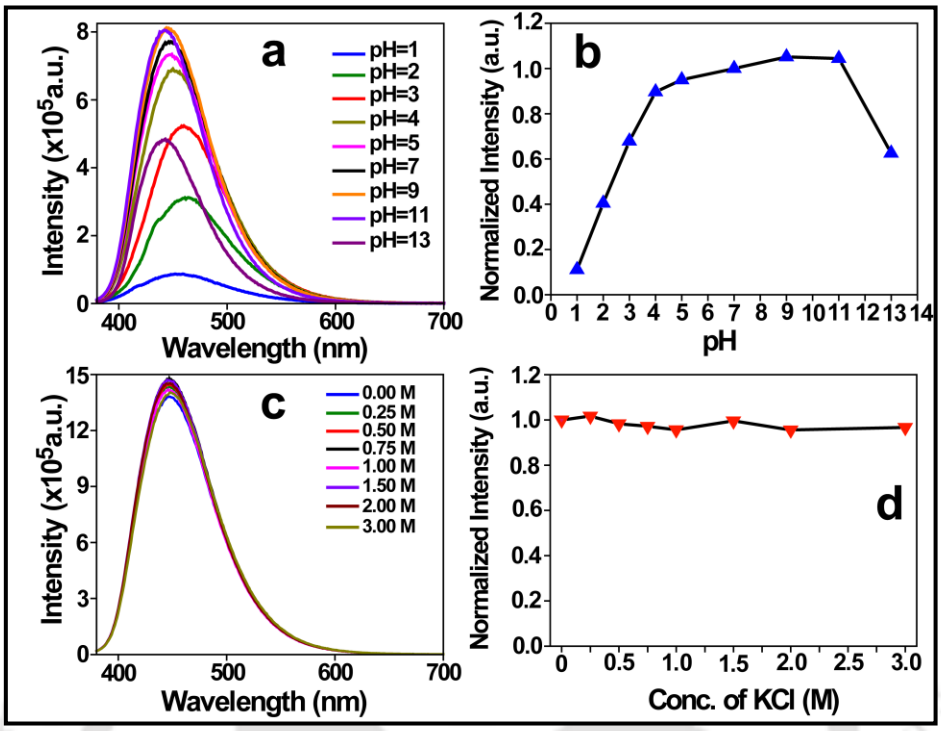

Figure 4.4. Dependence of photoluminescence of Cdots on **(a)** pH and **(b)** ionic strength of the medium.

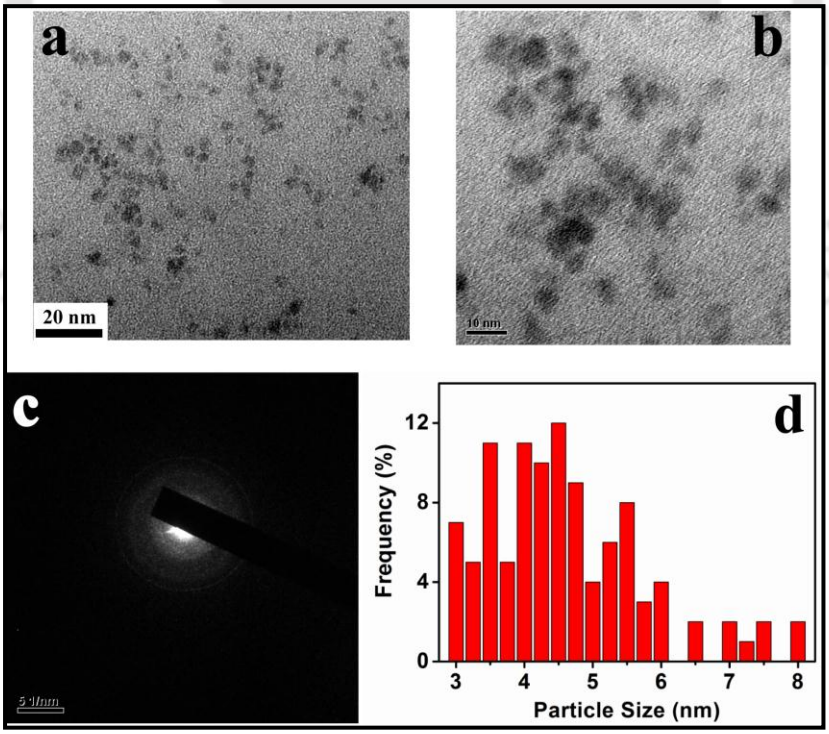

Figure 4.5. (a) TEM image of Cdots. **(b)** High resolution TEM image and **(c)** SAED pattern of Cdots. **(d)**Size distribution of Cdots as calculated from TEM images.

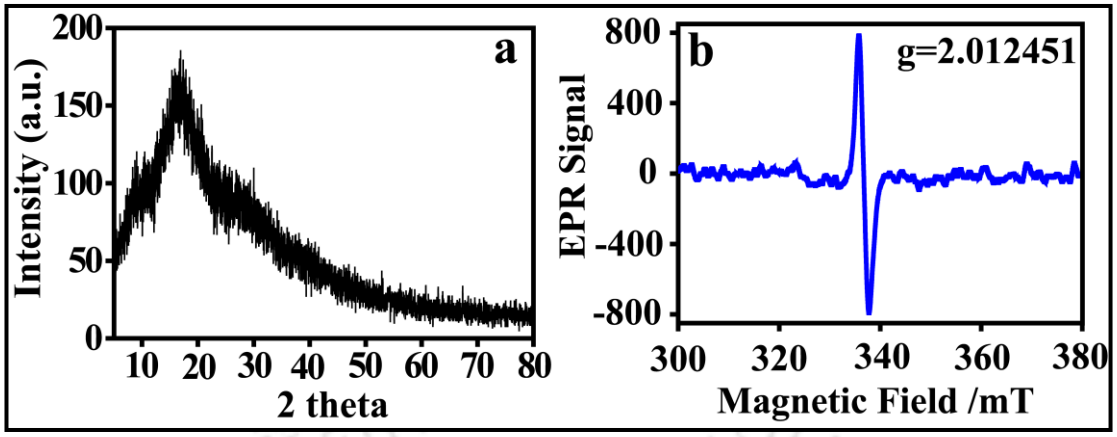

Figure 4.6. (a) Powder XRD pattern of Cdots. **(b)** EPR spectrum of solid Cdots.

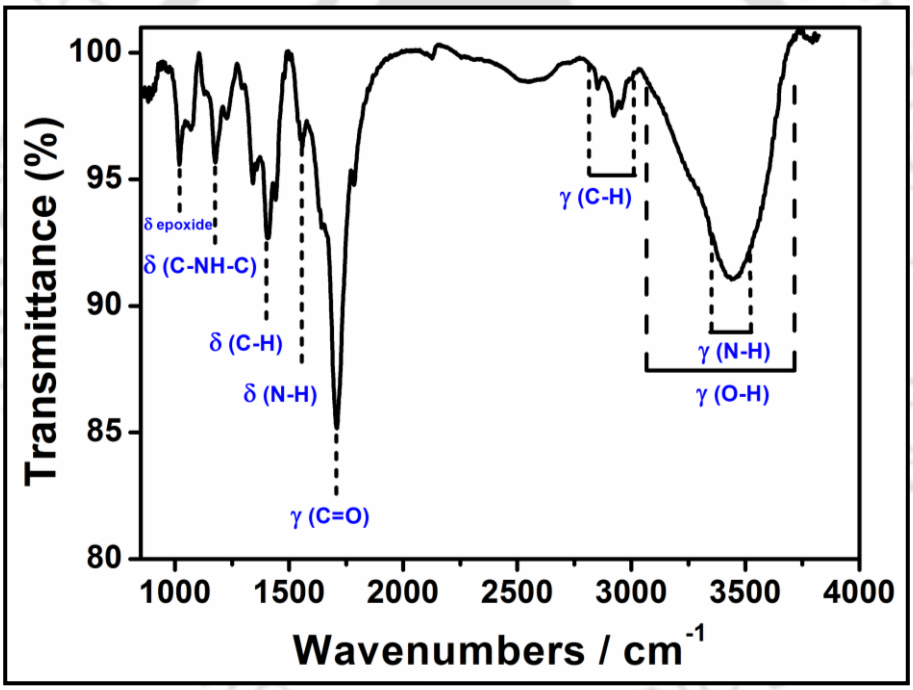

Figure 4.7. FTIR spectrum of Cdots.

Transmission electron microscopy (TEM) revealed that as-synthesized Cdots were nearly spherical with average particle size of 4.6 ± 1.2 nm (Figure 4.5a). The size distribution of Cdots as calculated from TEM images is shown at Figure 4.5d. The amorphous nature of the particles was established by lack of observation of clear lattice fringes in the high resolution TEM as well as any clear pattern in selected area electron diffraction (Figure 4.5b, c). X-ray diffraction (XRD)

pattern consisted of a broad peak at 2θ = 17°, suggesting the formation of amorphous carbon structure (Figure 4.6a). Elemental analysis confirmed that the Cdots contained 39.76% C, 6.31% H, 10.03% N and 43.90% O (as calculated). Further, ^{13}C NMR spectroscopy (Figure 4.8) revealed that sp^2 as well as sp^3 carbons were present in Cdots. The sp^2 carbons were carbonyl in nature (with peaks in the range of 170-185 ppm), which could be due to the presence of carboxylic or amide groups. The peaks around 30- 45 ppm are attributed to the presence of aliphatic sp^3 carbon atom. Another peak at 72 ppm suggested that alcoholic or C-O-C aliphatic sp^3 carbon atoms were present. Also, Fourier transform infrared (FTIR) spectrum confirmed the presence of -OH, C=O, C-N-C and -NH groups in the Cdots (Figure 4.7). The appearance of the peak at 1709 cm^{-1} instead of the peak of carbonyl group of citric acid at 1731 cm^{-1} indicated the formation of amide bond [159]. Further, the nature of bonding of carbon in the Cdots was confirmed by X-ray photoelectron spectroscopy (XPS) (Figure 4.9) [111, 154, 160]. The XPS result of C_{1s} is attributed to the presence of C-C or C=C (284.8 eV), oxygenated carbon or C-N (286.2 eV) and amide carbonyl group or C=O (287.9 eV) functional groups. The N_{1s} spectrum of Cdots contained two peaks at 399.9 eV and 401.5 eV, which correspond to the C-N-C and N-H respectively. Also, the O_{1s} spectrum showed two peaks at 531.6 eV (C=O) and 533.2 eV (C-O). Interestingly, electron paramagnetic resonance (EPR) spectroscopy studies (Figure 4.6b) indicated the presence of one or more singly occupied electron orbitals in the ground state (with g = 2.012451), suggesting electron donation and acceptance properties of the Cdots [161-163].

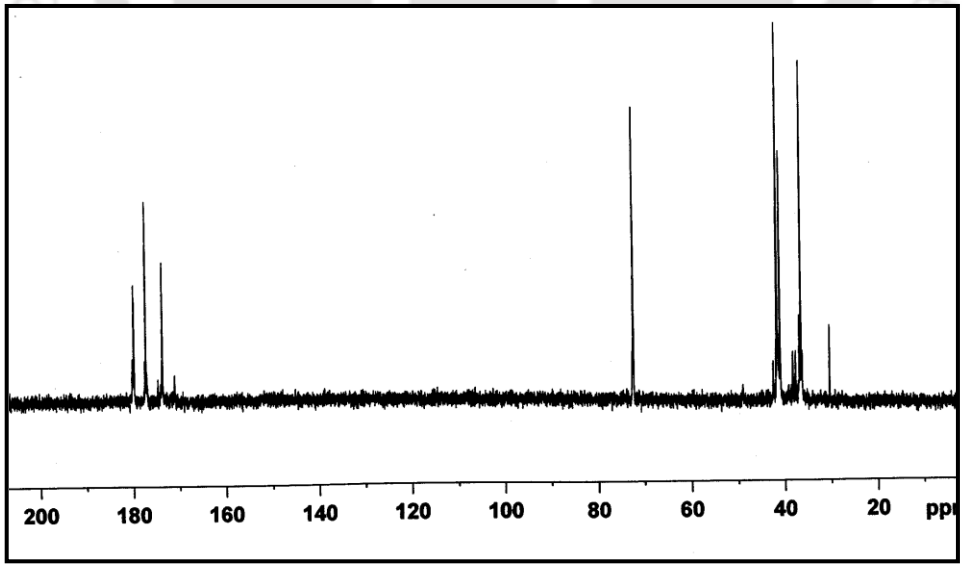

Figure 4.8. ^{13}C NMR spectrum of Cdots.

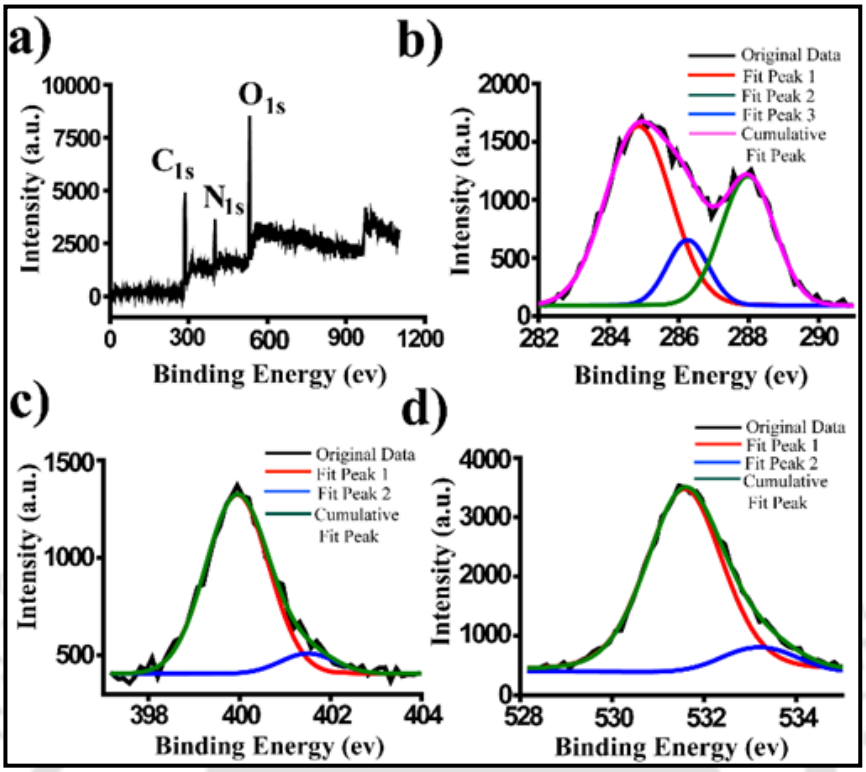

Figure 4.9. **(a)** X-ray photoelectron spectra of Cdots. **(b)** is for C_{1s}, c) is for N_{1s} and d) is for O_{1s}.

It is important to mention here that the Cdots were not only dispersible in water but also in organic solvents such as in N, N-dimethylformamide and dimethylsulfoxide, and weakly in methanol. Further, it was observed that the product formation could easily be scaled to higher amount primarily by using higher amounts of starting materials. The merit of high photoluminescence QY, scalability and ease of dispersion in various solvents, make the case for high application prospects of the Cdots. A versatile application could be in the form of UV-active ink, which would otherwise be undetectable to visible light. For this purpose, a gel was prepared using the so synthesized Cdots and chitosan biopolymer. The gel 'ink' was then used to fill up an ordinary ball-point pen refill, the images of which - under visible and UV light - are shown in Figure 4.10a-c. The refill could then be used to sketch images of different size and shapes on non-fluorescent currency notes. A few of these images, which were recorded in the presence of UV light, are shown in Figure 4.10b. Importantly, the ink adhered to the paper well such that following washing with water and then with detergent solution the imprint was still clearly discernible (Figure 4.10c). Further, as shown in Figure 4.10f, the gel could be converted into highly fluorescent film. An important application of the water dispersible Cdots could be to

follow water flow in fields. For this gram was incubated in the dispersion for 24 h, following which it was exposed to UV-light for imaging. As is clear from Figure 4.10d, the Cdots percolated into the gram with high efficiency and gave rise to clear fluorescent image in comparison to control sample kept in water.

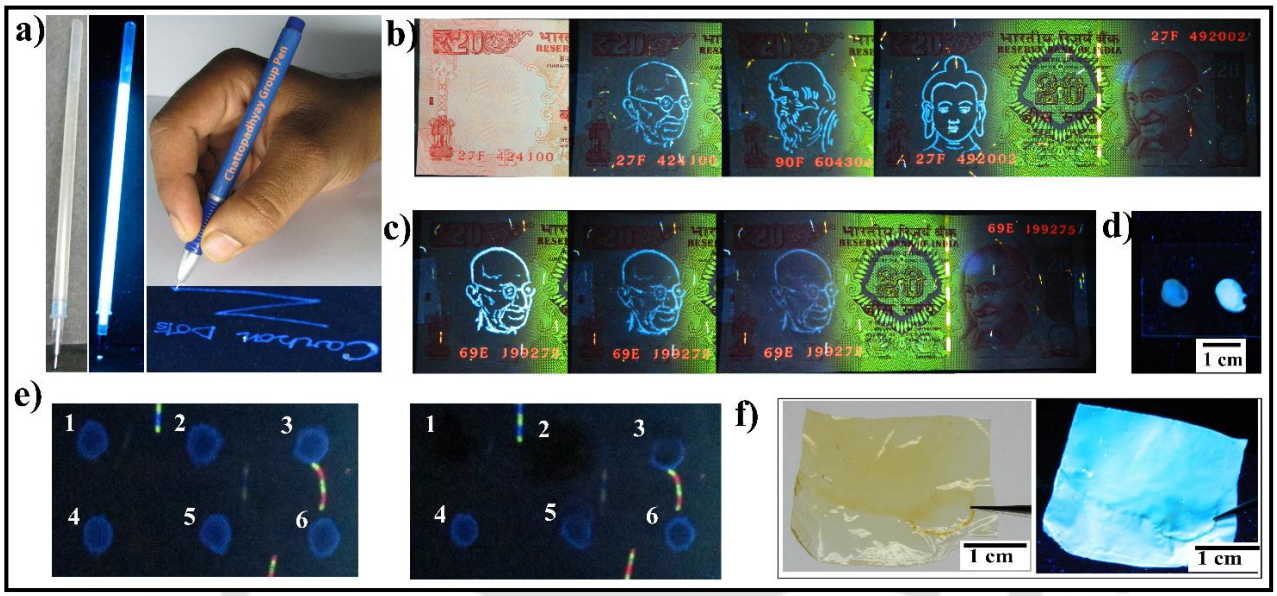

Figure 4.10. (a) Cdots filled ballpoint pen refill under visible light and UV light, respectively. **(b)** Sketches drawn using Cdot ink which were discernible in UV light. (**c)** UV-active sketch and its appearance following washing with water and then by soap solution. (**d)** Image of uptake of Cdots by gram (right) with control on the left. **(e)** Quenching of fluorescence of Cdot ink (concentration 0.1 mg / mL) marked on non-fluorescent paper before (left panel) and after addition of various analytes (2 µl of 1.0 mM) on the spots. 1. picric acid, 2. 2,4- dinitrophenol, 3. 4-nitrophenol, 4. nitrobenzene, 5. 1,4-benzoquinone, 6. 4-methoxybenzoic acid). **(f)** Appearance of Cdot film under daylight and UV light.

Finally, the highly fluorescent gel was also used for efficient detection of nitroaromatic phenols such as picric acid and 2, 4-dinitro phenol, the primary constituents of explosives. The Stern–Volmer binding constants (Ksv) for picric acid and 2, 4-dinitro phenol were found to be 3.72 x 10^4 M^{-1} and 3.23 x 10^4 M^{-1}, respectively, which are comparable with previously reported values [163-171]. The results are shown in Figure 4.11a-b, 4.12. The detection limit of picric acid was observed to be 75.6 ppb. I was also interested in finding the nature of quenching of luminescence of Cdots by picric acid. This was pursued by time-resolved photoluminescence (TRPL) studies which revealed that there was no change in average life time of Cdots in DMF

upon addition of picric acid (conc. range from 0 to 100 μM), suggesting static quenching (Figure 4.11d & Table 4.3). Additionally, I observed that the quenching efficiencies of picric acid and 2, 4-dinitro phenol were much more than benzoquinone or 4-methoxy benzoic acid, indicating selectivity of the process (Figure 4.10e & 4.11c). This is evident from the difference in luminescence intensities of the spots of Cdots in the presence of the above reagents, as shown in Figure 4.10e.

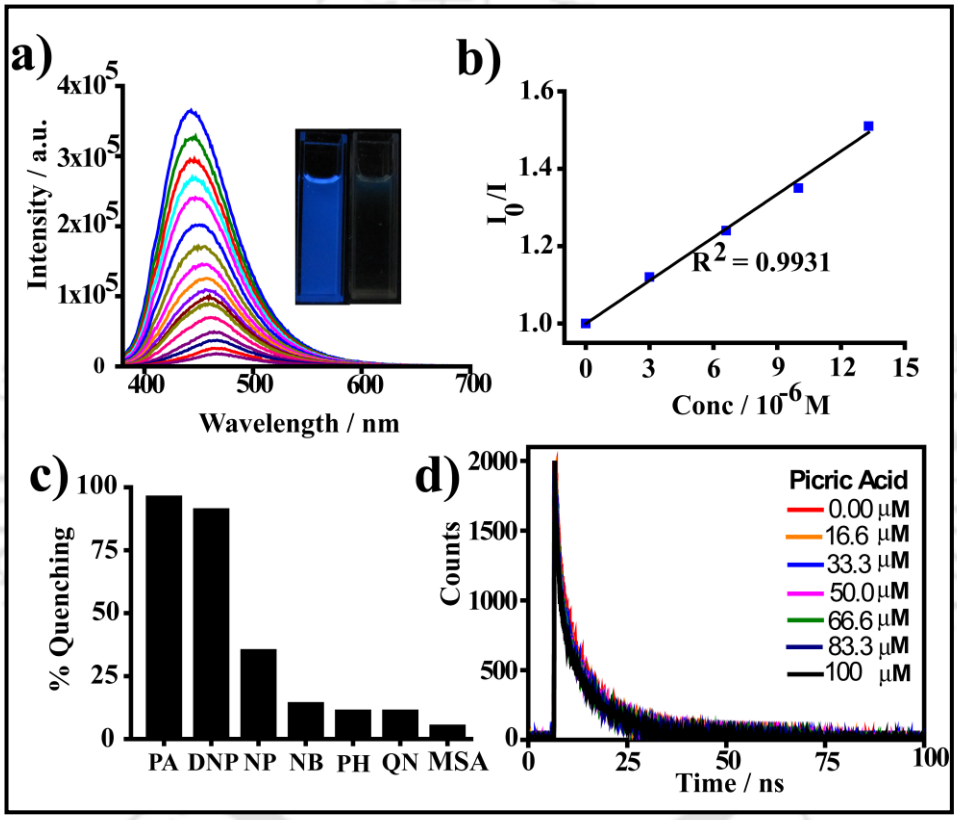

Figure 4.11. (a) Quenching of fluorescence of Cdots (0.01mg / mL) by picric acid (0 to 120 μM) in DMF (λex=365 nm). **(b)** Stern-Volmer plot of the quenching of fluorescence (conc. of picric acid used was up to a maximum of 13.3 μM). **(c)** Extent of quenching of fluorescence of Cdots (0.01 mg/ml in DMF) following addition of various analytes up to the concentration of 120 μM. (PA= picric acid, DNP= 2,4-dinitrophenol, NP= 4-nitrophenol, NB= nitrobenzene, PH= phenol, QN= 1,4-benzoquinone and MSA= 4-methoxybenzoic acid). **(d)** Time-resolved fluorescence decay curves of Cdots in DMF in absence and presence of gradually increasing concentration of picric acid. The excitation and emission (probe) wavelengths were set at 375 nm and 450 nm respectively.

Table 4.3. Decay parameters of the fluorescence of carbon dots in DMF in absence and presence of gradually increasing concentration of picric acid.

Conc. (μM)	A_1 (%)	τ_1 (ns)	A_2 (%)	τ_2 (ns)	$\langle\tau\rangle$ (ns)
0	23.14	1.431	76.86	9.642	9.3
16.6	22.09	1.426	77.91	9.66	9.3
33.3	22.11	1.428	77.89	9.628	9.3
50	22.6	1.417	77.4	9.59	9.25
66.6	37.88	1.415	62.12	9.612	8.94
83.3	23.33	1.401	76.67	9.513	9.2
100	26.96	1.355	73.04	9.483	9.1

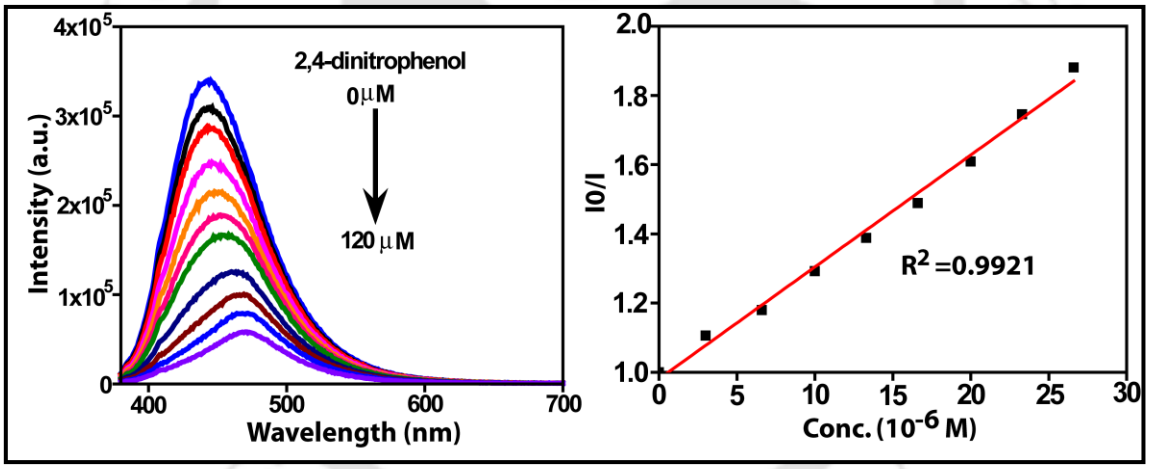

Figure 4.12. Quenching of fluorescence of Cdots (0.01 mg / mL) by 2,4-dinitrophenol (with concentration varying from 0 to 120 μM) in DMF (λex=365 nm). Stern-Volmer plot with respect to the quenching of fluorescence (conc. of 2,4-dinitrophenol used was up to 26.6 μM).

4.4. CONCLUSIONS

In conclusion, I have demonstrated a new and facile method of synthesis of highly photoluminescent Cdots. The use of commercial induction heater not only made the process fast and efficient but also may help the process commercially viable. While preparations using microwave oven have similar simplicity, induction coil heater offers unique advantages of

uniform solvent evaporation, workability under different solvent conditions and ease of control of temperature of heating of the sample. Further, the formation of a gel using chitosan demonstrated the ease and versatility of the application as UV-active marker as well as sensor for common explosives. The simplicity, scalability, generality and commercial viability of the process may lead to important applications of the highly fluorescent Cdots.

CHAPTER-5

Dual Phase Logic Operations using luminescent Carbon Dots

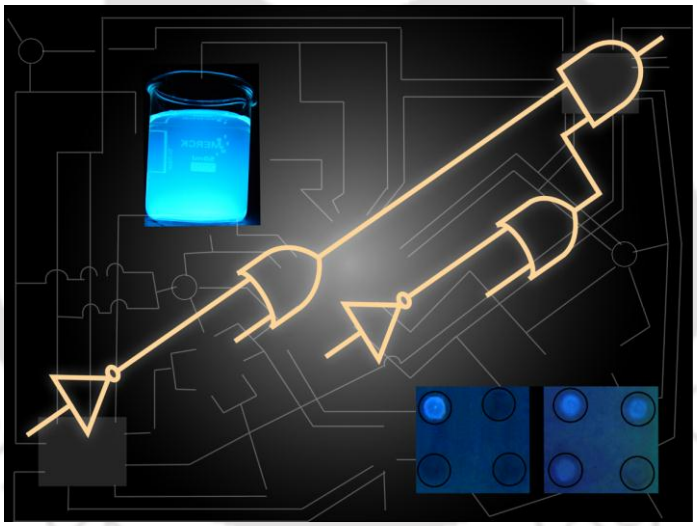

Highlights:

- *Exploitation of photoluminescence property of Cdots in simple and complex logic operations.*
- *Dual phase (in liquid & solid) logic system.*
- *Cdots based logic structure for versatile applications.*

5.1. INTRODUCTION

Complex decisive logic systems prevail ubiquitously in nature [174]. However, the effective understanding and implementation of these logical operations in artificial systems have only been used seriously only after the success of semiconductor based electronics. Regardless of the growing demands and existing advantages of conventional silicon based technology, these sublime naturally prevailing logical operations perfected over the course of evolution remain essential for smooth functioning of everyday life [175-176]. Importantly, molecule-based electronics – which promises significant improvement in computation power and speed – can adopt or learn from some of the key concepts of these nature-based logic operations. This may also help realize multifunctional 'lab-on-a-molecule' [177]. The inaugural works of de Silva and co-workers [178] have inspired recent developments in molecular computations using "bottom-up" approaches, based on organic and bio molecules, polymeric materials, molecular assemblies, quantum dots, nanoclusters, nanoparticles and other nanomaterials [179-187, 197-198]. Some of the key features of these low dimensional materials include structural tuneability of the function [188], fast processing [176], liquid phase operation [179-182, 184-187], environmental friendliness [187] and their ability to work in varied environment [182, 189]. However, an important requirement for their practical applications is the ability for complex operations, which could be based on cascading of simpler individual processes. In addition, the system would be more robust if it could be used in both liquid and solid phases. Interestingly, although there are a large number of proposed devices which work in single phase (mostly in liquid), multi-phase operative molecular logic systems are scarce [190-192]. To the best of our knowledge, except for a gel based systems [193], the solid phase depiction of integrated logical systems has not been demonstrated.

Herein I propose and demonstrate that carbon dot (Cdot) could be an important candidate for cascade logic operations independently in two phases. This would be based on interactions of molecular species with Cdot, leading to changes in photophysical properties (especially luminescence) of its liquid dispersion and dried solid particles. More importantly, my observations suggest that photophysical properties of Cdots are equally affected by molecular

The work contained herein is published in the peer reviewed journal [Sk *et al.* *ChemPhysChem,* **2015**, *16*, 723.] Reproduced with permission of John Wiley and Sons.

species both in their aqueous dispersions and solid phase. My experiments also suggest that these properties make Cdot an ideal candidate for the development of multi-phase (medium) molecule based computational material. Interestingly, except for a single example of a few logic gate operations, the functionality of Cdots in complex computation has not been demonstrated [194].

In this chapter I have developed basic logic gates like NOT, YES, AND, OR, IMPLIES; universal gates NOR, NAND and molecular switch using Cdot as fluorophore and picric acid, Fe^{3+}, Fe^{2+} and hydrogen peroxide as luminescence tuning inputs. I further constructed higher order logic structures through appropriate integration of the chemical inputs. Also, a typical demonstration of integration by cascading two individually functioning simple logic gates was made for detection of Fe^{3+} ions. These logic structures are not only good for operation in the liquid medium but also are engineered to be operative in a simple solid phase, i.e., typically on a non-fluorescent paper. For the demonstration of various logic functions, photoluminescence of the Cdot was considered to be the logical output. When the output luminescence crossed the marked threshold, the logic was considered high (1) and on the other hand when it failed to do so, it was considered to be low (0). The excitation wavelength for all the logic functions was set at 365 nm, while the emission wavelength was taken as 443 nm. The luminescence in solid phase was monitored using a commercially available digital photographic camera while the sample was under the UV radiation.

5.2. EXPERIMENTAL

Materials. Citric acid, ethylenediamine, $CoCl_2$, $CuSO_4$, $NiCl_2$, $HgCl_2$, $ZnCl_2$, $FeCl_2$, KCl, NaCl, $PbSO_4$, $Al_2(SO_4)_3$, $CaCl_2$, $MgSO_4$, $MnCl_2$, Cetyl trimethylammonium bromide (CTAB), picric acid, ascorbic acid cysteine were purchased from Merck. $FeCl_3$ and 1KDa dialysis membrane were procured from Aldrich. Chitosan was obtained from Merine Chemicals, India. All were used as received without further purification. Milli-Q grade water was used in all the experiments. Induction coil heater and non-stick frying pan were bought from Philips and Prestige (India) respectively.

Synthesis of Cdots. Cdots were synthesized by our previously reported method as discussed in chapter-4, where a mixture of 50 ml of 60 mM aqueous solution of citric acid was taken in a non-stick frying pan and then 134 µl ethylenediamine (final conc. of ethylenediamine was 40 mM) was added to it. Then the solution was heated using induction heater at 100 ^oC

(500W) for 12 min which eventually led to the formation of Cdots. The product was dialysed by 1KDa dialysis membrane. The quantum yield of the Cdots was measured to be 73.5 %.

Optical Measurements. Optical measurements of Cdots were carried out by directly adding aliquots of different molecules and metal ions in a quartz cuvette containing 3.0 mL Cdot (0.01 mg/ mL) aqueous dispersion (measured using fluorescence spectroscopy, Horiba Fluoromax-4 Spectrofluorometer). Fluorescence was recorded at room temperature.

Emission Quenching Phenomena of Cdots with Picric acid. The quenching of photoluminescence of Cdots by picric acid has already been discussed in chapter-4. For reversibility of emission, phase transfer process was introduced where Cdot-picric acid dispersion was taken in a test tube. To this, a mixture of acetonitrile and ethyl acetate in a ratio of 1:1.5 was added and then the mixture was shaken, coupled with addition of small amount of sodium chloride. Then the organic layer which was yellowish in colour was separated from the colourless aqueous layer by decanting. Then the fluorescence of aqueous layer was recorded. This behaviour can be used to construct a molecular switch as shown in Figure 5.1.

Quenching of Emission of Cdots by Metal ions. The titration of the Cdots with different metal ions in water medium (measured using fluorescence spectroscopy) was carried out by directly adding aliquots of metal ions to the 3 mL of the dispersion (containing 0.01 mg/mL carbon dots) in a quartz cuvette, at room temperature. The excitation wavelength was 365 nm and emission was set at 443 nm. The relative luminescence emission is shown in Figure 5.2. In particular, the effect of Fe^{3+} ions on Cdots was studied since they were found to be much responsive, as shown in Figure 5.3. The reversible recovery of emission following quenching by Fe^{3+} was obtained by simply adding of 50 µL of 0.1 M ascorbic acid or cysteine. After immediate adding of 50 µL of 0.1 M ascorbic acid or cysteine to the Cdots - Fe^{3+} mixture, 71% and 47% emission revival was observed, respectively. But, after 30 min, there was almost 75% and 69% revival of emission, respectively.

Logic Implementation on Non-Fluorescent Paper. For constructing logic structures on non-fluorescent paper, Cdot ink (gel) was prepared by dissolving 150 mg chitosan in 20 mL water with further addition of 100 µL acetic acid, keeping the concentration of Cdot at 0.01 mg/mL. Cdot ink (5 µL) was used for making spot on non-fluorescent paper, which was then dried at room temperature or at 60 ^{o}C.

For hardware system, the inputs are same as in liquid phase unless until mentioned here. 5 µL of Cdot ink was used for making spot on non-fluorescent paper and also 2 µL picric acid

(1mM), 5 uL $FeCl_3$ (1 mM) were used to quench the luminescence where needed and then the paper was dried. In a particular case of OR logic system, 5 µL citric acid or mercaptopropionic acid (0.2 M) was used as an input in place of ascorbic acid (as done in liquid media) with another input as cysteine (5 uL, 0.1M). I found ascorbic acid was not suitable for solid phase logic system but it was good for the reversibility of emission in solution phase logic system. Also, for the case of AND or integrated logic system, phase transfer process which was used in solution phase logic system was found to be not suitable and recover was achieved alternatively by pouring 4 µL CTAB (0.1M) on the spot where needed and was very gently wiped using tissue paper or washed with a mixture of acetonitrile/ethylacetate (1:1.5) after drying the spot. Also, cysteine was used as an input in place of ascorbic acid for AND logic system. For NAND logic system, 5 µL $FeCl_2$ (1 mM) and 5 µL hydrogen peroxide (1%) were used. Except for phase transfer process, in all other cases the spot was dried after addition of analyte.

5.3. RESULTS & DISCUSSION

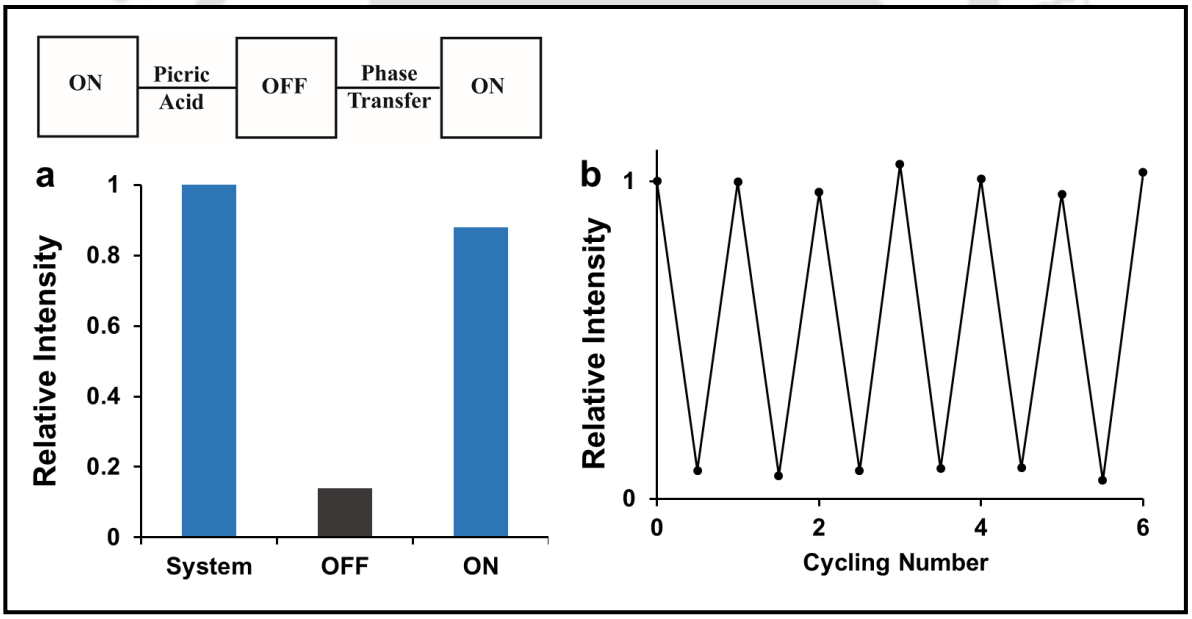

Figure 5.1. Molecular Switch. **(a)** The inherent fluorescence of the Cdots could be quenched through the exposure to picric acid (OFF condition). The fluorescence can be revived (ON condition) through the phase transfer process. **(b)** Switching of fluorescence (on and off) for six cycles.

Molecular Switch. An aqueous dispersion of the as-synthesized Cdots showed optical emission at 443 nm upon excitation at 365 nm. This inherent photoluminescence of the Cdots can be quenched, by exposure to picric acid, which is based on static quenching mechanism as discussed in chapter-4 [163]. I observed that the fluorescence could easily be recovered by transfer of the quencher (picric acid) to organic phase (Figure 5.1). The reversible change in luminescence could be used to build molecular switch. The OFF condition is achieved by interaction of Cdots with picric acid (no fluorescence) and the ON condition is through the phase transfer of the acid.

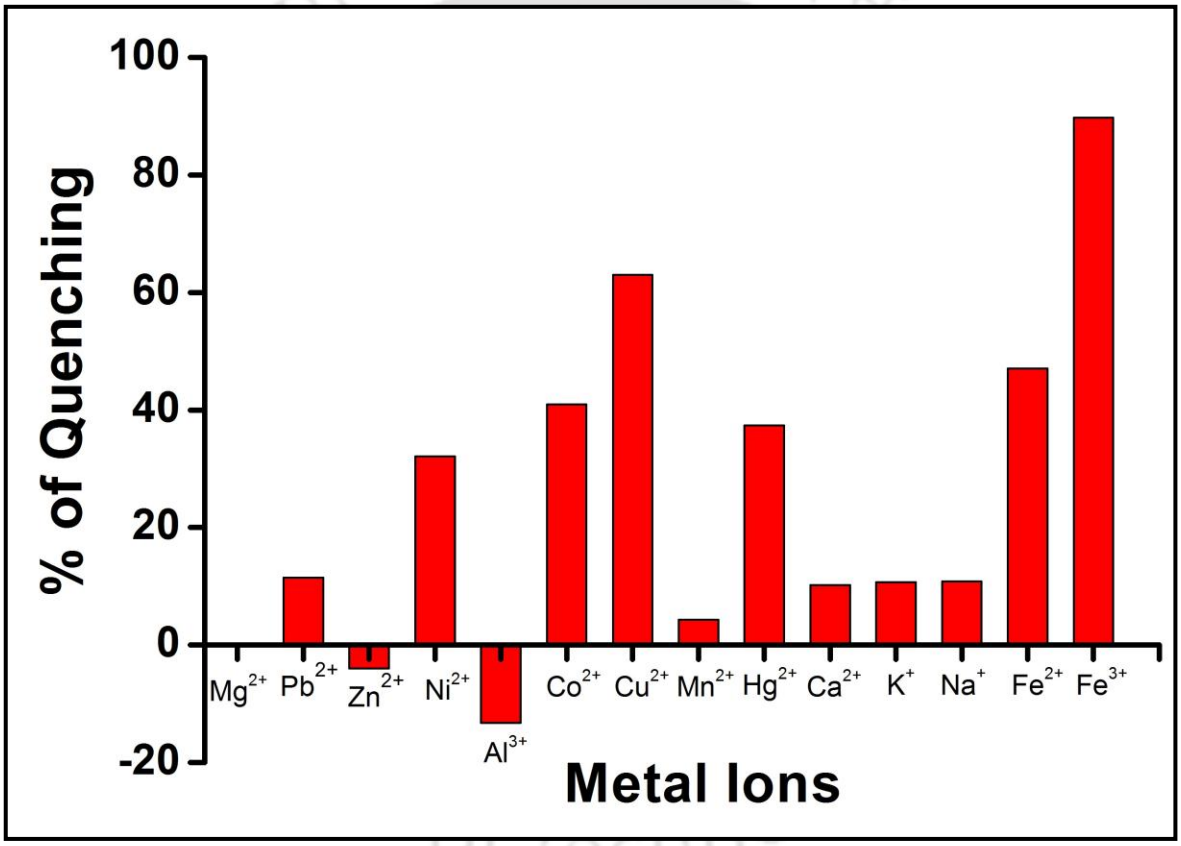

Figure 5.2. Relative photoluminescence emission of Cdots (0.01 mg/ml) following addition of various ions with final concentration of 100 μM for each ion.

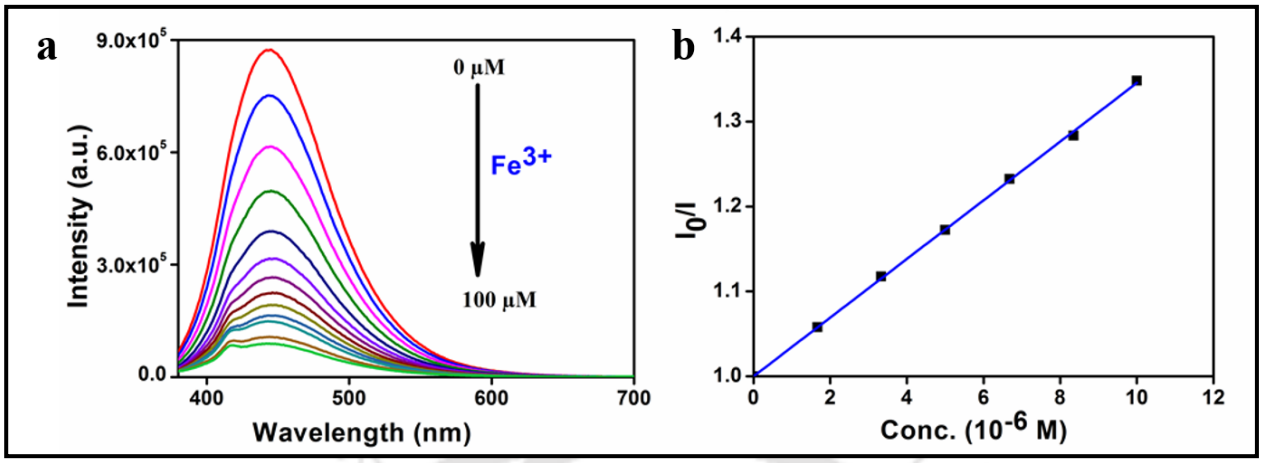

Figure 5.3. (a) Quenching of emission of Cdots (0.01 mg / mL) by Fe^{3+} ions (with $FeCl_3$ concentration varying from 0 to 100 μM) in water (λ_{ex}=365 nm). **(b)** Stern-Volmer plot with respect to the quenching of luminescence (conc. of $FeCl_3$ used was up to 10 μM). Stern-Volmer constant (K_{sv}) was calculated to be 3.46 x 10^4 M^{-1}.

Basic Gates. The as-synthesized luminescent Cdots were considered as the initial system for demonstration of NOT logic. On exposure to picric acid (input logic 1), the photoluminescence was quenched (output logic 0). When picric acid was absent (input logic 0), the inherent emission had remained (output logic 1). The behaviour suits the logical NOT operation as shown in Figure 5.4a. However, the same demonstration can also be made with Fe^{3+} input - as shown in the Figure 5.4a - in place of picric acid. It has been established that photoluminescence of Cdots can be quenched through the interaction with metal ions [111]. The relative variations in emissions when the Cdots were treated with metal ions is shown in the Figure 5.2 & 5.3. The Cdots were found to be highly responsive to Fe^{3+} ions as evident from the figures. Literature reports suggest that quenching of Cdot emission by metal ions could be due to dynamic quenching based on the ultrafast electron-transfer between the two species [111].

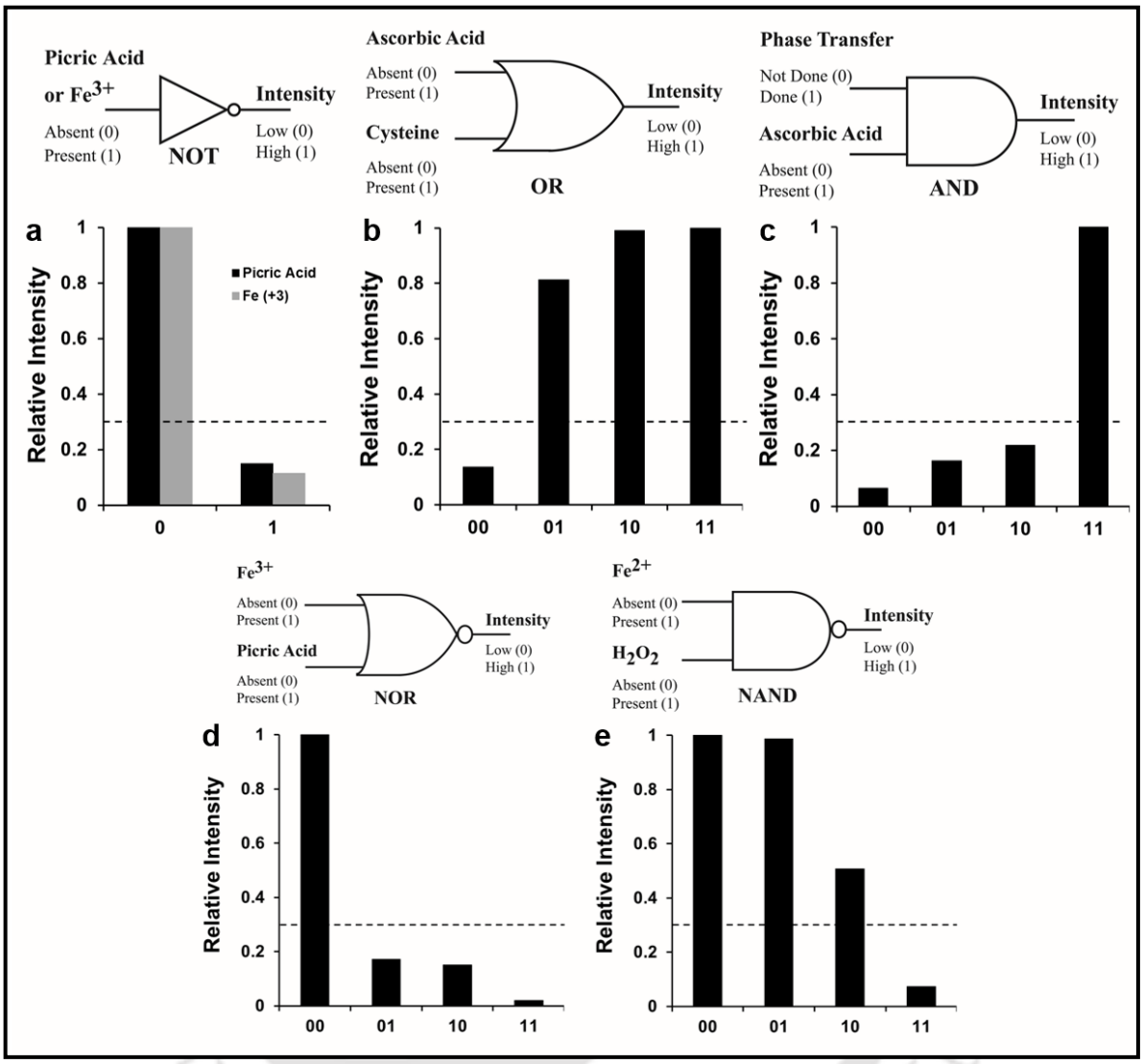

Figure 5.4. Basic and Universal Gates. (a) The NOT gate was constructed by probing the carbon dot luminescence with picric acid or Fe^{3+} as the input. **(b)** OR logic was obtained using a composite system comprised of Cdots and Fe^{3+} with ascorbic acid and cysteine as inputs. **(c)** AND logic behaviour was also obtained using a composite system constructed with Cdots, picric acid and Fe^{3+}. The inputs for this logic were chosen to be the phase transfer process and ascorbic acid. **(d)** The as synthesized Cdots functioned as NOR gate in presence of inputs Fe^{3+} and picric acid. **(e)** The Cdots functionality could be tuned with Fe^{2+} and H_2O_2 to develop NAND logic structure. (λex = 365 nm, λem = 443 nm)

Interestingly, when Fe^{3+}-treated Cdots were subsequently exposed to cysteine, the recovery of luminescence could be observed. This is possibly due to the formation of Fe^{3+}-cysteine

complex [195], which led to the removal of Fe^{3+} attached to the Cdots. The quenching of fluorescence in the presence of Fe^{3+} ions and then recovery following treatment with cysteine could be considered as cascading of two NOT gates, resulting in the formulation of YES gate as shown in the Figure 5.5.

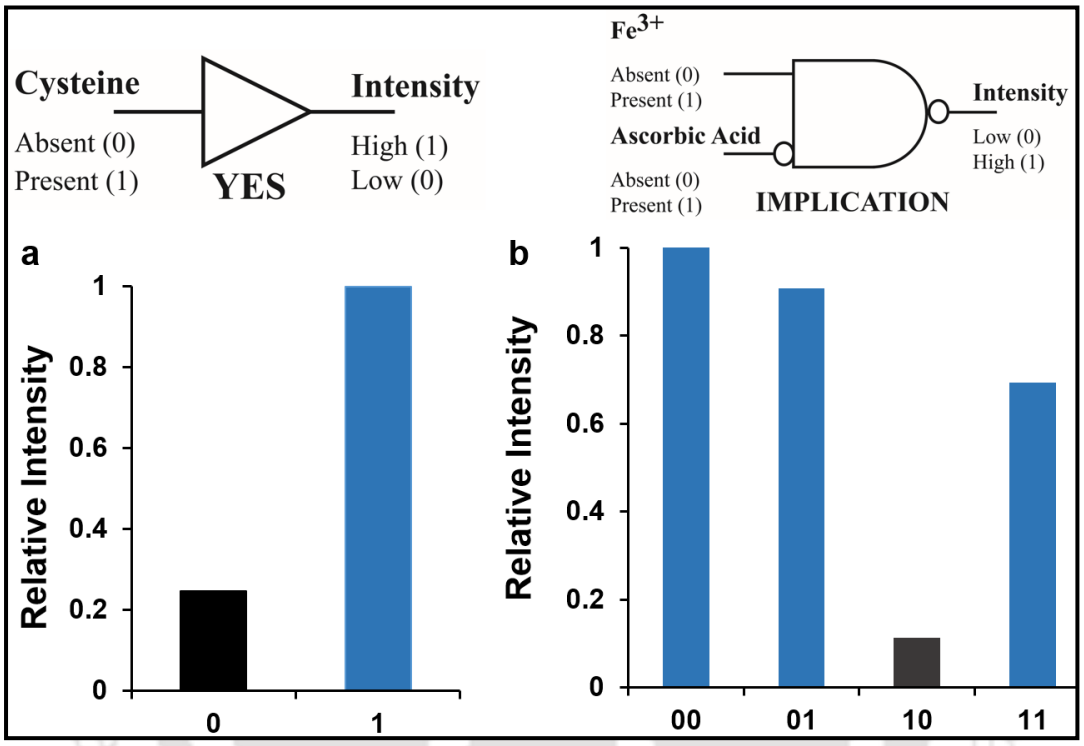

Figure 5.5. Basic Gates. **(a)** The basic logic gate YES was built from the composite system of Cdots and Fe^{3+} with cysteine as the input. The system is non- fluorescent in the absence of the input Cysteine (input logic 0) but is luminescent only in the presence of the input (input logic 1). **(b)** The other basic logic structure IMPLICATION could be constructed by probing the Cdots with the inputs Fe^{3+} and ascorbic acid. The logic table can be found in the Table 5.1(refer to page no. 94).

As mentioned earlier, the fluorescence of the composite system of Cdots and Fe^{3+} is absent or considerably low below the threshold. However, the fluorescence can be generated back upon treatment with either ascorbic acid or cysteine or both. While ascorbic acid reduces Fe^{3+} to Fe^{2+}, cysteine forms complex with Fe^{3+} leading to the recovery of fluorescence [195-196]. This composite system of Cdots and Fe^{3+} with ascorbic acid and cysteine as inputs suits OR logic, as shown in Figure 5.4b. When both the inputs were absent (input logic 00), the luminescence

intensity was low (output logic 0). On introduction of any one of the inputs (input logic 01, 10) or both the inputs (input logic 11), the luminescence recovered (output logic 1).

Another composite system consisting of a mixture of Cdots, picric acid and Fe^{3+} ions exhibits no fluorescence emission as it is collectively quenched by picric acid and Fe^{3+}. The recovery of fluorescence of this composite system can only be achieved if the effects of both picric acid and Fe^{3+} ions were nullified. The effect of picric acid can be negated with the transfer of the quencher (picric acid) to organic phase (Figure 5.1). On the other hand, addition of ascorbic acid reduces the Fe^{3+} ion to Fe^{2+} ion thus eliminating the quencher's effect. Hence, to revive the fluorescence (output logic 1), both the inputs are essential (input logic 11) and cannot be achieved (output logic 0) with no input (input logic 00) or single input (input logic 10 or 01). Thus, the system demonstrated the capability of the AND logic operation as shown in Figure 5.4c.

Another basic logic, i.e. IMPLICATION could be achieved by probing the Cdots with inputs Fe^{3+} and ascorbic acid as shown in Figure 5.5b. The output of this logic stays low (output logic 0) i.e. absence of luminescence above threshold, only when the first input, i.e. Fe^{3+} is solely present (input logic 10). In all other cases, i.e. input logic (00), (01) and (11), the output is high. The logic tables for the basic gates are illustrated in the Table 5.1 (refer to page no. 94).

Universal Gates. The universal gate i.e. NOR logic gate was built using the as-synthesized Cdots. The inputs for this gate were chosen to be picric acid and Fe^{3+}. The system exhibits inherent fluorescence (output logic 1) when inputs are absent (input logic 00). Introduction of picric acid or Fe^{3+} (input logic 10 or 01) or both (input logic 11) quenched the luminescence of Cdots (output logic 0) as illustrated in Figure 5.4d justifying the logic of NOR gate. Another universal gate, NAND is presented in Figure 5.4e. Here, the system was constructed with synthesized Cdots using inputs as Fe^{2+} and hydrogen peroxide. It is observed that the luminescence of Cdots was present (output logic 1) in all three cases of inputs, i.e. either both inputs were absent (input logic 00) or any one of the inputs was present (input logic 10 or 01). But when both Fe^{2+} and H_2O_2 were introduced (input logic 11), H_2O_2 oxidized Fe^{2+} to Fe^{3+} which eventually resulted in quenching of fluorescence (output logic 0). The logic tables for the universal gates are illustrated in Table 5.2 (refer to page no. 94).

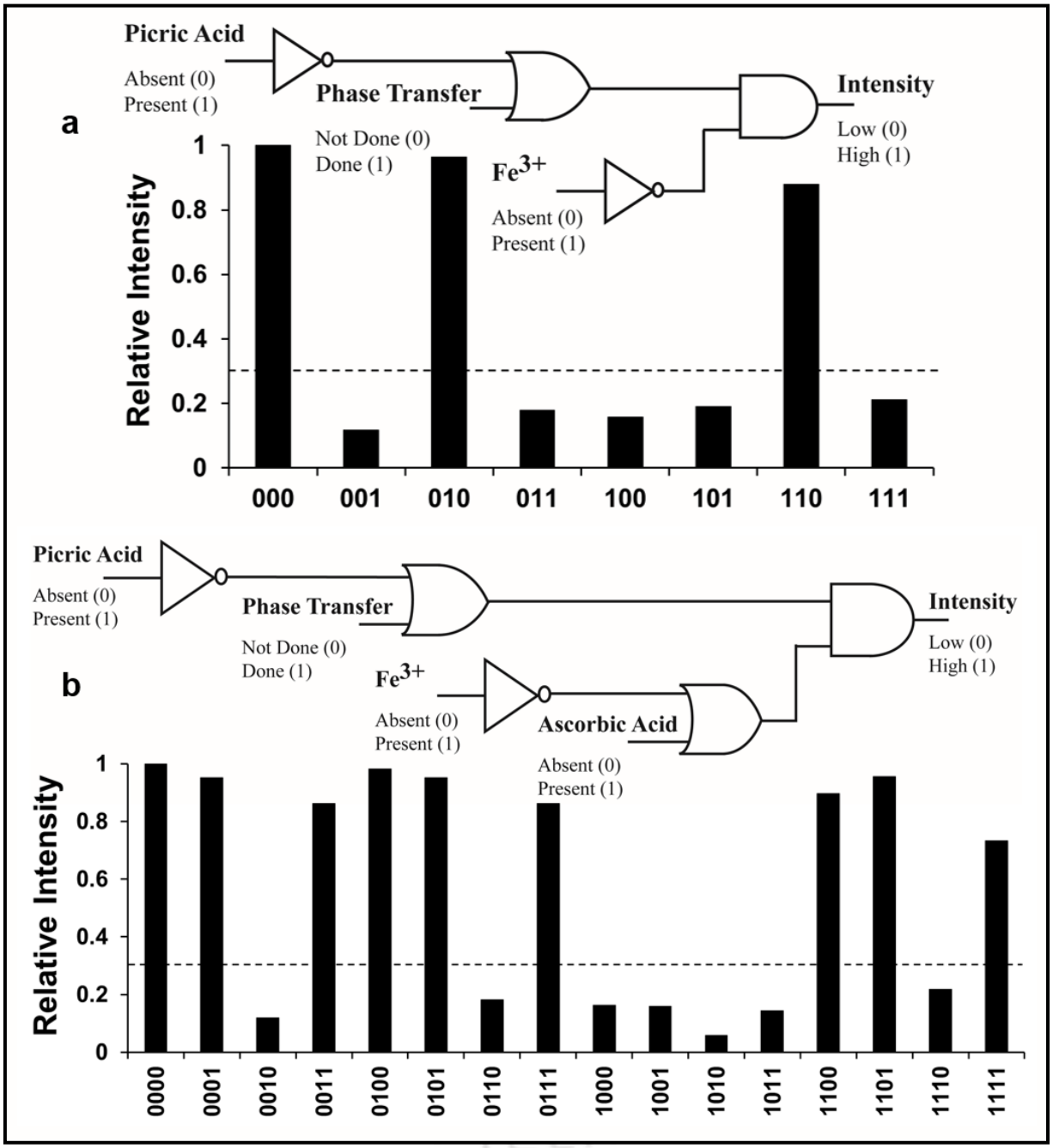

Figure 5.6. Higher Logical Systems. A hierarchical logic system was built using a three input system or four input system to obtain higher logical function such as,

(a) $(\overline{Picric\ Acid} + Phase Transfer) \cdot \overline{Fe^{3+}}$

(b) $(\overline{Picric\ Acid} + Phase Transfer) \cdot (\overline{Fe^{3+}} + Ascorbic\ Acid)$

Construction of Higher Logical Functions. Evidently from above, the luminescence of Cdots could be tuned with different inputs. I observed that the combination of the inputs could also be used effectively in constructing higher order logic systems through effective integration. Thus, construction of two integrated structures were demonstrated with Cdots as initial system as shown in Figure 5.6. In both the proposed logic, the inputs must be provided in sequential order; i.e., picric acid, phase transfer, Fe^{+3} and ascorbic acid are to be given in that sequential order. The first integration, as shown in Figure 5.6a, was done using three inputs, while the second one was achieved with four inputs as shown in Figure 5.6b. In the first of the integrated systems, picric acid, the phase transfer based recovery of Cdots and the Fe^{3+} ions were used as inputs. The function that was achieved is $(\overline{Picric\ Acid} + Phase\ Transfer) \cdot \overline{Fe^{3+}}$. While picric acid was used in the first stage, the phase transfer process was carried out in the next level. Following this, Fe^{3+} ions were introduced as shown in Figure 5.6a. The Cdots were inherently luminescent in the absence of all the inputs (input logic 000). The introduction of picric acid or Fe^{3+} separately or collectively (input logic 001, 100, 101) quenched the luminescence of the Cdots. Further the system possesses the capability to reset the effect of picric acid through phase transfer (input logic 110, 111). The logic table for the function is shown in Table 5.3 (refer to page no. 95).

In the second integrated structure, in addition to the above mentioned inputs, another input in the form of ascorbic acid was added in the last stage, as shown in Figure 5.6b. The logical function which was achieved this way is $(\overline{Picric\ Acid} + Phase\ Transfer) \cdot (\overline{Fe^{3+}} + Ascorbic\ Acid)$. The introduction of individual inputs, i.e. picric acid and Fe^{3+}, either separately or collectively quenched the luminescence as earlier (input logic 1000, 1010, and 0010). However, the system further possesses the capability to reset the individual or combined effects of picric acid and Fe^{3+} inputs through the other inputs, i.e. phase transfer process and ascorbic acid (logic input 1100, 0011, 1111). The logical output and the sequencing of gates are shown in Figure 5.6b. All the logical combinations are illustrated in Table 5.4 (refer to page no. 95).

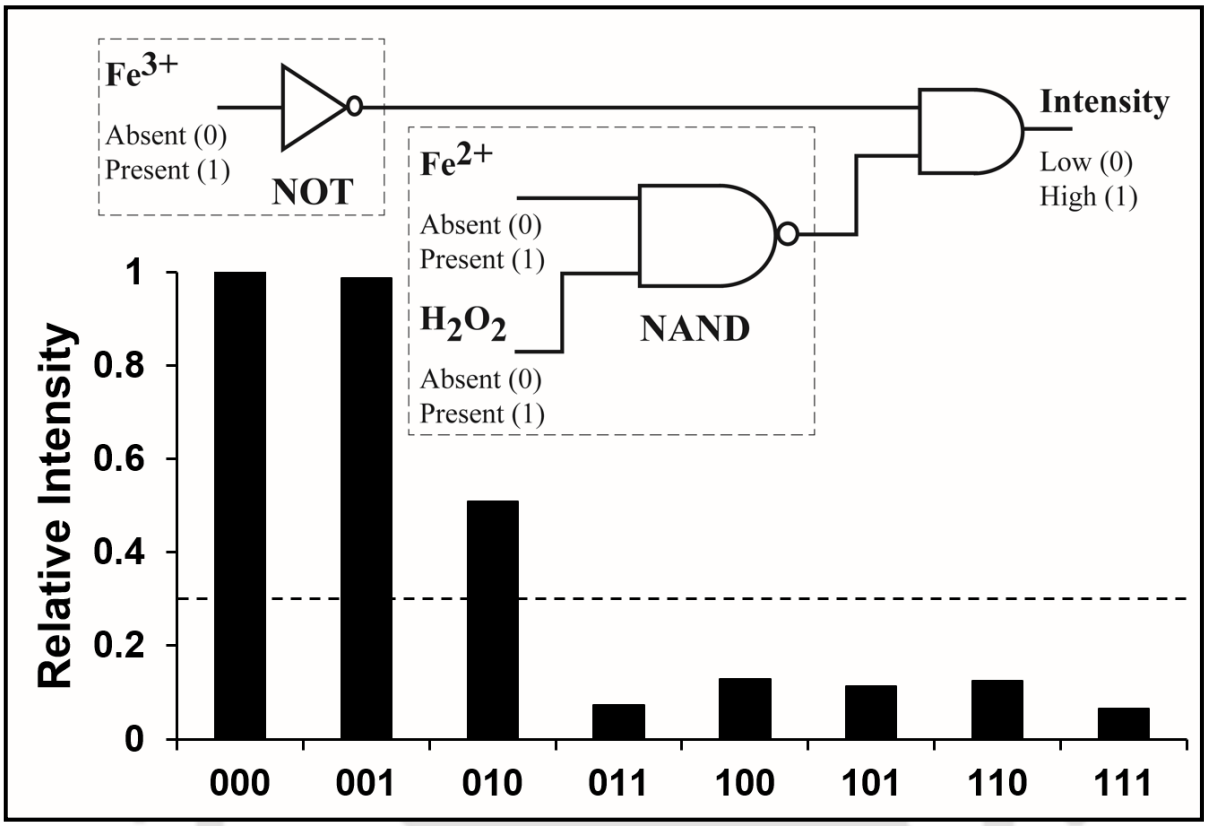

Figure 5.7. Cascading of Simple gates for Complex Logic Formulation. Here, two independently functional gates, i.e., the basic gate NOT in the first stage and the universal gate NAND in the second stage were cascaded in the third stage to be logically ANDed to obtain the function, $\overline{Fe^{3+}} \cdot (\overline{Fe^{2+} \cdot H_2O_2})$. Through this formulation, Cdots could be used to probe Fe^{3+} over Fe^{2+} using H_2O_2. (λ_{ex} = 365 nm, λ_{em} = 443 nm).

Cascading of Individual Gates for Higher Logical Functions. A deeper investigation revealed the possibility of cascading the above mentioned simple logic gates (basic, universal) into higher logical functions. Here, the ones demonstrated could achieve the logic function, $\overline{Fe^{3+}} \cdot (\overline{Fe^{2+} \cdot H_2O_2})$ through cascading of basic gate NOT and universal gate NAND, which were demonstrated earlier in Figure 5.4. The inputs can be added in any order to achieve a particular input combination. The starting system for this integration was the as-prepared Cdots. The basic gate NOT was operated in first stage and the universal gate NAND was operated in second stage. Finally, the outcome of those two stages (gates) was combined with logic operation AND in the third stage. This is an important logical function particularly in biological environment[111], which identifies that the Cdots were responsive towards Fe^{3+} alone

(input logic 011,100,101,110,111) and not Fe^{2+} (input logic 001, 010) as shown in Figure 5.7. This logic system is typically useful to detect Fe^{3+} over Fe^{2+}. Thereby, Cdots could be used as a probe to discriminate Fe^{3+} and Fe^{2+} using hydrogen peroxide. The detection of Fe^{2+} ion was made possible through the oxidation of Fe^{2+} to Fe^{3+} using hydrogen peroxide as the oxidizing agent. The logical combinations for the cascaded system are given in Table 5.5 (refer to page no. 96).

Solid Phase Simple, Integrated and Cascaded Logic Systems. One of the important requirements of molecular electronics for its future development is the ability to function in versatile environment. It would be even more useful if the functional components behave in a similar fashion in environment such as in different phases. For example, if the properties of the Cdots were similar in liquid and solid phases, with respect to interactions with molecular species, then the same principle could be used for computation. I report here that photoluminescence properties of Cdots with respect to interactions with molecular species as mentioned above were identical when they (Cdots) were dispersed in water or in the solid phase. More importantly, the logical structures, including integration to higher levels, could be achieved following deposition of the Cdots on non-fluorescent paper. In other words, the Cdots drop-cast on non-fluorescent paper exhibited similar change in emission in the presence of the above mentioned species. The solid phase depiction of these logic systems under UV excitation is shown in Figure 5.8.

The procedure to construct these logical structures is described in experimental section. Typically, starting with the liquid ink spotted on the non-fluorescent paper, the initial system for a particular logic is defined by the dried spot. The inputs (in the liquid phase) are placed on the dried spot one after the other as per combination and dried. The presence of blue spot under UV illumination suggested the existence of fluorescence (output logic 1) for that particular input combination listed above/below the spot. On the other hand, absence of the blue spot suggests the lack of fluorescence (output logic 0). The corresponding truth tables for the denoted logic is given in Table 5.1-5.5 (refer to page no. 94-96). It is worth mentioning here, that the substrate – a non-fluorescent paper - did not get affected even after achieving four-level-integration. More importantly, sequential addition of chemical species provided exact reproduction of emission behaviour of the Cdots as in the liquid phase. Such unique behaviour of Cdot based logic systems offers great scope in construction of logic based bioassays and environmental logical sensors. Thus the robust solid state bio-friendly logic systems could demonstrate not only simple but also cascaded and integrated higher logic. They offer a bright prospective to develop systems akin to conventional silicon based electronics to be able to operate in places where the conventional electronics might fail.

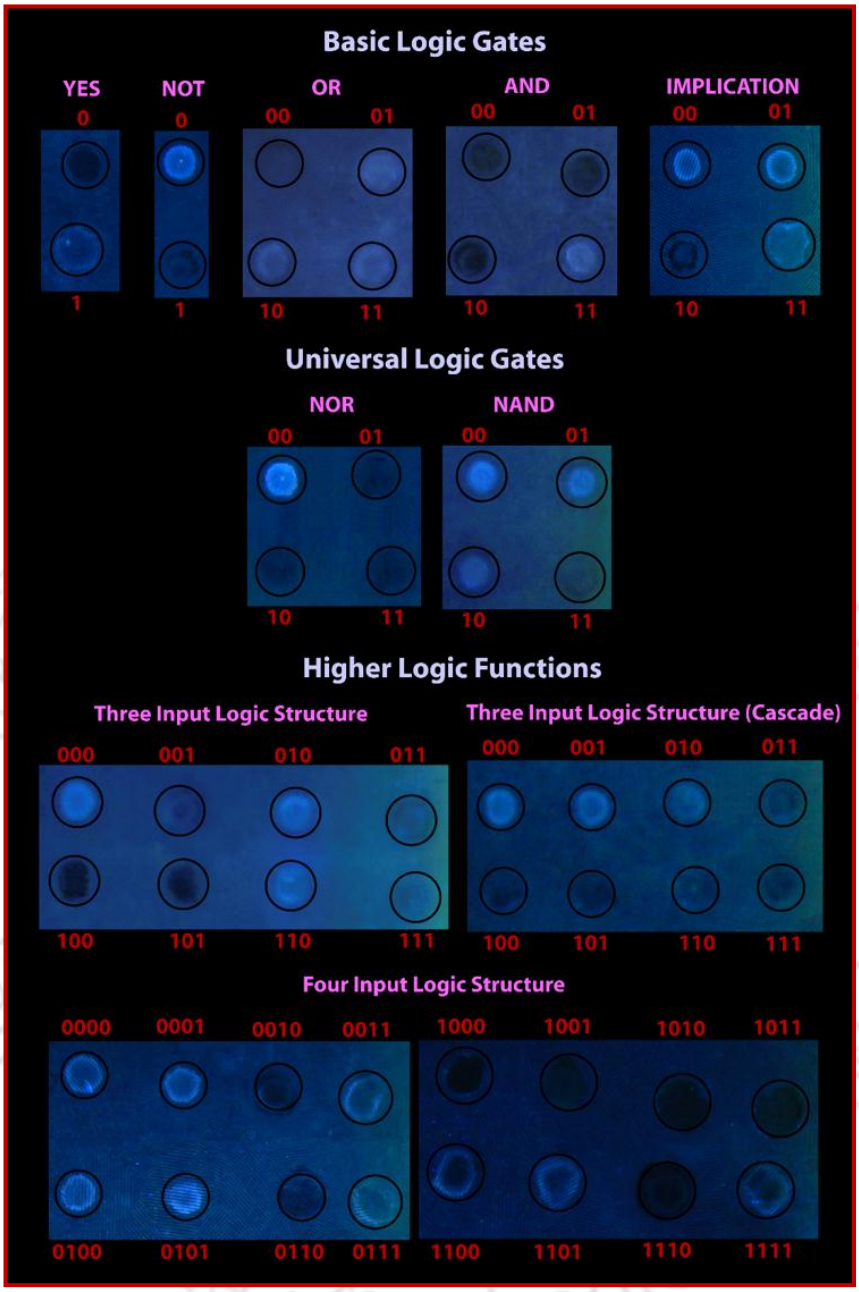

Figure 5.8. Solid Phase Logic Implementation on a Non-Fluorescent Paper. The logic, both simple and complex could also be performed in solid form of the substrate in addition to being in the liquid media. The demonstration of logic in solid state was achieved on typical non-fluorescent paper. The output logic was monitored under the UV illumination. The output logic 1 is indicated here through the fluorescence (blue dot) and the absence denotes the output logic 0 for a particular combination of inputs as indicated in liquid phase (refer to Logic Table, Table 5.1-5.5, refer to page no. 94-96). (λ_{ex} = 365 nm, λ_{em} = 443 nm)

5.4. CONCLUSIONS

In conclusion, I constructed a series of basic logic gates, universal logic gates, molecular switch and also integrated basic structures to higher levels through introduction of Cdots in the molecular logic family, in order to provide further advances in molecular logic systems. The system is robust and could operate in dual phases, i.e., in both liquid media as well as in the solid phase. Building such dual phase operative simple and complex logic systems offers various applications for analytical purposes in biological system, such as detection of hazardous materials in environment, implementation of solid state logic for detection of chemicals. This work is expected to draw attention towards constructing logical systems - in terms of both simple and complex - which are functional in multiple phases and would operate in diverse environment.

Logic Tables

The initial system for the logic is indicated below the respective gate name. The inputs used are also indicated for each gate. Output 1 denotes the existence of luminescence crossing the threshold.

Table 5.1. Logic table of Basic Gates.

YES		NOT	
Cdots and Fe^{3+}		Cdots	
Input	Output	Input	Output
Cysteine		Picric Acid or Fe^{3+}	
0	**0**	0	**1**
1	**1**	1	**0**

OR			AND			IMPLICATION		
Cdots and Fe^{3+}			Cdots, Fe^{3+} and Picric Acid			Cdots		
Input 1	Input 2	Output	Input 1	Input 2	Output	Input 1	Input 2	Output
Ascorbic Acid	Cysteine		Phase Transfer	Ascorbic Acid		Fe^{3+}	Ascorbic Acid	
0	0	**0**	0	0	**0**	0	0	**1**
0	1	**1**	0	1	**0**	0	1	**1**
1	0	**1**	1	0	**0**	1	0	**0**
1	1	**1**	1	1	**1**	1	1	**1**

Table 5.2. Logic table of Universal Gates.

NOR			NAND		
Cdots			Cdots		
Input 1	Input 2	Output	Input 1	Input 2	Output
Fe^{3+}	Picric Acid		Fe^{2+}	H_2O_2	
0	0	**1**	0	0	**1**
0	1	**0**	0	1	**1**
1	0	**0**	1	0	**1**
1	1	**0**	1	1	**0**

Table 5.3. Integration to Higher Logic (3 Input Logic Function).

3 INPUT COMPLEX LOGIC			
Cdots			
$(\overline{Picric\ Acid} + Phase\ Transfer) \cdot \overline{Fe^{3+}}$			
Input 1	Input 2	Input 3	Output
Picric Acid	Phase Transfer	Fe^{3+}	
0	0	0	**1**
0	0	1	**0**
0	1	0	**1**
0	1	1	**0**
1	0	0	**0**
1	0	1	**0**
1	1	0	**1**
1	1	1	**0**

Table 5.4. Integration to Higher Logic (4 Input Logic Function).

4 INPUT COMPLEX LOGIC									
Cdots									
$(\overline{Picric\ Acid} + Phase\ Transfer) \cdot (\overline{Fe^{3+}} + Ascorbic\ Acid)$									
Input 1	Input 2	Input 3	Input 4	Output	Input 1	Input 2	Input 3	Input 4	Output
Picric Acid	Phase Transfer	Fe^{3+}	Ascorbic Acid		Picric Acid	Phase Transfer	Fe^{3+}	Ascorbic Acid	
0	0	0	0	**1**	1	0	0	0	**0**
0	0	0	1	**1**	1	0	0	1	**0**
0	0	1	0	**0**	1	0	1	0	**0**
0	0	1	1	**1**	1	0	1	1	**0**
0	1	0	0	**1**	1	1	0	0	**1**
0	1	0	1	**1**	1	1	0	1	**1**
0	1	1	0	**0**	1	1	1	0	**0**
0	1	1	1	**1**	1	1	1	1	**1**

Table 5.5. Integration to Higher Logic through Cascading of Individual Gates.

3 INPUT COMPLEX LOGIC			
Cdots			
$\overline{Fe^{3+}} \cdot \overline{(Fe^{2+} \cdot H_2O_2)}$			
Input 1	Input 2	Input 3	Output
Fe^{3+}	Fe^{2+}	H_2O_2	
0	0	0	**1**
0	0	1	**1**
0	1	0	**1**
0	1	1	**0**
1	0	0	**0**
1	0	1	**0**
1	1	0	**0**
1	1	1	**0**

CHAPTER-6

Cu^{2+} - embedded Carbon Nanoparticle as an Anticancer Agent

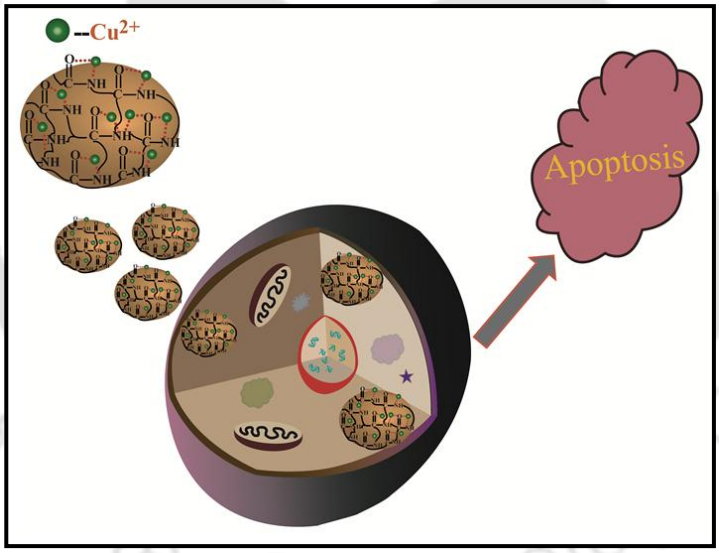

Highlights:

- *Design of CNP based fluorescent anticancer agent.*
- *'Apoptosis' mode of cell death due to ROS generation.*

6.1. INTRODUCTION

Metal-complexes offer a different platform for therapeutics [199-201]. In this regard, the clinical success of anti-cancer drug cisplatin (a Pt-complex) could be considered to have been a precursor to search for other complexes as more potent drugs, with improved pharmacological properties, for cancer and other diseases. Thus complexes of copper, gold, titanium and ruthenium have been synthesized for cancer therapy with increased pharmacological values [201]. Copper complexes are more popular as the metal is endogenous and thus less cytotoxic; also, there are sequestering agents available for removal of excess copper from human body [199]. Importantly, it has been reported that copper complex can alter the metabolism of cancer cells as well as induce apoptotic cell death [199]. Further, recent reports on the use of copper oxide nanoparticles (Cu_xO; x=1,2) and copper nanoclusters suggest generation of reactive oxygen species (ROS), leading to DNA damage [202-205]. It may be that the dissolution of copper ions (from the nanomaterials) and the redox activity of the surface ions are responsible for ROS generation in biological and environmental media [204]. Thus the use of copper ions as a drug itself may be of significance. However, an important challenge would be to deliver copper ions to target sites with high efficiency and with minimum circulation loss [199-201, 207]. In addition, efficient cellular uptake of copper related nanomaterials or metal-complexes is vital to their potential for practical usage [202, 204, 206]. A conventional option is to develop suitable delivery vector for the materials [208- 211]. On the other hand, it could also be possible through designing a new system where metal-complexes are formed on the surface of appropriate carriers to deliver metal ions. An ideal carrier could be made out of carbon nanoparticle (CNP).

In this chapter I have presented an easy and bio-friendly method of synthesis of Cu^{2+} embedded in CNP (Cu-CNP) in aqueous medium, which was used as an effective anticancer agent for killing cervical cancer HeLa cells. The average size of the Cu-CNP was 92.7 ± 49.8 nm. The size was chosen so that the Cu^{2+}-containing CNPs could be used for practical application using enhanced permeation and retention (EPR) effect. Further, the inherent blue emission of CNP could be used to monitor the cellular uptake using a confocal microscope. The cell viability study in presence of Cu-CNP was carried out by standard MTT assay followed by cell cycle analysis, where it has been found to undergo apoptosis. Further, evidences suggest that the generation of ROS in the cells might have led to apoptosis.

6.2. EXPERIMENTAL

Materials. Citric acid, ethylenediamine, NaOH and $CuSO_4.5H_2O$ were purchased from Merck, India. The dialysis membrane (dialysis tubing, benzoylated) was purchased from Sigma-Aldrich, India. All the materials were used as received without further purification. Elix grade water was used in all the experiments. The induction cooker and non-stick frying pan were procured from Philips (model no. HD4908, 220-240V AC, 50/60 Hz) and Prestige, India, respectively.

Preparation of Carbon Nanoparticlecs (CNP). CNP were synthesized by slight modification of a previously reported method from the laboratory as discussed in chapter-4. In brief, 50 mL aqueous solution containing mixture of 630 mg citric acid and 134 μL ethylenediamine (in 3:2 molar ratio) in a non-stick frying pan was heated using induction heater at 100 ^oC for 15 min. Then the dark brownish syrup was purified by dialysis method using 1 KDa dialysis membrane. TEM image of the particles synthesized is shown at Figure 6.3(e). The longer heating time possibly made the sizes of CNP bigger than those reported earlier in chapter-4.

Preparation of Cu^{2+} embedded Carbon Nanoparticlecs (Cu-CNP). The whole amount of purified aqueous CNP was taken in a round bottom flask and the final volume was made up to 12 mL. Then, solid NaOH (~ 80 mg) was added to it with stirring to ensure the pH of the solution to be in between 9-11. After 5 min of stirring, 100 mg $CuSO_4$ (0.4 mM) was added to it and the mixture was stirred for 2 h at 50 ^oC. The color of the reaction mixture turned greenish.

Purification of Cu-CNP. The as-synthesized Cu-CNP was purified by centrifugation. The reaction mixture was centrifuged at 12000 rpm for 10 min using acetone (the ratio of reaction mixture and acetone was 3:1). The dark greenish pellet was isolated but not used for further application as the quantum yield of redispersion of the dark greenish pellet was low (15.9%). On the other hand, the supernatant was separated out and centrifuged at 25000 rpm using acetone (the ratio of reaction mixture and acetone was 11:1) and the final centrifuged Cu-CNP was then dried at 40 ^oC for 12 h. The greenish dry pellet was redispersed in water prior to further use as well as for characterizations. The redispersion of Cu-CNP appeared brownish orange in visible light (with a photoluminescence quantum yield of 27.9%, the details of which are mentioned below).

Analytical Measurements. The products were characterized using transmission electron microscopy (JEOL 2100 UHR-TEM, operating at 200 KV), UV-vis spectroscopy (Hitachi U 2900 spectrophotometer), photoluminescence spectroscopy (Horiba Fluoromax-4 spectro fluorometer), powder X-ray diffraction (Brucker D8 advanced X-ray diffraction measurement system) with Cu Kα source (λ=1.54 Å), nuclear magnetic resonance spectroscopy (Bruker, 600 MHz), Fourier transform infrared spectroscopy (Perkin Elmer IR spectrometer), electron paramagnetic resonance (JEOL, Model: JESFA200) spectrometry, particle size analysis (Malvern zeta size; Nano ZS 90). Inductive coupled plasma optical emission spectrometer-optical emission spectrometer (ICP-OES) measurement was performed with Thermo-iCAP 6000 Series. Cell cycle was analyzed by FACS (fluorescence-activated cell sorting) Calibur, BD Biosciences. Field Emission Scanning Electron Microscope (FESEM) analysis for untreated and treated Cells was done with Zeiss (Sigma) FESEM.

Quantum Yield Calculation with respect to Quinine sulphate (QS) in 0.1 M H_2SO_4. I have calculated Quantum yield with respect to quinine sulphate using the formula:

$$Q_S = Q_R \times \frac{I_S}{I_R} \times \frac{A_R}{A_S} \times \frac{\eta_S^2}{\eta_R^2}$$

Where, Q_S = quantum yield of sample; Q_R = quantum yield of reference; I_S = area under PL curve of sample; I_R = area under PL curve of reference; A_R = absorbance of the reference; A_S = absorbance of the sample; η_S = refractive index of sample; η_R = refractive index of reference.

Q.Y. of quinine sulphate = 0.54, Refractive Index of water = 1.33

(The concentration of all samples and the reference quinine sulphate were adjusted so that the optical densities of all samples were 0.100 ± 0.003 at the excitation wavelength (365 nm).

Cell Based Experiments:

Cell Culture. HeLa cells (human cervical carcinoma) were acquired from National Centre for Cell Sciences (NCCS), Pune. For growing HeLa cells Dulbecco's Modified Eagle's Medium was used which was purchased from Sigma Aldrich along with L-glutamine (4 mM), penicillin (50 units/mL), streptomycin (50 mg/mL) which were mixed with the medium. Into

that, 10% (v/v) fetal bovine serum was added, which was procured from PAA Laboratories, Austria. The cells were grown in CO_2 incubator with 5% CO_2 at 37 °C.

Cell viability assay. To quantify the viable cells following the 48 h treatment with Cu-CNP, the cell viability assay was carried out. In this regard, approximately 1×10^5 cells/well were seeded in 96-well micro plate and was kept for overnight incubation, in the presence of 5% CO_2 at 37 °C. The grown cells were then treated with various concentrations of Cu-CNP with copper concentration of (0.75 ppm – 2.5 ppm), along with various CNP concentrations separately (20-80 ppm), under identical conditions for 48 h. After the treatment, the number of viable cells was estimated by performing MTT assay. For MTT reaction 7 µl of [3-(4,5-dimethylthiazol-2-yl)-2,5-diphenyltetrazolium bromide] was added and incubated for 2 h in the above mentioned condition wherein respiratory mitochondria reduced MTT into color formazan. After the incubation, the medium was discarded and the absorbance of formazan was measured at 550 nm by adding 70 µl of DMSO, which provides the number of viable cells. All the experiments were carried out in three sets with 100% number of viable cells for each experiment.

FACS Analysis for Reactive Oxygen Species Generation. Generation of reactive oxygen species was analysed by fluorescence based assay in FACS with the help of 2, 7-dichlorofluoresceindiacetate (DCFH-DA) dye. For this, the overnight grown cells (2 x 10^6 in 6 well plates) were treated with IC_{50} value dose of Cu-CNP and CNP for 3 h, prior to the incubation with 10 µL of 1 mM DCFH-DA at 37 °C for 10 min. DCFH-DA a non-fluorescent dye after its diffusion inside the cell is deacetylated by cellular esterase and is oxidized by ROS into 2, 7-dichlorofluroscein (DCF), which has high fluorescence with absorbance at 480 nm and emission at 530 nm. To determine the fluorescence, the treated cells were trypsinized and redispersed in fresh 1 mL DMEM medium and analyzed in a flow cytometer (FACS Calibur, BD Biosciences). The fluorescence data were recorded in cell Quest Program with fixed 15000 cells for each sample and was collected in Fl-1 channel (530/30), which corresponds to green fluorescence.

FESEM Analysis for Untreated and Treated Cells. For FESEM analysis cells were grown in 35 mm culture plate for 12 h followed by treatment with IC_{50} dose of Cu-CNP for 24 h in case of treated sample. After trypsinization, the cells were fixed with 4% formaldehyde and kept for 10 min incubation at 37 °C.The cells were collected after centrifuging at 670 rcf for 6 min and immediately redispersed in chilled 70% ethanol. Then 20 µL of the sample was drop casted on a clean glass side with aluminum foil over it.

Cell Cycle Analysis by Propidium Iodide. Cell cycle analysis in FACS was carried out by using propidium iodide (PI) dye. For this 2 x 10^6 cells were seeded in 6 well culture plates for 12 h, in the same condition as mentioned above. The Cu-CNP at IC_{50} dose as well as CNP (separately) was added and kept for 48 h. After trypsinization, the cells were fixed with chilled 70% ethanol and kept for 1 h incubation at -20 ^oC. The fixed cells were re-dispersed in 1 mL PBS and were incubated in water bath at 37 ^oC with 100 µg/mL of RNase A for 45 min, followed by addition of 10 µL of PI under dark condition. After 30 min of incubation the PI fluorescence data for 15000 cells were analyzed in FACS Calibur by using cell quest program. PI binds with DNA and gives red emission which is collected at FL-2 channel (band pass filter 585/42nm).

Caspase 3-Assay. To further study apoptosis caspase 3-assay was conducted. The 6 well plates were seeded with 2x10^6 cells and were kept for 12 h as mentioned earlier. The cells were treated in a same manner as mentioned in other experiments and were incubated for 24 h. The cells were trypsinized and were fixed with 0.1% (v/v) formaldehyde and kept in dark for 10 min. To permeabilise the harvested cells, 0.5% Tween20 was added along with 1 mL of PBS. This was followed by two repetitive washing with PBS buffer and finally 8 µL of Caspase 3 (PE conjugated antibody) was added with 500 µL PBS buffer under dark condition. After 30 min the data were collected in FL-2 channel (band pass filter 585/42nm) with the help of cell quest program in FACS.

ICP-OES Analysis for Untreated and Treated Cells. Metal concentration inside the cells was determined by an ICP-OES. To carry out these experiments 6 well plates with 1x10^6 cells in 1.8 mL medium for each was incubated. The cells were than treated with IC_{50} dose of Cu-CNP or CNP for 4 h. After treatment and washing, the cells were treated with 3% sub-boiled HNO_3 for 2 h at room temperature. Afterwards the solutions were collected 15 mL tubes and prepared for ICP measurement. For the untreated cells the same procedure was repeated (in the absence of any nanoparticles).

6.3. RESULTS & DISCUSSION

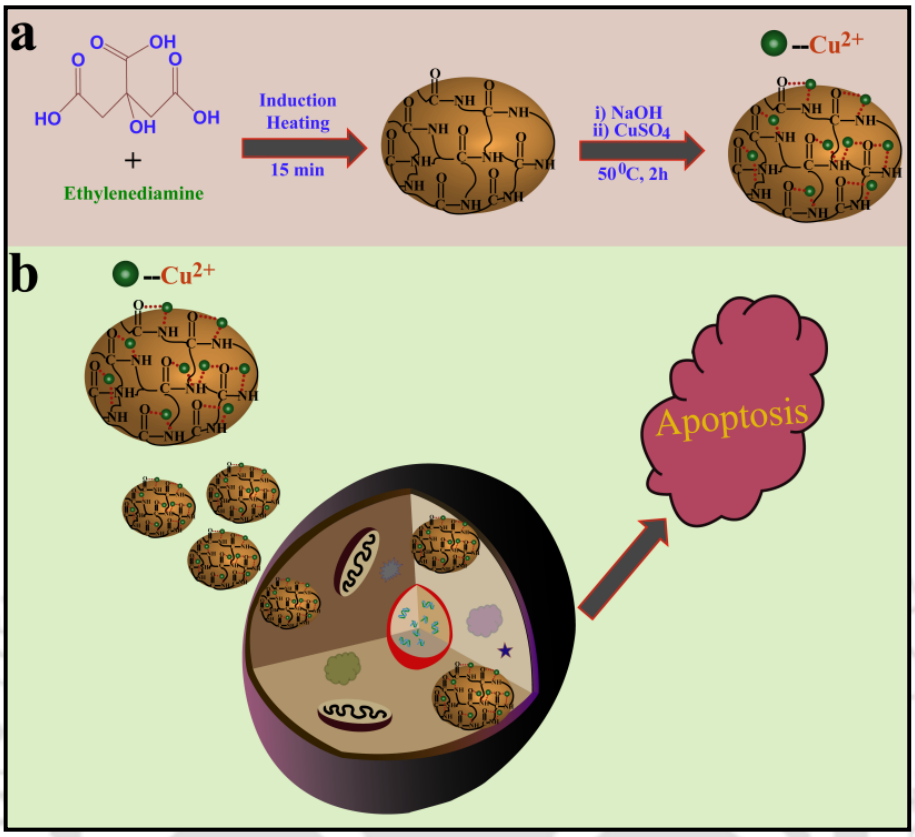

Scheme 6.1. Schematic representation of the (a) synthesis of Cu-CNP and (b) possible mode of uptake of Cu-CNP, leading to apoptotic cell death.

The synthesis of CNP was carried out based on a slight modification of a method developed in the laboratory as discussed in chapter-4 and using an induction coil heater. The Cu-CNP composite was synthesized using CNP and $CuSO_4$ in basic aqueous medium (pH=9-11) with constant stirring for 2 h, at 50 ^oC and the product was purified prior to further use. The brownish orange aqueous solution of dispersed Cu-CNP was used for further characterizations. The UV-visible spectra of the dispersed CNP and Cu-CNP are shown in Figure 6.1(a). The UV-vis spectrum of CNP consisted of a clear peak at 342 nm. On the other hand, the presence of Cu^{2+} led to significant change with a hump at the same peak position. The change in the UV-vis spectrum could be attributed to complex formation between Cu^{2+} and CNP. Further, the dispersion of Cu-CNP in water exhibited weak wavelength tunability in its emission (Figure. 6.1b). This is in consonance with earlier observations of emission of CNP as discussed in

chapter-4 prepared similarly. On the other hand, the photoluminescence quantum yield of the Cu-CNP was observed to be lower (27.9%) than that of the CNP (45.6%). This could be due to the quenching of the luminescence of CNP in the presence of Cu^{2+} as found in chapter-5.

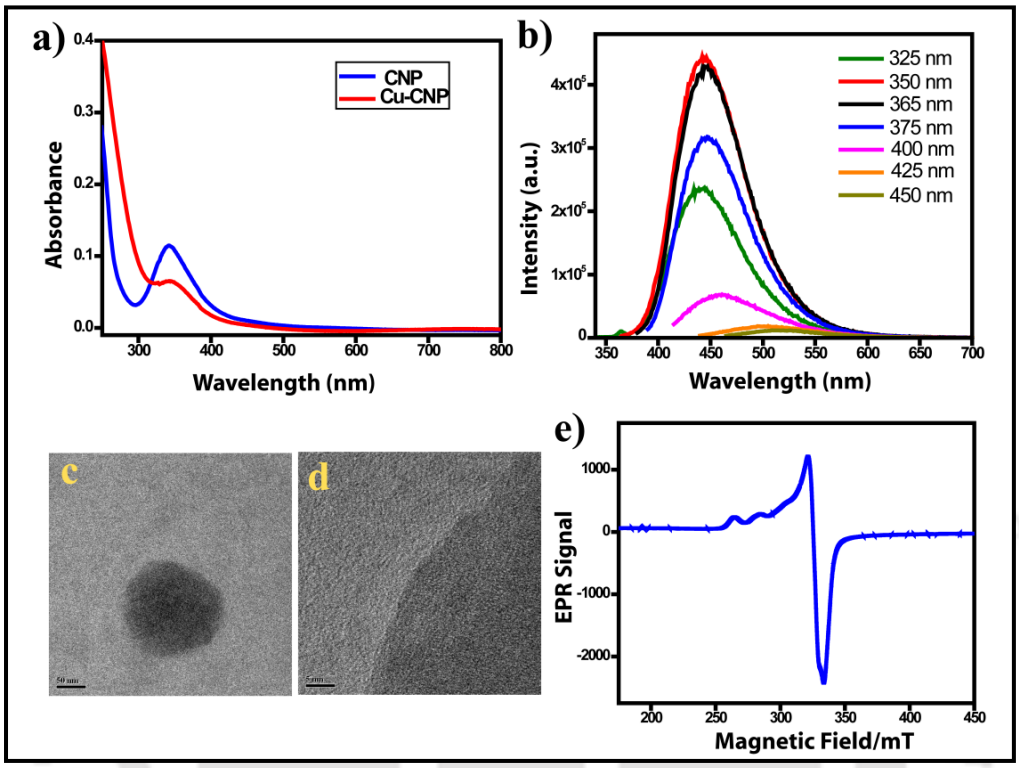

Figure 6.1. (a) Absorption spectra of the CNP and Cu-CNP in water. **(b)** Wavelength-dependent emission spectra of Cu-CNP in water. **(c)** TEM image of the Cu-CNP in a scale of 50 nm. **(d)** High resolution TEM image of Cu-CNP in a scale of 5 nm. **(e)** EPR spectrum of solid Cu-CNP.

It has been established that CNPs consist of different surface functional groups such as –OH, C–N–C, –NH, C=O and amide carbonyl group as discussed in chapter-4. Therefore, the surface functional groups of CNP could be reactive to metal ions, leading to the formation of inorganic complex. In the current context, the evidence of complexation of Cu^{2+} on the surface of the CNP was confirmed by Fourier transform infrared (FTIR) spectroscopy, the results of which indicated carbonyl stretching frequency shifts from 1709 cm^{-1} for the free amide carbonyl group on surface of the CNP to 1647 cm^{-1} upon complexation with Cu^{2+} (Figure 6.2). However, the peak at 1704 cm^{-1} of Cu-CNP may be due to the free amide carbonyl group not involved in complexation with Cu^{2+} on the surface of Cu-CNP.

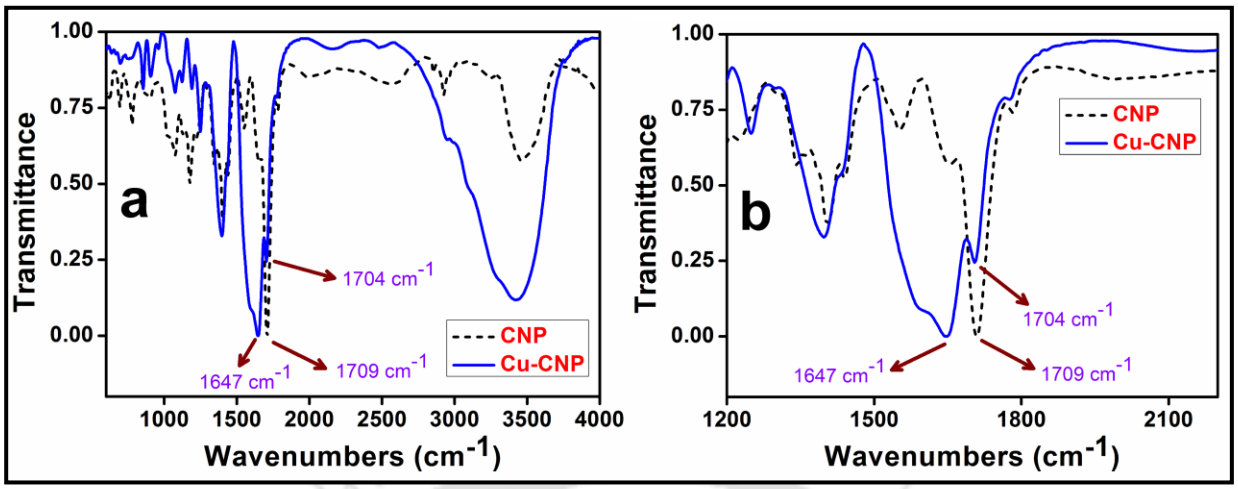

Figure 6.2. (a) FTIR spectra of CNP and Cu-CNP and **(b)** expanded view of the same for the region 1200 – 2100 cm^{-1}.

The oxidation state of copper in the complex was established by electron paramagnetic resonance (EPR) spectroscopy (Figure 6.1e). The Cu-CNP powder showed characteristic four-line X-band EPR spectrum for Cu^{2+} for the sample measured at room temperature [212]. The four-line hyperfine splitting pattern of Cu-CNP suggested the coupling of the unpaired electron and the ^{63}Cu nucleus (I = 3/2) and also revealed that there was complexion on the surface of CNP. On the other hand, atomic absorption spectroscopy (AAS) confirmed the loading of Cu^{2+} on the surface of CNP, which was found to be 8.1 wt%. Transmission electron microscopy (TEM) revealed the formation of nearly spherical Cu-CNP particles with average size of 92.7 ± 49.8 nm (Figure 6.1c and Figure 6.3a-c). However, the dynamic light scattering (DLS) based particle size analysis study of Cu-CNP showed the average size of 172.2 ± 23.8 nm (Figure 6.3d). This difference in average size could be explained based on the presence of the polymeric layer surrounding these particles (in addition to the measured property being the hydrodynamic diameter). Thus TEM which could image the CNP only revealed a smaller size than the particles would have in the presence of polymeric surrounding. It is worthy of mentioning here that the TEM analysis of Cu-CNP ruled out the possibility of formation of NPs of copper or its oxide on the surface of CNP. This was further supported by the high resolution TEM (Figure 6.1d) and X-ray diffraction (XRD) studies (Figure 6.4). The lack of any peak except a broad background centered at $2\theta=17.1^{o}$ in the XRD pattern indicated the absence of any copper related NPs. Additionally, the as-prepared Cu-CNP was found to have zeta potential of −7.43 mV, indicating

sufficient stability in the aqueous dispersion. The results presented above point towards the formation of a Cu^{2+}-complex on the surface of the CNP.

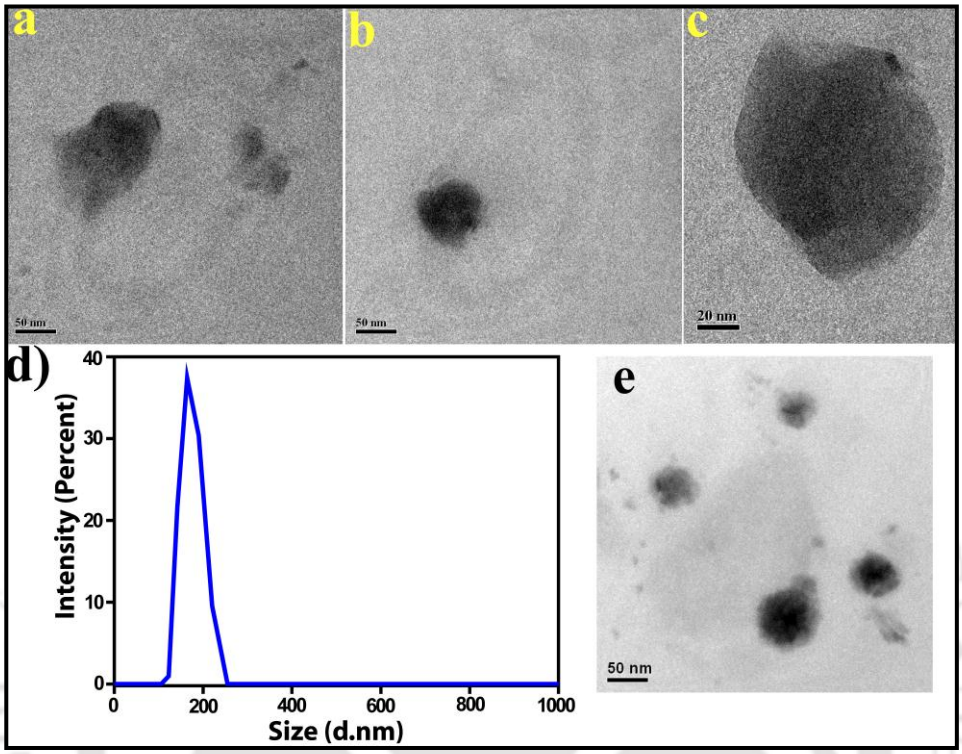

Figure. 6.3. (a, b & c) Representative additional TEM images of the Cu-CNP. **(d)** Dynamic light scattering based particle size analysis of Cu-CNP. **(e)** TEM image of CNP.

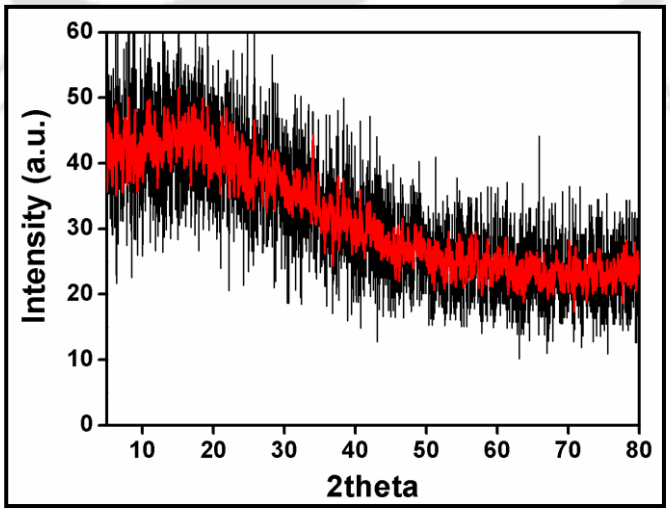

Figure 6.4. Powder XRD pattern of Cu-CNP.

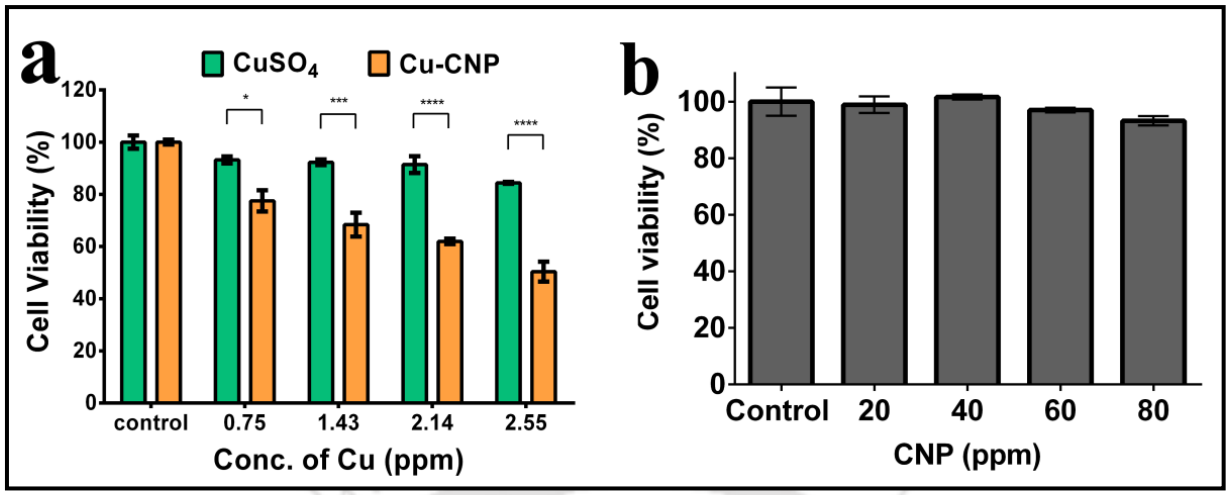

Figure 6.5. (a) Effects of Cu-CNP and $CuSO_4$ after 48h treatment on HeLa cancer cell lines viability determined by the MTT assay. Experiments were carried out in triplicate. Statistical significance has been determined by one-way ANOVA where *p<0.05; ***p<0.001; ****p<0.0001. **(b)** Cytotoxicity analysis of the CNPs (24h post-treatment) by MTT based cell viability assay. Results are presented as mean ± standard error.

In order to probe the anticancer activity of Cu-CNP, I performed cell viability assay using human cervical carcinoma (HeLa) cells. It was observed that the Cu-CNP showed significant cytotoxic activities towards HeLa cells (Figure 6.5a). In addition, cells were also treated with various concentrations of CNP (20 ppm– 80 ppm) for control experiments. However, no apparent cytotoxicity was observed for only CNP, as is evident from the Figure 6.5b. Thus it can be concluded that the cytotoxicity of Cu-CNP originated due to the presence of Cu^{2+} on the surface of CNP. Further, 3-(4,5-dimethylthiazolyl-2)-2,5-diphenyltetrazolium bromide (MTT) assay confirmed the inhibition of cell proliferation by Cu-CNP (Figure 6.5a). In this regard, cells were incubated with Cu-CNP (with the range of copper concentrations from 0.75 ppm - 2.55 ppm in Cu-CNP and the concentration range of Cu-CNP composite was 9.26 ppm – 31.4 ppm) at 37 ^{o}C for 48 h. Further, IC_{50} value of Cu-CNP was found out to be 2.55 ppm, which denotes the copper concentration in the Cu-CNP.

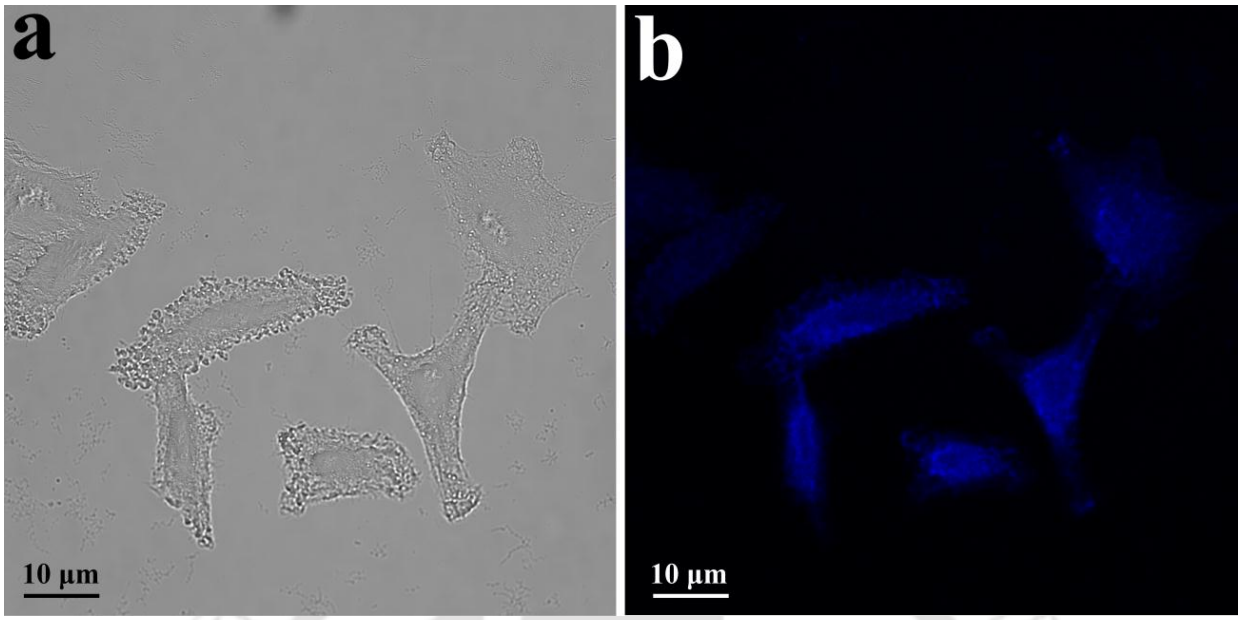

Figure. 6.6. Confocal microscopic images of HeLa cells treated with Cu-CNP, recorded after 6 h of incubation. **(a)** Image under bright field and **(b)** Fluorescence image of HeLa cells showing blue emission. Scale bar is 10 µm.

The theranostic potential of Cu-CNP was tested by using the luminescence of the CNPs following cellular uptake, which was probed by confocal microscopy (Figure 6.6). Intense blue emission was observed when HeLa cells were incubated with Cu-CNP for 6 h. Additionally, inductively coupled plasma – optical emission spectroscopy (ICP-OES) measurements were made to find out the concentration of copper inside the cells. For this, 10^5 HeLa cells (10^5) were incubated with Cu-CNP at the concentration of IC_{50} value (i.e. Cu concentration at 2.55 ppm in the composite) for 4 h. The control cells were not treated with any agent. The results showed the copper concentration in the treated cells to be 0.0221 ppm as opposed to 0.0079 ppm in the control HeLa cells. Thus the presence of Cu in the composite might have led to the observed cellular cytotoxicity. The results presented above revealed the cellular uptake of copper through Cu-CNP and role of CNP as a transport vehicle for delivering copper into the cells.

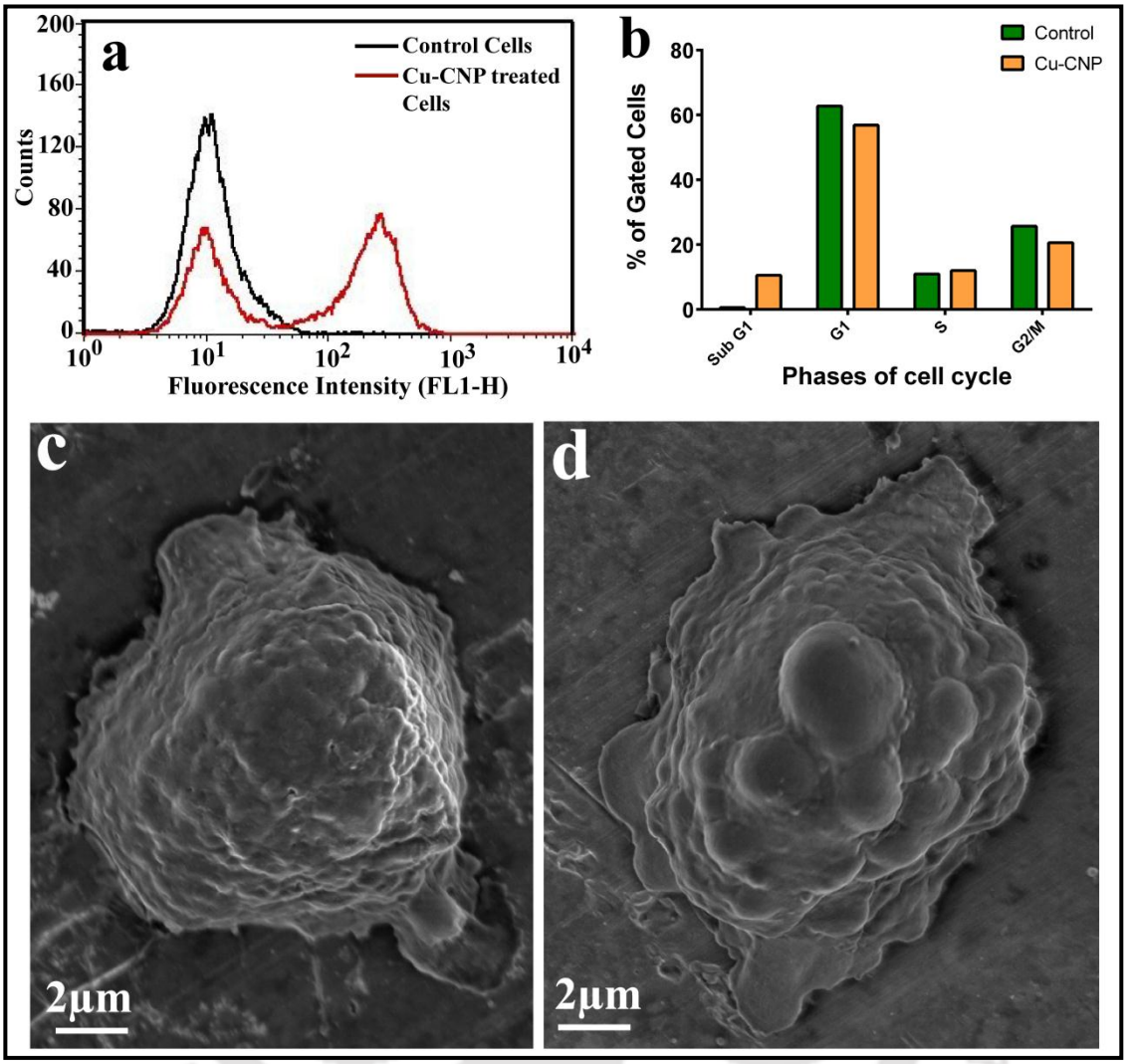

Figure 6.7. (a) Flow cytometric analysis of ROS production in HeLa cells: untreated cells (black line) and cells treated with Cu-CNP (red line). **(b)** Cell cycle analysis by FACS of PI-stained cells: quantitative analysis of Sub G1, G1, S and G2/M. Sub G1 populations of treated cells was 10.05% where control cell populations 0.34% which confirmed the apoptotic cell death. **(c)** FESEM image of a control cell **(d)** FESEM image of a cell treated with Cu-CNP indicating the apoptosis mode of cell death.

An important aspect of the copper based nanomaterials is their ability to generate reactive oxygen species (ROS) in the cellular environment. The ROS could be produced by dissolution of copper ions (Cu^{+} or Cu^{2+}) into the medium and as highly redox active species they can generate hydroxyl radicals via Fenton type reactions or by heterogeneous reactions at the particle surfaces [204]. Hence ROS production and subsequent oxidative stress generated in the cellular

environment could be the reason behind the toxicity of copper related nanomaterials. That Cu-CNP is also capable of generating ROS inside the cells was proved through flow cytometric studies of the HeLa cells treated with Cu-CNP for 3 h. The cytometric probe for ROS study is carried out by staining the cells with cell permeable flurogenic dye DCFH-DA (2',7'-Dichlorodihydroflurescin diacetate), which gets oxidized by intracellular ROS to DCF (2′ ,7′ -dichlorofluorecein) having green fluorescence. Increase in fluorescence intensity due to DCF formation for the Cu-CNP treated cells indicated enhanced level of ROS (Figure 6.7a) as compared to control cells. In order to distinguish between live and dead cells AO/EtBr (acridine orange / ethidium bromide) dual staining was performed after treatment of the cells with Cu-CNP for 24 h and was then observed under fluorescence microscope. AO stains the nucleus of live cells and gives green emission, when excited with blue light, whereas EtBr stains the dead cells and gives red fluorescence upon excitation with green light. Treatment with Cu-CNP at IC_{50} turned more cells red as compared to control cells (Figure 6.8). The results clearly established the killing of cancer cells by Cu-CNP. Control experiments involving CNP did not result in the significant killing of the cancer cells.

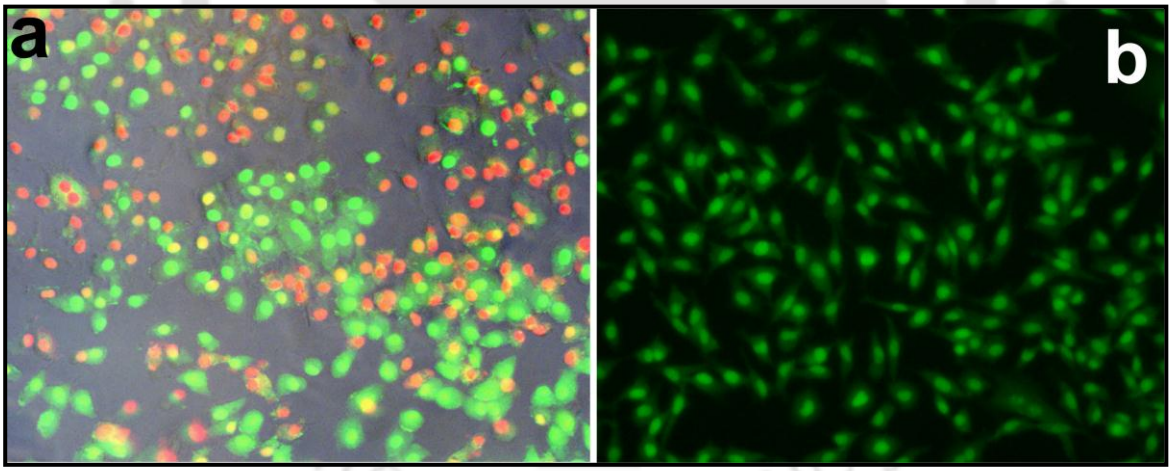

Figure 6.8. Dual staining (acridine orange / ethidium bromide) of HeLa Cells treated with **(a)** Cu-CNP and **(b)** CNP.

To investigate the mode of cell death, cell cycle analysis was carried out by using propidium iodide (PI), which is a membrane impermeant dye. It gets inside the cell after the cell is damaged and intercalates between base pairs of dsDNA and gives fluorescence emission maximum at 617 nm. This property is exploited to evaluate the DNA content of cells at different

stages of cell cycle, such as sub G1, G1, S and G2/M by flow cytometric analysis. On treatment with Cu-CNP significantly, higher sub G1 population was found (10.05%) which denotes the apoptotic population (Figure 6.7b, 6.9-6.10, refer to cell cycle analysis on page no-113). At the same time, in case of untreated and cells treated with CNP, sub G1 population was found to be 0.34% and 1.76% respectively, which are much lower as compared with cells treated with Cu-CNP (Figure 6.11, refer to cell cycle analysis on page no-114). Higher percentage of sub G1 population in case of Cu-CNP treated cells supports apoptosis as the primary mode of cell death. To further support the above results, Caspase 3 assays on the above mentioned samples were carried out. Caspase 3 is a caspase protein which exists as inactive proenzymes in cells. During the early phase of apoptosis it gets activated by proteolysis or by cleavage by some other proteases. In Cu-CNP treated HeLa cells, 10.84% cells were found to be apoptotic after 24 h of treatment, whereas there was no apoptosis for the cells treated with CNP, as shown in Figure 6.12-6.14, refer to cell cycle analysis on page no-114-115. This was substantiated by field-emission scanning electron microscopy (FESEM) measurements. FESEM image of the control cell did not show the formation of apoptotic bodies, whereas the treated cell clear showed their formation (Figure 6.7d). Thus it can be concluded that Cu-CNP induced apoptotic cell deaths in the cancerous HeLa cells.

6.4. CONCLUSIONS

In conclusion, I have developed a new and easy method for the synthesis of anticancer agent Cu^{2+} embedded in carbon NPs (Cu-CNP). To the best of our knowledge, this is for the first time a CNP based anticancer agent is being reported. Good biocompatibility and high photoluminescence for cellular imaging of the CNP, and anticancer effect of Cu-CNP will make the composite a promising candidate for future theranostic applications. That the copper complex formation on the surface of carbon NPs could be used for anticancer activity provides a new and potent use of carbon based nanomaterials.

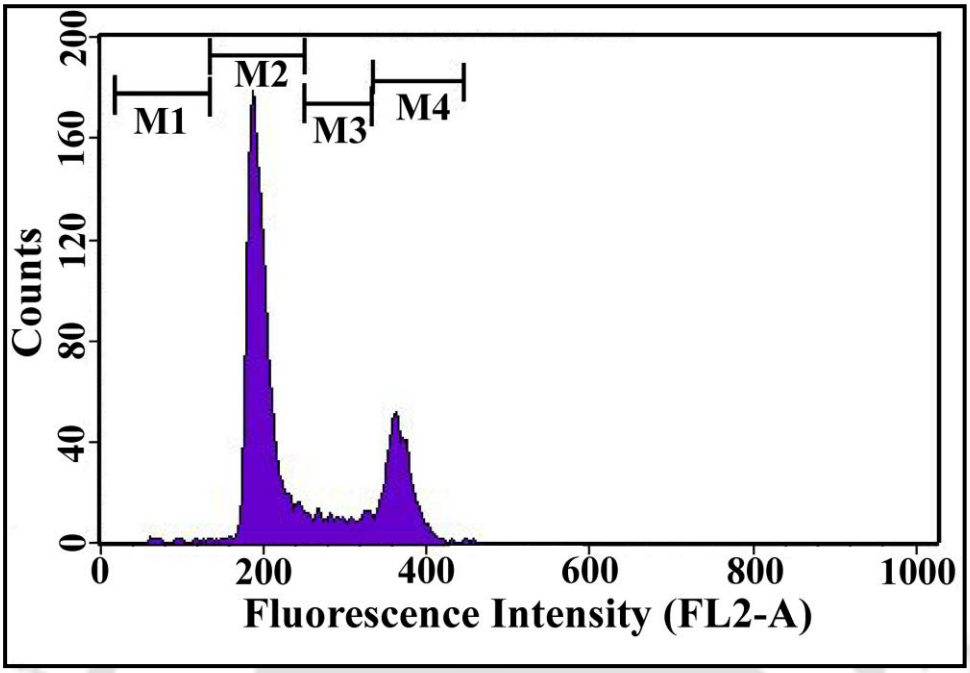

Figure 6.9. Cell cycle analysis by FACS of PI-stained HeLa cells (control).

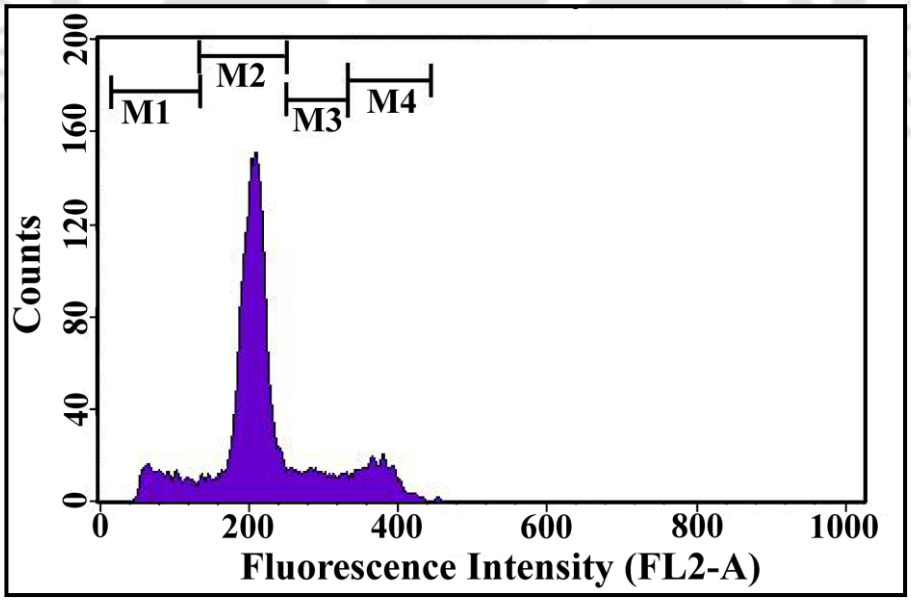

Figure 6.10. Cell cycle analysis by FACS of PI-stained HeLa cells treated with Cu-CNP.

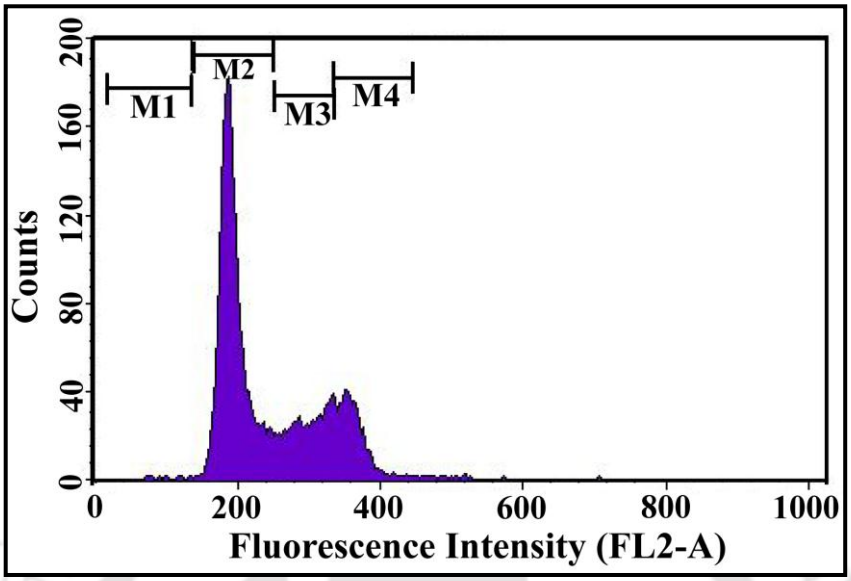

Figure 6.11. Cell cycle analysis by FACS of PI-stained HeLa cells treated with CNP.

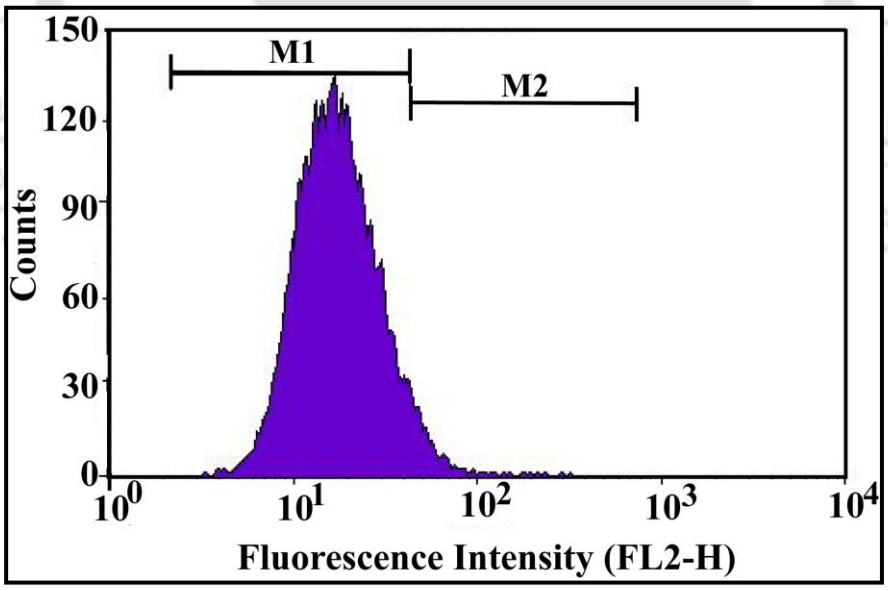

Figure 6.12. Caspase 3 assay of control HeLa cells.

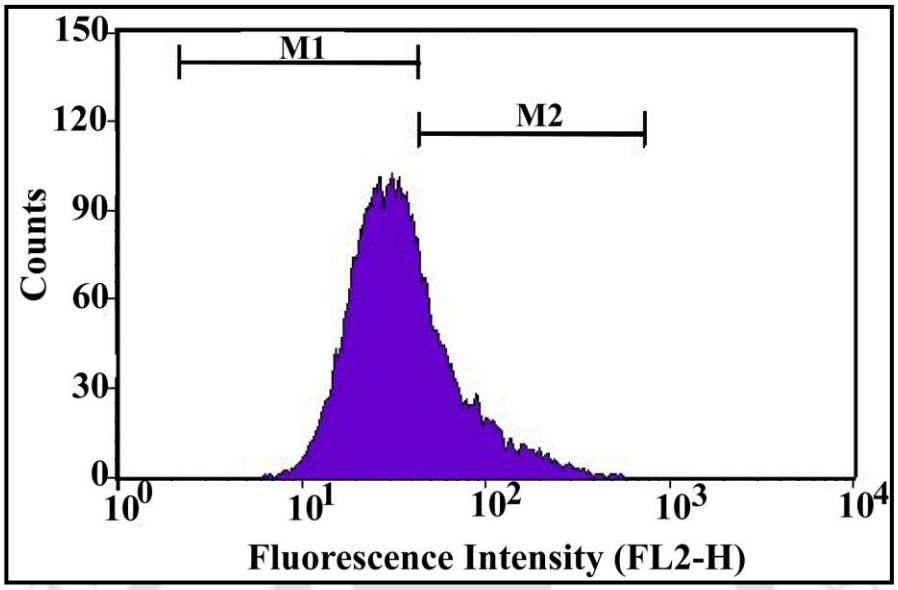

Figure 6.13. Caspase 3 assay of Cu-CNP treated HeLa cells.

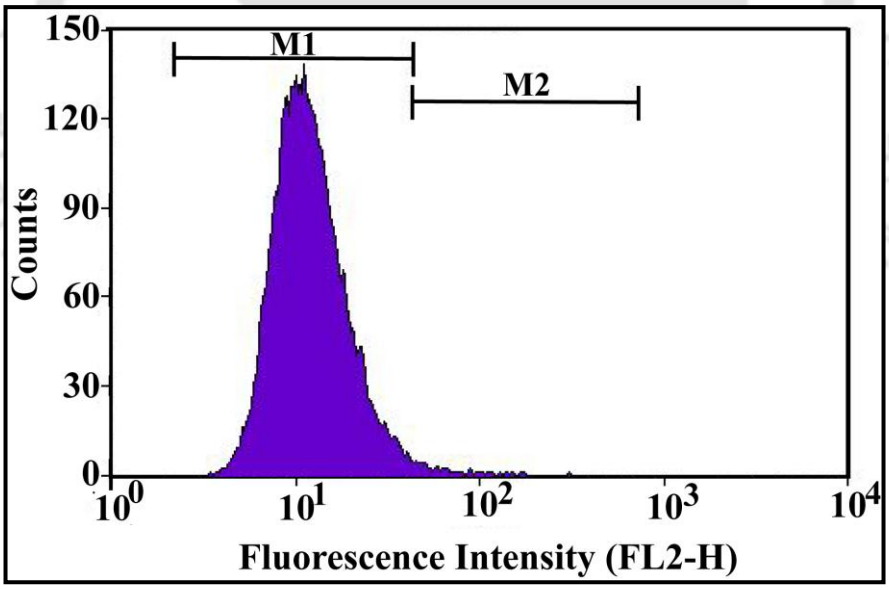

Figure 6.14. Caspase 3 assay of CNP treated HeLa cells.

CHAPTER-7

Overview and Future Prospects of the Thesis

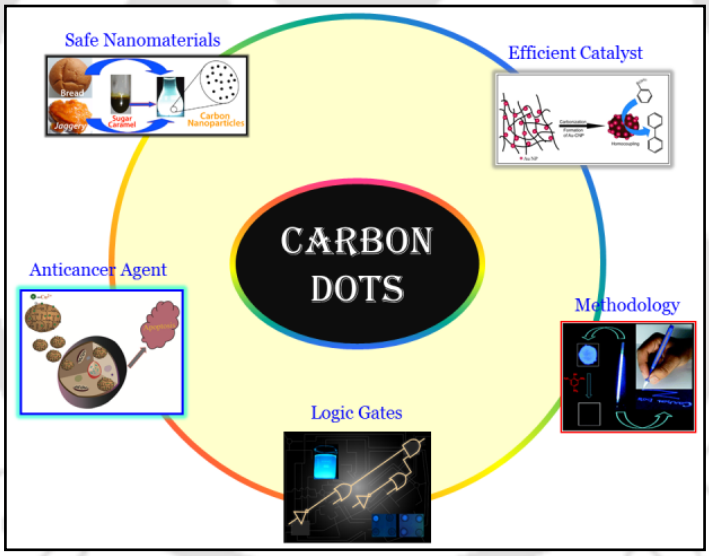

7.1. SUMMARY OF THE THESIS

The works presented in the thesis adress several of the issues related to carbon nanoparticles (CNPs). In particular, the first work of the thesis (chapter-2) provides the best solution to a prolonging ambiguity on whether or not nanomaterials are suitable for biological applications. As reported in the chapter, carbon nanoparticles (CNPs)- were isolated from bread, sugar derived *jaggery*, biscuits and cornflakes, some of which human beings have been eating for centuries. These particles are amorphous in nature and non-toxic to mammalian cells. They have wavelentgh tunable fluorescence. The surface of CNPs contains polymeric layer of sugars. This paradigm espouses the non-toxicity of CNPs and thus brings in an important application aspects in healthcare.

CNPs have been found as good support material for catalyst similar to charcoal-supported Pd or Pt metal catalysts as reported in chapter-3. Synthesis of Au NPs supported on CNPs made the composite catalysts and their catalytic acitivity in homocoupling reaction of phenylboronic acid have been demonstrated. The composite catalyst showed potentiality in terms of efficiency, selectivity as well as recyclability .

A new synthetic method for production of Cdots, with high photoluminescence quantum yield, based on traditional knowledge has been developed in chapter-4. Cdots were produced using faster, safer and energy efficient induction coil heating replacing existing microwave or hydrothermal heating techniques. Then their pH and ionic strength independent bright emission properties were employed as marker and selective sensor for explosive like picric acid. However, a gel was prepared using Cdots and chitosan for the above mentioned applications. In addition, Cdots were introduced as fluorescent probe to design basic and higher integrated logic gate in chapter-5. These logic systems are able to work in two phases such as liquid and solid, through interactions with metal ions and organic molecules.

Further to previous chapter, larger sized CNPs have been used as carrier of Cu^{2+} for cancerous cells which is illustrated in chapter-6. Synthesis of Cu^{2+} embedded CNP (Cu-CNP) has been described in this chapter, where complexion between Cu^{2+} and surface functional groups of CNP was confirmed. Then the anticancer activity of Cu-CNP was investigated in HeLa cells. The results indicated that Cu-CNP acts as potential anticancer agent generating reactive oxygen species and following apoptosis mechanism. Also, the emission property of Cu-CNP was used for cellular imaging.

All the works discussed in the thesis are connected with promising applications of CNPs, which is the main theme of the thesis and thus justify the title of the thesis.

7.2. FUTURE PROSPECTS OF THE THESIS

The works which have been described throughout the thesis have considerable contribution in the area of CNP research. In this regard, various aspects of CNPs are yet to be explored and thus a large number of future scopes can be envisaged, based on the work presented in this thesis. All the possible scopes for future work are being presented chapter-wise.

Chapter-2

The CNPs which were derived from various daily eating foods are considered as safe nanomaterials. So, they could be potentially safe to use for biomedical applications replacing inorganic toxic nanomaterials such as quantum dots. They could be exploited in drug delivery applications *in vivo*, when conjugated with biomolecules and drugs and also in imaging as well as tracking applications.

Chapter-3

The work provides new opportunity to modify the existing catalyst or design new catalyst with CNPs. This catalyst could be used for the large-scale production of fine chemicals, pharmaceuticals of industrial importance and in polymerization reactions of materials importance.

Chapter-4

The facile and energy efficient synthesis method of highly fluorescent Cdots can easily be extended to produce large-scale Cdots for commercial purposes. The robust optical and biocompatible property of Cdots could be applied in agriculture science. The gel could be used as invisible ink for security purposes and in paper based sensor.

Chapter-5

The study may open new doors to construct Cdots based logic system for further advances in molecular logic family. These biphasic logic systems could be used for various analytical applications in diverse environments. Even it may be possible to distinguish Fe^{2+} and Fe^{3+} using higher integrated logic system. These logic operations could serve as the basis of small devices for analytical application purposes.

Chapter-6

The concept of Cu-CNP may encourage researcher for designing metal based anticancer agent on the surface of CNPs for future theranostic applications. Detailed studies will be required to develop anticancer agents for practical applications.

Bibliography

(1) G. Cao, Nanostructures & nanomaterials: synthesis, properties & applications. *World Scientific Publishing Company*, 2004.

(2) Gabor L. Hornyak, H.F. Tibbals, Joydeep Dutta, John J. Moore, Introduction to Nanoscience and Nanotechnology. *Taylor & Francis, CRC Press,* **2008**.

(3) H. M. Chen and R. Liu, *J. Phys. Chem. C,* **2011**, *115*, 3513.

(4) E. Roduner, *Chem. Soc. Rev.* **2006**, ***35***, 583.

(5) M.C. Daniel and D. Astruc, *Chem. Rev*. **2003**, *104*, 293.

(6) S. Link and M. A. E. Sayed, *Int. Reviews in Physical Chemistry,* **2000,** *19,* 409.

(7) S. K. Ghosh, S. Kundu, M. Mandal and T. Pal, *Langmuir,* **2002**, *18*, 8756.

(8) A. M. Schwartzberg and J. Z. Zhang, *J. Phys. Chem. C,* **2008***, 112, 10323*.

(9) E. Sayed, *Acc. Chem. Res.*, **2001**, *34*, 257.

(10) G. Mie, *Ann. Phys*., **1908**, *25*, 377.

(11) M. Rycenga, C. M. Cobley, J. Zeng, W. Li, C. H. Moran, Q. Zhang, D. Qin and Y. Xia, *Chem. Rev*.**2011**, *111*, 3669.

(12) Y. Sun and Y. Xia, *Anal. Chem*. **2002**, *74*, 5297.

(13) K. L. Kelly, E. Coronado, L. L. Zhao and G. C. Schatz, *J. Phys. Chem B* **2003**, *107*, 668.

(14) J. N. Anker, W. P. Hall, O. Lyandres, N. C. Shah, J. Zhao and R. P. V. Duyne, *Nature Materials,* **2008**, *7*, 442.

(15) A. H. Lu, E. L. Salabas and F. Schuth, Angew. *Chem. Int. Ed.* **2007**, *46*, 1222.

(16) L. H. Reddy, J. L. Arias, J. Nicolas and P. Couvreur, *Chem. Rev.* **2012**, *112*, 5818.

(17) A. P. Alivisatos, *The J. Phys. Chem.* **1996,** *100,* 13226.

(18) J. Y. Kim, O. Voznyy , D. Zhitomirsky and E. H. Sargent, *Adv. Mater*. **2013**, *25*, 4986.

(19) M. Bruchez, M. Moronne, P. Gin, S. Weiss and A. P. Alivisatos, *Science,* **1998,** *281,* 2013.

(20) I.L. Medintz, H. Mattoussi and A. R. Clapp*, Int. J. Nanomedicine*, **2008**, *3,* 151.

(21) C. Warren, W. Chan and S. Nie, *Science,* **1998**, *281,* 2016.

(22) A. M. Smith, H. Duan, A. M. Mohs and S. Nie, *Advanced Drug Delivery Reviews*, **2008**, *60*, 1226.

(23) M. Dahan, S. Levi, C. Luccardini, P. Rostaing, B. Riveau and A. Triller, *Science,* **2003**, *302,* 442.

(24) X. Y Wu, H. J. Liu, J. Q. Liu, K. N. Haley, J. A. Treadway, J. P. Larson, N. F. Ge, F. Peale and M. P. Bruchez. *Nat. Biotechnol*. **2003**, *21*, 41.

(25) A. Sukhanova, M. Devy, L. Venteo, H. Kaplan, M. Artemyev, V. Oleinikov, D. Klinov, M. Pluot, J. H. M. Cohen and I. Nabiev, *Anal. Biochem*. **2004**, *324*, 60.

(26) D. Alexson, Y. Li, D. Ramadurai, P. Shi, L. George, L. George, M. Uddin, P. Thomas, S. Rufo, M. Dutta and M. A. Stroscio, *IEEE T. Nanotechnol*. **2004**, *3*, 86.

(27) R. Nisman, G. Dellaire, Y. Ren, R. Li and D. P. Bazett-Jones, *J. Histochem. Cytochem*. **2004**, *52*, 13.

(28) S. Pathak, S. K. Choi, N. Arnheim and M. E. Thompson, *J. Am. Chem. Soc.* **2001**, *123*, 4103.

(29) Y. Xiao and P. E. Barker, *Nucleic Acids Res.* **2004**, *32,* e28.

(30) M. E. Akerman, W. C. W. Chan, P. Laakkonen, S. N. Bhatia and E. Ruoslahti, *Proc. Natl. Acad. Sci. USA,* **2002**, *99*, 12617.

(31) Y. Wang, R. Hu, G. Lin, I. Roy and K.T. Yong, *ACS Appl. Mater. Interfaces*, **2013**, *5*, 2786.

(32) W. R. Algar, A. J. Tavares and U. J. Krull, *Analytica Chimica Acta*, **2010**, *673*, 1.

(33) R. D. Schaller and V. I. Klimov, *Physical Review Letters,* **2004**, *92*, 186601.

(34) C.H. M. Chuang, P. R. Brown, V. Bulović and M. G. Bawendi, *Nature Materials*, **2014**, *13*, 796.

(35) A. J. Nozik, M. C. Beard, J. M. Luther, M. Law, R. J. Ellingson and J. C. Johnson, *Chem. Rev*. **2010**, *110,* 6873.

(36) V. Wood and V. Bulovic, *Nano Reviews*, **2010**, *1*, 5202.

(37) P. O. Anikeeva, J. E. Halpert, M. G. Bawendi and V. Bulovic, *Nano Lett*. **2009**, *9*, 2532.

(38) K.H. Lee, J.H. Lee, W.S. Song, H. Ko, C. Lee, J.H. Lee and H. Yang, *ACS Nano*, **2013**, *7*, 7295.

(39) G. Konstantatos, I. Howard, A. Fischer, S. Hoogland, J. Clifford, E. Klem, L. Levina and E. H. Sargent, *Nature,* **2006**, *442*, 180.

(40) J. Lovric, H. S. Bazzi, Y. Cuie, G. R. A. Fortin, F. M. Winnik and D. Maysinger, *J. Mol. Med.* **2005**, *83*, 377.

(41) C. Kirchner, T. Liedl, S. Kudera, T. Pellegrino, A. M .Javier, H. E. Gaub, S. Stolzle, N. Fertig and W. Parak, *J. Nano Lett*. **2005**, *5*, 331.

(42) N. Chen, Y. He, Y. Y. Su, X. M. Li, Q .Huang, H. F. Wang, X. Z. Zhang, R. Z. Tai and C. H. Fan, *Biomaterials*, **2012**, *33*, 1238.

(43) A. Hoshino, K. Fujioka, T. Oku, M. Suga, Y. F. Sasaki, T. Ohta, M. Yasuhara, K. Suzuki and K. Yamamoto, *Nano Lett*.**2004**, *4*, 2163.

(44) A. M. Derfus, W. C. W. Chan and S. N. Bhatia, *Nano Lett*. **2004**, *4*, 11.

(45) R. F. Domingos, D. F. Simon, C. Hauser and K. Wilkinson, *J. Environ. Sci. Technol*. **2011**, *45*, 7664.

(46) Y. Y. Su, M. Hu, C. H. Fan, Y. He, Q. N. Li, W. X. Li, L. H. Wang, P. P. Shen and Q. Huang, *Biomaterials* , **2010**, *31*, 4829.

(47) B. I. Ipe, M. Lehnig and C. M. Niemeyer, *Small,* **2005**, *1*, 706.

(48) P. Juzenas, R. Generalov, A. Juzeniene and J. Moan, J. Biomed. *Nanotechnol.* **2008**, *4*, 450.

(49) S. W. Kim, J. P. Zimmer, S. Ohnishi, J. B. Tracy, J. V. Frangioni and M. G. Bawendi, *J. Am. Chem. Soc.* **2005**, *127*, 10526.

(50) N.Pradhan, D. M. Battaglia,Y. C. Liu and X. G. Peng, *Nano Lett*. **2007**, *7*, 312.

(51) M. Geszke, M. Murias, L. Balan, G. Medjandi, J. Korczynski, M. Moritz, J. Lulek and R. Schneider, *Acta Biomater*. **2011**, *7*, 1327.

(52) M. Helle, E. Cassette, L. Bezdetnaya, T. Pons, A. Leroux, F. Plenat, F. Guillemin, B. Dubertret and F. Marchal, *PLoS One*, **2012**, *7*, e44433.

(53) D. Jariwala, V. K. Sangwan, L. J. Lauhon, T. J. Marksab and M. C. Hersam, *Chem. Soc. Rev.* **2013**, *42*, 2824.

(54) L. Dai , D. W. Chang , J.B. Baek and W. Lu, *small*, 2012, **8**, 1130.

(55) C. Cha, S. R. Shin, N.Annabi, M. R. Dokmeci and A. Khademhosseini, *ACS Nano*, **2013**, *7*, 2891.

(56) M.M. Titirici, R. J. White, N. Brun, V. L. Budarin, D. S. Su, F. del Monte, J. H. Clark and Mark J. MacLachlan, *Chem. Soc. Rev.* **2015**, *44*, 250.

(57) J. Wang, Z. Hu, J. Xu and Y. Zhao, *NPG Asia Materials*, **2014**, *6*, e84; doi:10.1038/am.2013.79.

(58) S. N. Baker and G. A. Baker, *Angew. Chem. Int. Ed.* **2010**, *49*, 6726.

(59) H. Li, Z. Kang, Y. Liu and S.T. Lee, *J. Mater. Chem.* **2012**, *22*, 24230.

(60) P. G. Luo, F. Yang, S. T. Yang, S. K. Sonkar, L. Yang, J. J. Broglie, Y. Liua and Y.P. Sun, *RSC Adv.* **2014**, *4*, 10791.

(61) K. Hola, Y. Zhangb, Y. Wang, E. P. Giannelis, R. Zboril and A. L. Rogach, *Nano Today*, **2014**, *9*, 590.

(62) S. Y. Lim, W. Shen and Z. Gao, *Chem. Soc. Rev.* **2015**, *44*, 362.

(63) A. Zhao, Z. Chen, C. Zhao, N. Gao, J. Ren and X. Qu, Carbon, doi:10.1016/j.carbon.2014.12.045.

(64) X. Xu, R. Ray, Y. Gu, H. J. Ploehn, L. Gearheart, K. Raker and W. A. Scrivens, *J. Am. Chem Soc.* **2004**, *126*, 12736.

(65) Y. P. Sun, B. Zhou, Y. Lin, W. Wang, K. A. S. Fernando, P. Pathak, M.J. Meziani, B. A. Harruff, X. Wang, H. Wang, P. G. Luo, H. Yang, M. E. Kose, B. Chen, L. M. Veca and S. Y. Xie, *J. Am. Chem Soc.* **2006**, *128*, 7756.

(66) H. Liu, T. Ye and C. Mao, *Angew. Chem. Int. Ed.* **2007**, *46*, 6473.

(67) L. Cao, X. Wang, M. J. Meziani , F. Lu , H. Wang, P. G. Luo , Y. Lin, B. A. Harruff , L. M. Veca , D. Murray , S.Y. Xie and Y.P. Sun , *J. Am. Chem Soc.* **2007**, *129*, 11318.

(68) Q. L. Zhao, Z.L. Zhang, B.H. Huang, J. Peng, M. Zhang and D.W. Pang, *Chem. Commun.* **2008**, 5116.

(69) A. B. Bourlinos, A. Stassinopoulos, D. Anglos, R. Zboril, V. Georgakilas, and E. P. Giannelis, *Chem. Mater.* **2008, *20*,** 4539.

(70) S.T. Yang, L. Cao, P.G. Luo, F. Lu, X. Wang, H. Wang, M. J. Meziani, Y. Liu, G. Qi and Y.P. Sun, *J. Am. Chem Soc.* **2009**, *131*, 11308.

(71) H. Zhu , X. Wang , Y. Li , Z. Wang , F. Yang and X. Yang , *Chem. Commun.* **2009**, 5118.

(72) S.L. Hu, K.Y. Niu, J. Sun, J. Yang, N.Q. Zhao and X.W. Du, *J. Mater. Chem.* **2009**, *19*, 484.

(73) J. Lu, J.X. Yang, J. Wang, A. Lim, S. Wang, and K. P. Loh, *ACS Nano*, **2009**, *3*, 2367.

(74) L. Y. Zheng, Y. W. Chi, Y. Q. Dong, J. P. Lin, B. B. Wang, *J. Am. Chem. Soc.* **2009**, *131*, 4564.

(75) J. Zhou, C. Booker, R. Li, X. Zhou, T.K. Sham, X. Sun and Z. Ding, *J. Am. Chem. Soc.* **2007**, *129*, 744.

(76) S. C. Ray, A. Saha, N. R. Jana, R. Sarkar, *J. Phys. Chem. C*, **2009**, *113*, 18546.

(77) L. Tian, D. Ghosh, W. Chen, S. Pradhan, X. Chang and S. Chen, *Chem. Mater.* **2009**, *21*, 2803.

(78) R. L. Liu, D. Q. Wu, S. H. Liu, K. Koynov, W. Knoll and Q. Li, *Angew. Chem. Int. Ed.* **2009**, *48*, 4598.

(79) A. Jaiswal, S. S. Ghosh and A. Chattopadhyay, *Chem. Commun.* **2012**, *48*, 407.

(80) H. T. Li, X. D. He, Y. Liu, H. Huang, S. Y. Lian, S. T. Lee and Z. H. Kang, *Carbon*, **2011**, *49*, 605.

(81) X. H. Wang, K. G. Qu, B. L. Xu, J. S. Ren and X. G. Qu, *J. Mater. Chem.* **2011**, *21*, 2445.

(82) A. B. Bourlinos, A. Stassinopoulos, D. Anglos, R. Zboril, M. Karakassides and E. P. Giannelis, *Small*, **2008**, *4*, 455.

(83) F. Wang, M. Kreiter, B. He, S. Pang and C.-Y. Liu, *Chem. Commun.* **2010**, *46*, 3309.

(84) Z.-C. Yang, M. Wang, A. M. Yong, S. Y. Wong, X.-H. Zhang, H. Tan, A. Y. Chang, X. Li and J. Wang, *Chem. Commun.* **2011**, *47*, 11615.

(85) S. Chandra, P. Das, S. Bag, D. Laha and P. Pramanik, *Nanoscale*, **2011**, *3*, 1533.

(86) J. Jiang, Y. He, S. Li and H. Cui, *Chem. Commun.* **2012**, *48*, 9634.

(87) P.-C. Hsu and H.-T. Chang, *Chem. Commun.* **2012**, *48*, 3984.

(88) H. T. Li, H. Ming, Y. Liu, H. Yu, X. D. He, H. Huang, K. M. Pan, Z. H. Kang and S.T. Lee, *New J. Chem.* **2011**, *35*, 2666.

(89) Z.-C. Yang, X. Li and J. Wang, *Carbon*, **2011**, *49*, 5207.

(90) B. Zhang, C.-Y. Liu and Y. Liu, *Eur. J. Inorg. Chem.* **2010**, 4411.

(91) J. J. Zhou, Z. H. Sheng, H. Y. Han, M. Q. Zou and C. X. Li, *Mater. Lett.* **2012**, *66*, 222.

(92) W. B. Lu, X. Y. Qin, S. Liu, G. H. Chang, Y. W. Zhang, Y. L. Luo, A. M. Asiri, A. O. Al-Youbi and X. P. Sun, *Anal. Chem.* **2012**, *84*, 5351.

(93) S. Sahu, B. Behera, T. K. Maiti and S. Mohapatra, *Chem. Commun.* **2012**, *48*, 8835.

(94) H. Huang, J. J. Lv, D. L. Zhou, N. Bao, Y. Xu, A. J. Wang and J. J. Feng, *RSC Adv.* **2013**, *3*, 21691.

(95) V. N. Mehta, S. Jha and S. K. Kailasa, *Mater. Sci. Eng.* **2014**, *38*, 20.

(96) J. R. Neabo, C. Vigier-Carriere, S. Rondeau-Gagne and J. F. Morin, *Chem. Commun.* **2012**, *48*, 10144.

(97) Q. H. Liang, W. J. Ma, Y. Shi, Z. Li and X. M. Yang, *Carbon*, **2013**, *60*, 421.

(98) L. Zhu, Y. Yin, C.-F. Wang and S. Chen, *J. Mater. Chem. C*, **2013**, *1*, 4925.

(99) J. Wei, J. Shen, X. Zhang, S. Guo, J. Pan, X. Hou, H. Zhang, L. Wang and B. Feng, *RSC Adv.* **2013**, *3*, 13119.

(100) B. De and N. Karak, *RSC Adv.* **2013**, *3*, 8286.

(101) Q. Wang, X. Liu, L. Zhang and Y. Lv, Analyst, **2012**, *137*, 5392.

(102) J. Wang, S. Sahu, S. K. Sonkar, K. N. Tackett II, K. W. Sun, Y. Liu, H. Maimaiti, P. Anilkumar and Y.-P. Sun, *RSC Adv.* **2013**, *3*, 15604.

(103) Z. L. Wu, P. Zhang, M. X. Gao, C. F. Liu, W. Wang, F. Leng and C. Z. Huang, *J. Mater. Chem. B*, **2013**, *1*, 2868.

(104) Q. Wang, X. Huang, Y. Long, X. Wang, H. Zhang, R. Zhu, L. Liang, P. Teng and H. Zheng, *Carbon*, **2013**, *59*, 192.

(105) D. Sun, R. Ban, P.-H. Zhang, G.-H. Wu, J.-R. Zhang and J. J. Zhu, *Carbon*, 2013, **64**, 424.

(106) D. Chowdhury, N. Gogoi and G. Majumdar, *RSC Adv.* **2012**, *2*, 12156.

(107) L. Wang, S.J. Zhu, H.Y. Wang, S.N. Qu, Y.L. Zhang, J.H. Zhang, Q.D. Chen, H.L. Xu, W. Han, B. Yang and H.B. Sun, *ACS Nano*, **2014**, *8*, 2541.

(108) Q. L. Zhao, Z. L. Zhang, B. H. Huang, J. Peng, M. Zhang and D. W. Pang, *Chem. Commun*. **2008**, 5116.

(109) J. C. Vinci, I. M. Ferrer, S. J. Seedhouse, A. K. Bourdon, J. M. Reynard, B. A. Foster, F. V. Bright and L. A. Colón, *J. Phys. Chem. Lett*. **2013**, *4*, 239.

(110) Y.P. Sun, X. Wang, F. Lu, L.Cao, M. J. Meziani, P. G. Luo, L. Gu, and L. M. Veca, *J. Phys. Chem. C*, **2008**, *112*, 18295.

(111) S. Zhu, Q. Meng, L. Wang, J. Zhang, Y. Song, H. Jin, K. Zhang, H. Sun, H. Wang and B. Yang, *Angew. Chem. Int. Ed.* **2013**, *52*, 3953.

(112) N. Sozer and J. L. Kokini, *Trends Biotechnol*. **2009**, *27*, 82.

(113) P. Sanguansri, and M.A. Augustin, *Food Sci. Tech*. **2006**, *17*, 547.

(114) T. V. Duncan, *Nat. Nanotechnol*. **2011**, *6*, 683.

(115) C. Bass, Scientific American Home Page, http://www.scientificamerican.com/article.cfm?id=will-nano-particles-present-big-health-problems (accessed Dec 26, 2011).

(116) R. A. Petros, and J. M. DeSimone, *Nat. Rev. Drug Discov*. **2010**, *9*, 615.

(117) J. Panyam and V. Labhasetwar, *Adv. Drug Deliv. Rev*. **2003**, *55*, 329.

(118) M. M. Hong, J. M. Oh and J. H. Choy, *J. Nanosci. Nanotechnol*. **2008**, *8*, 5018.

(119) W. J. Stark, *Angew. Chem. Int. Ed*. **2011**, *50*, 1242.

(120) E. Miele, G. P. Spinelli, E. Miele, F. Tomao and S. Tomao, *Int. J. Nanomedicine*. **2009**, *4*, 99.

(121) R. Bawa, *Nanotechnology Law and Business*, **2008**, *5*, 135.

(122) R. Khundkar, C. Malic and T. Burge, *Burns*, **2010**, *36*, 751.

(123) P. Walter et al. *Nano Lett*. **2006**, *6*, 2215.

(124) D. J. Barber, and I. C. Frestone, *Archaeometry*, **1990**, *32*, 33.

(125) M. Reibold, P. Paufler, A. A. Levin, W. Kochmann, N. Patzke, and D. C. Meyer, *Nature*, **2006**, *444*, 286.

(126) G. Eggleston, B. J. Trask-Morrell and R. V. John, *J. Agric. Food Chem*. 1996, 44, 3319.

(127) H. Blaser and M. Studer, *Appl. Catal. A*, **1999**, *189*, 191.

(128) M. J. Climent, A. Corma and S. Iborra, *Chem. Rev*. **2011**, *111*, 1072.

(129) H. Li, X. He, Z. Kang, H. Huang, Y. Liu, J. Liu, S. Lian, C H. A. Tsang, X. Yang and S. Lee, *Angew. Chem., Int. Ed*. **2010**, *49*, 4430.

(130) P. Luo, C. Li and G. Shi, *Phys. Chem. Chem. Phys*. **2012**, *14*, 7360.

(131) J. Guo and K. S. Suslick, *Chem. Commun*. **2012**, *48*, 11094.

(132) R. Liu, S. M. Mahurin, C. Li, R. R. Unocic, J. C. Idrobo, H. Gao, S. J. Pennycook and S. Dai, *Angew. Chem., Int. Ed*. **2011**, *50*, 6799.

(133) M. Stratakis and H. Garcia, *Chem. Rev*. **2012**, *112*, 4469.

(134) M. M. Maye, N. N. Kariuki, J. Luo, L. Han, P. Njoki, L. Wang, Y. Lin, H. R. Naslund and C. Zhong, *Gold Bull*. **2004**, *37,* 217.

(135) A. Sanchez, S. Abbet, U. Heiz, W. D. Schneider, H. Hakkinen, R. N. Barnett and U. Landman, *J. Phys. Chem. A,* **1999**, *103*, 9573.

(136) D. A. Horton, G. T. Bourne and M. L. Smythe, *Chem. Rev.* **2003**, *103*, 893.
(137) J. H. Schön, H. Meng and Z. Bao, *Nature*, **2001**, *413*, 713.
(138) S. Carrettin, J. Guzman and A. Corma, *Angew. Chem. Int. Ed.* **2005**, *44*, 2242.
(139) L. Wang, W. Zhang, D. S. Su, X. Meng and F. Xiao, *Chem. Commun.* **2012**, *48*, 5476.
(140) H. Tsunoyama, H. Sakurai, N. Ichikuni, Y. Negishi and T.Tsukuda, *Langmuir*, **2004**, *20*, 11293.
(141) A. Primo and F. Quignard, *Chem. Commun.* **2010**, *46*, 5593.
(142) A. S. Demir , Ö. Reis and M. Emrullahoglu, *J. Org. Chem.* **2003**, *68*, 10130.
(143) B. Kaboudin,T. Haruki and T.Yokomatsu, *Synthesis*, **2011**, *1*, 91.
(144) T. Vogler and A.Studer, *Adv. Synth. Catal.* **2008**, *350*, 1963.
(145) K. Mitsudo, T. Shiraga and H. Tanaka, *Tetrahedron Lett.* **2008**, *49*, 6593.
(146) L. Yin and J. Liebscher, *Chem. Rev.* **2007**, *107*, 133.
(147) C. Gonza´lez-Arellano, A. Corma, M. Iglesiasc and F. Sa´nchez, *Chem. Commun.* **2005**, 1990.
(148) M. Boronat and A. Corma, *Dalton Trans.* **2010**, *39*, 8538.
(149) D. T. Sawyer and J. S. Valentine, *Acc. Chem. Res.* **1981**, *14*, 393.
(150) N. Weiher, A. M. Beesley, N. Tsapatsaris, L. Delannoy, C. Louis, J. A. v. Bokhoven and S. L. M. Schroeder, *J. Am. Chem. Soc*, **2007**, *129*, 2240.
(151) V. F. Lapko, I. P. Gerasimyuk, V. S. Kuts and Y. A. Tarasenko, *Russ. J. Phys. Chem. A,* **2010**, *84*, 934.
(152) X. Dou, Z. Lin, H. Chen, Y. Zheng, C. Lua and J. Lin, *Chem. Commun.* **2013**, *49*, 5871.
(153) F. Wang, S. Pang, L. Wang, Q. Li, M. Kreiter and C. Liu, *Chem. Mater.* **2010**, *22*, 4528.
(154) Y. Dong, H. Pang, H. B. Yang, C. Guo, J. Shao, Y. Chi, C. M. Li and T. Yu, *Angew. Chem., Int. Ed.* **2013**, *52*, 7800.
(155) M. J. Krysmann, A. Kelarakis, P. Dallas and E. P. Giannelis, *J. Am. Chem. Soc.* **2012**, *134*, 747.
(156) R. Piner, H. Li, X. Kong, L. Tao, I. N. Kholmanov, H. Ji, W. H. Lee, J. W. Suk, J. Ye, Y. Hao, S. Chen, C. W. Magnuson, A. F. Ismach, D. Akinwande and R. S. Ruoff, *ACS Nano*, **2013**, *7*, 7495.
(157) X. Wang, Li. Cao, S. Yang, F. Lu, M. J. Meziani, L.Tian, K. W. Sun, M. A. Bloodgood, and Y. Sun, *Angew. Chem., Int. Ed.* **2010**, *49*, 5310.
(158) J. C. Vinci, I. M. Ferrer, S. J. Seedhouse, A. K. Bourdon, J. M. Reynard, B. A. Foster, F. V. Bright and L. A. Colon, *J. Phys. Chem. Lett.* **2013**, *4*, 239.
(159) S. Jaeqx, W. Du, E. J. Meijer, J. Oomens, and A. M. Rijs, *J. Phys. Chem. A*, **2013**, *117*, 1216.
(160) S. Qu, X. Liu, X. Guo, M. Chu, L. Zhang and D. Shen, *Adv. Funct. Mater.* **2013**, *24*, 2689.
(161) D. Pan, J. Zhang, Z. Li, C. Wu, X. Yana and M. Wu, *Chem. Commun.* **2010**, *46*, 3681.
(162) Z. Lin, W. Xue, H. Chen and J. Lin, *Chem. Commun.* **2012**, *48*, 1051.
(163) X. Wang, L. Cao, F. Lu, M. J. Meziani, H. Li, G. Qi, B. Zhou, B. A. Harruff, F. Kermarrec and Y. Sun, *Chem. Commun.* **2009**, 3774.
(164) J. Liu, Y. Zhong, P. Lu, Y. Hong, J. W. Y. Lam, M. Faisal, Y. Yu, K. S. Wong and B. Z. Tang, *Polym. Chem.* **2010**, *1*, 426.
(165) V. Bhalla, A. Gupta and M. Kumar, *Org. Lett.* **2012**, *14*, 3112.

(166) B. Roy, A. K. Bar, B. Gole, and P.S. Mukherjee, *J. Org. Chem.* **2013**, *78*, 1306.

(167) D. A. Olley, E. J. Wren, G. Vamvounis, M. J. Fernee, X. Wang, P. L. Burn, P. Meredith and P. E. Shaw, *Chem. Mater.* **2011**, *23*, 789.

(168) S. Shanmugaraju, S. A. Joshi and P. S. Mukherjee, *J. Mater. Chem.* **2011**, *21*, 9130.

(169) M. S. Meaney and V. L. McGuffin, *Anal. Chim. Acta*, **2008**, *610*, 57.

(170) Q. Niu, K. Gao, Z. Linb and W. Wu, *Anal. Methods*, **2013**, *5*, 6228.

(171) V. Vij, V. Bhalla and M. Kumar, *ACS Appl. Mater. Interfaces*, **2013**, *5*, 5373.

(172) X. Zhai, P. Zhang, C. Liu, T. Bai, W. Li, L. Daic and W. Liu, *Chem. Commun.* **2012**, *48*, 7955.

(173) F. Li, C. Liu, J. Yang, Z. Wang, W. Liu and F. Tian, *RSC Adv.* **2014**, *4*, 3201.

(174) Principles of Neural Science, 3rd ed. (Eds.: E. R. Kandel, J. H. Schwatz, T. M. Jessel), *Elsevier,* New York, **1991**.

(175) A. P. de Silva and S. Uchiyama, *Nature Nanotech.* **2007**, *2*, 399.

(176) C. Joachim, J. K. Gimzewski and A. Aviram, *Nature*, **2000**, *408*, 541.

(177) D. C. Magri, G. J. Brown, G. D. McClean and A. P. de Silva, *J. Am. Chem. Soc.* **2006**, *128*, 4950.

(178) A. P. de Silva, H. Q. N. Gunaratne and C. P. McCoy, *Nature*, **1993**, *364*, 42.

(179) A. Credi, V. Balzani, S. J. Langford and J. F. Stoddart, *J. Am. Chem. Soc.* **1997**, *119*, 2679.

(180) S. Uchiyama, N. Kawai, A. P. de Silva and K. Iwai, *J. Am. Chem. Soc.* **2004**, *126*, 3032.

(181) R. Guliyev, S. Ozturk, Z. Kostereli and E. U. Akkaya, *Angew. Chem. Int. Ed.* **2011**, *50*, 9826.

(182) G. Seelig, D. Soloveichik, D. Y. Zhang and E. Winfree, *Science*, **2006**, *314*, 1585.

(183) X. Li, Y. Wu, D. Steel, D. Gammon, T. H. Stievater, D. S. Katzer, D. Park, C. Piermarocchi and L. J. Sham, *Science*, **2003**, *301*, 809.

(184) S. K. Sailapu, A. K. Sahoo, S. S. Ghosh and A. Chattopadhyay, *Small,* **2014**, *10*, 4067.

(185) M. Elstner, J. Axthelm and A. Schiller, *Angew. Chem. Int. Ed.* **2014**, *53*, 7339.

(186) M. Ikeda, T. Tanida, T. Yoshii, K. Kurotani, S. Onogi, K. Urayama and I. Hamachi, *Nature Chem.* **2014**, *6*, 511.

(187) D. Liu, W. Chen, K. Sun, K. Deng, W. Zhang, Z. Wang and X. Jiang, *Angew. Chem. Int. Ed.* **2011**, *50*, 4103.

(188) F. M. Raymo and S. Giordani, *J. Am. Chem. Soc.* **2001**, *123*, 4651.

(189) M. Chuang, J. R. Windmiller, P. Santhosh, G. V. Ramı´rez, E. Katz and J.Wang, *Chem. Commun.* **2011**, *47*, 3087.

(190) A. W. Martinez, S. T. Phillips, M. J. Butte and G. M. Whitesides, *Angew. Chem. Int. Ed.* **2007**, *46*, 1318.

(191) T. Gupta and M. E. van der Boom, *Angew. Chem. Int. Ed.* **2008**, *47*, 5322.

(192) Y. Lin, C. Xu, J. Ren and X. Qu, Angew. *Chem. Int. Ed.* **2012**, *51*, 12579.

(193) P. Xue, R. Lu, J. Jia, M. Takafuji and H. Ihara, *Chem. Eur. J.* **2012**, *18*, 3549.

(194) L. Feng, A. Zhao, J. Ren and X. Qu, *Nucleic Acids Res.* **2013**, *41*, 7987.

(195) M. Kumar, R. Kumar and V. Bhalla, *Org. Lett.* **2011**, *13*, 366.

(196) H. Y. Au-Yeung, J. Chan, T. Chantarojsiri and C. J. Chang, *J. Am. Chem. Soc.* **2013**, *135*, 15165.

(197) U. Pischel, J. Andréasson, D. Gust and V. F. Pais, *ChemPhysChem*, **2013**, *14*, 28.

(198) D. Margulies, C. E. Felder, G. Melman and A. Shanzer, *J. Am. Chem. Soc.* **2007**, *129*, 347.

(199) C. Santini, M. Pellei, V. Gandin, M. Porchia, F. Tisato, and C. Marzano, *Chem.Rev.* **2014**, *114*, 815.

(200) J. J. Wilson and S. J. Lippard, *Chem. Rev.* **2014**, *114*, 4470.

(201) K. J. Kilpin and P. J. Dyson, *Chem. Sci.*, **2013**, *4*, 1410.

(202) P. Cronholm , H. L. Karlsson , J. Hedberg , T. A. Lowe , L. Winnberg , K. Elihn , I. O. Wallinder , and L. Möller, *Small*, **2013**, *9*, 970.

(203) R. Ghosh, U. Goswami, S. S. Ghosh, A. Paul, and A. Chattopadhyay, *ACS Appl. Mater. Interfaces*, **2015**, *7*, 209.

(204) Z. Wang, A. Bussche, P. K. Kabadi, A. B. Kane, and R. H. Hurt, *ACS Nano*, **2013**, *7*,8715.

(205) C. Hou, H. Quan, Y. Duan, Q. Zhang, H. Wang and Y. Li, *Nanoscale*, **2013**,*5*, 1227.

(206) S. Tardito, I. Bassanetti, C. Bignardi, L. Elviri, M. Tegoni, C. Mucchino, O. Bussolati, R. F. Gazzola, and L. Marchio, *J. Am. Chem. Soc.* **2011**, *133*, 6235.

(207) W. R. Sanhai, J. H. Sakamoto, R. Canady & M. Ferrari, *Nat. Immunol.* **2008**, *3*, 242.

(208) Z. Chen, *Trends Mol. Med.* **2010**, *16*, 594.

(209) D. Peer, J. M. Karp, S. Hong, O. C. Farokhzad, R. Margalit and R. Langer, *Nature Nanotech.* **2007**, *2*, 751.

(210) R. Khandelia, A. Jaiswal, S. S. Ghosh and A. Chattopadhyay, *Small*, **2013**, *9*, 3494.

(211) O. C. Farokhzad and R. Langer, *ACS Nano*, **2009**, *3*, 16.

(212) V. Kumar, A. Kalita and B. Mondal, *Dalton Trans.* **2013**, *42*, 16264.

(213) M. K. Barman, B. Jana, S. Bhattacharyya, and A. Patra, *J. Phys. Chem. C*, **2014**, *118*, 20034.

(214) M.K. Mishra, A. Chakravarty, K. Bhowmik and G. De, *J. Mater. Chem. C*, **2015**, *3*, 714.

Publications

1) Amaresh Kumar Sahoo, **Md Palashuddin Sk**, Siddhartha Sankar Ghosh and Arun Chattopadhyay, Plasmid DNA linearization in the antibacterial action of a new fluorescent Ag nanoparticle–paracetamol dimer composite. *Nanoscale*, **2011**, 3, 4226.

2) **Md Palashuddin Sk**, Amit Jaiswal, Anumita Paul, Siddhartha Sankar Ghosh, Arun Chattopadhyay, Presence of Amorphous Carbon Nanoparticles in Food Caramels. *Sci. Rep*. **2012**, 2, 383. (*Highlighted in COSMOS-Australian Science Magazine, 2020 Science, Food Production daily.com, Food Engineering, NanoWiki, Nanotechnology Law Report, New Heaven Independent newspaper, European Observatory on NanoSafety, etc.)*

3) **Md Palashuddin Sk**, Chandan K Jana, Arun Chattopadhyay, A gold–carbon nanoparticle composite as an efficient catalyst for homocoupling reaction. *Chem.Commun*. **2013**, 49, 8235.

4) **Md Palashuddin Sk**, Arun Chattopadhyay, Induction coil heater prepared highly fluorescent carbon dots as invisible ink and explosive sensor. *RSC Adv*., **2014**, 4, 31994.

5) **Md Palashuddin Sk**, Arun Chattopadhyay, Luminescent Carbon Dots for Logic Operations in Two Phases. *ChemPhysChem*, **2015**, 16, 723. *(Appeared on the front cover page with cover profile).*

6) **Md Palashuddin Sk**, Upashi Goswami, Siddhartha Sankar Ghosh and Arun Chattopadhyay, Cu^{2+}- embedded Carbon Nanoparticle as an Anticancer Agent (Submitted).

Highlights of our work

Appeared on cover page, 4th issue 2015.

ChemPubSoc Europe DOI: 10.1002/cphc.201500136 CHEMPHYSCHEM Cover Profile

Luminescent Carbon Dots for Logic Operations in Two Phases

Indian Institute of Technology Guwahati Assam, India E-mail: arun@iitg.ernet.in

Md Palashuddin Sk Sunil Kumar Sailapu Prof. Arun Chattopadhyay

The front cover artwork is provided by the group of Prof. Arun Chattopadhyay (Indian Institute of Technology Guwahati, India). The cover picture depicts luminescent carbon dot based logic operations that occur in liquid media and the solid phase with organic molecules and metal ions as inputs. Read the full text of the article at 10.1002/cphc.201402747.

What is the key achievement of this work?

Photoluminescence of carbon dots (Cdots) was observed in both liquid dispersions and solid-supported films. Moreover, the emission was responsive to the presence of selected metal ions and organic molecules. These formed the basis of simple and complex logic functions, which were operative in both liquid (water) and solid phases. Significant results include the demonstration of simple basic logic gates such as NOT, YES, AND, OR, and IMPLIES and universal gates NOR and NAND. Complex logic function was achieved in two or more stages. Also, cascading of two individually functioning basic gates was possible. These environmentally friendly Cdots could potentially be used for sensing analytes under diverse conditions.

What future opportunities do you see (in the light of the results presented in this paper)?

Complex decisive logic systems are ubiquitous in nature. Digital electronics have revolutionised artificial ways of carrying out complex logical operations at great speeds. Currently, alternative methods of computing, based on the stimuli-sensitive responses of nanoscale particles or molecular species, are of great interest. These methods are expected to provide artificial intelligence with the power to make decisions under diverse environmental conditions. The integral idea in the present work may offer multiphase basic and complex logic systems that would be responsive solely or collectively to physical, chemical, mechanical, and electrical stimuli. This diversity in operation may be useful in building automated lab-on-a-chip or lab-on-a-molecule devices.

What other relevant work is your group doing in this field?

We have recently looked at the use of ultra-small highly luminescent gold nanoclusters for the development of logical operative devices in aqueous media. The luminescent clusters responded to pH, temperature, and metal ions present in the medium. Thus, these clusters could be used to construct basic logic gates, decoders, and even hierarchical logic structures using both physical and chemical inputs. The clusters could also be used as a 'molecular' thermometer, pH sensor, and metal-ion detector. We expect these ideas to be relevant to the fabrication of contactless devices for biomimetic applications.

What is your next target in this field?

Carbon dots can be considered as environmentally friendly nanomaterials, and thus, may be used on a large scale. An important area that needs development is lithographic patterning and printing of carbon dots. We are working on developing such a method that would make fabrication of sensors simple and inexpensive.

Acknowledgments

We thank the Department of Electronics and Information Technology, Government of India for funds (No. 5(9)/2012-NANO-VoI(II)). M.P.S is thankful to CSIR for a fellowship (09/731(0095)/2010-EMR-I).

Title: Presence of Amorphous Carbon Nanoparticles in Food Caramels

Author: Md Palashuddin Sk, Amit Jaiswal, Anumita Paul, Siddhartha Sankar Ghosh, Arun Chattopadhyay

Publication: Scientific Reports

Publisher: Nature Publishing Group

Date: Apr 26, 2012

Creative Commons

The request you have made is considered to be non-commercial/educational. As the article you have requested has been distributed under a Creative Commons license (Attribution-Noncommercial 2.5), you may reuse this material for non-commercial/educational purposes without obtaining additional permission from Nature Publishing Group, providing that the author and the original source of publication are fully acknowledged.

For full terms and conditions of the Creative Commons license, please see the attached link http://creativecommons.org/licenses/by-nc/2.5

TH-1424_09612225

RSC | Advancing the Chemical Sciences

Royal Society of Chemistry
Thomas Graham House
Science Park
Milton Road
Cambridge
CB4 0WF

Tel: +44 (0)1223 420 066
Fax: +44 (0)1223 423 623
Email: contracts-copyright@rsc.org

www.rsc.org

Acknowledgements to be used by RSC authors

Authors of RSC books and journal articles can reproduce material (for example a figure) from the RSC publication in a non-RSC publication, including theses, without formally requesting permission providing that the correct acknowledgement is given to the RSC publication. This permission extends to reproduction of large portions of text or the whole article or book chapter when being reproduced in a thesis.

The acknowledgement to be used depends on the RSC publication in which the material was published and the form of the acknowledgements is as follows:

- For material being reproduced from an article in *New Journal of Chemistry* the acknowledgement should be in the form:
  - [Original citation] - Reproduced by permission of The Royal Society of Chemistry (RSC) on behalf of the Centre National de la Recherche Scientifique (CNRS) and the RSC
- For material being reproduced from an article *Photochemical & Photobiological Sciences* the acknowledgement should be in the form:
  - [Original citation] - Reproduced by permission of The Royal Society of Chemistry (RSC) on behalf of the European Society for Photobiology, the European Photochemistry Association, and RSC
- For material being reproduced from an article in *Physical Chemistry Chemical Physics* the acknowledgement should be in the form:
  - [Original citation] - Reproduced by permission of the PCCP Owner Societies
- For material reproduced from books and any other journal the acknowledgement should be in the form:
  - [Original citation] - Reproduced by permission of The Royal Society of Chemistry

The acknowledgement should also include a hyperlink to the article on the RSC website.

The form of the acknowledgement is also specified in the RSC agreement/licence signed by the corresponding author.

Except in cases of republication in a thesis, this express permission does not cover the reproduction of large portions of text from the RSC publication or reproduction of the whole article or book chapter.

A publisher of a non-RSC publication can use this document as proof that permission is granted to use the material in the non-RSC publication.

JOHN WILEY AND SONS LICENSE TERMS AND CONDITIONS

Feb 15, 2015

This Agreement between md palashuddin sk ("You") and John Wiley and Sons ("John Wiley and Sons") consists of your license details and the terms and conditions provided by John Wiley and Sons and Copyright Clearance Center.

License Number	3570251156343
License date	Feb 15, 2015
Licensed Content Publisher	John Wiley and Sons
Licensed Content Publication	ChemPhysChem
Licensed Content Title	Luminescent Carbon Dots for Logic Operations in Two Phases
Licensed Content Author	Md Palashuddin Sk,Sunil Kumar Sailapu,Arun Chattopadhyay
Licensed Content Date	Jan 7, 2015
Pages	1
Type of use	Dissertation/Thesis
Requestor type	Author of this Wiley article
Format	Print and electronic
Portion	Full article
Will you be translating?	No
Title of your thesis / dissertation	Versatile Applications of Carbon Nanoparticles
Expected completion date	May 2015
Expected size (number of pages)	150
Requestor Location	md palashuddin sk Dept. of Chemistry IIT Guwahati North Guwahati Guwahati, India 781039 Attn: md palashuddin sk
Billing Type	Invoice
Billing Address	md palashuddin sk Dept. of Chemistry IIT Guwahati North Guwahati Guwahati, India 781039 Attn: md palashuddin sk
Total	0.00 USD
Terms and Conditions	

TERMS AND CONDITIONS

This copyrighted material is owned by or exclusively licensed to John Wiley & Sons, Inc. or one of its group companies (each a"Wiley Company") or handled on behalf of a society with which a Wiley Company has exclusive publishing rights in relation to a particular work

JOHN WILEY AND SONS LICENSE TERMS AND CONDITIONS

Feb 15, 2015

This Agreement between md palashuddin sk ("You") and John Wiley and Sons ("John Wiley and Sons") consists of your license details and the terms and conditions provided by John Wiley and Sons and Copyright Clearance Center.

License Number	3570241116715
License date	Feb 15, 2015
Licensed Content Publisher	John Wiley and Sons
Licensed Content Publication	Angewandte Chemie International Edition
Licensed Content Title	Luminescent Carbon Nanodots: Emergent Nanolights
Licensed Content Author	Sheila N. Baker,Gary A. Baker
Licensed Content Date	Aug 4, 2010
Pages	19
Type of use	Dissertation/Thesis
Requestor type	University/Academic
Format	Print and electronic
Portion	Figure/table
Number of figures/tables	1
Original Wiley figure/table number(s)	Figure 1
Will you be translating?	No
Title of your thesis / dissertation	Versatile Applications of Carbon Nanoparticles
Expected completion date	May 2015
Expected size (number of pages)	150
Requestor Location	md palashuddin sk Dept. of Chemistry IIT Guwahati North Guwahati Guwahati, India 781039 Attn: md palashuddin sk
Billing Type	Invoice
Billing Address	md palashuddin sk Dept. of Chemistry IIT Guwahati North Guwahati Guwahati, India 781039 Attn: md palashuddin sk
Total	0.00 USD
Terms and Conditions	

TH-1424_09612225

TERMS AND CONDITIONS

Title: (CdSe)ZnS Core−Shell Quantum Dots: Synthesis and Characterization of a Size Series of Highly Luminescent Nanocrystallites

Author: B. O. Dabbousi, J. Rodriguez-Viejo, F. V. Mikulec, et al

Publication: The Journal of Physical Chemistry B

Publisher: American Chemical Society

Date: Nov 1, 1997

PERMISSION/LICENSE IS GRANTED FOR YOUR ORDER AT NO CHARGE

This type of permission/license, instead of the standard Terms & Conditions, is sent to you because no fee is being charged for your order. Please note the following:

- Permission is granted for your request in both print and electronic formats, and translations.
- If figures and/or tables were requested, they may be adapted or used in part.
- Please print this page for your records and send a copy of it to your publisher/graduate school.
- Appropriate credit for the requested material should be given as follows: "Reprinted (adapted) with permission from (COMPLETE REFERENCE CITATION). Copyright (YEAR) American Chemical Society." Insert appropriate information in place of the capitalized words.
- One-time permission is granted only for the use specified in your request. No additional uses are granted (such as derivative works or other editions). For any other uses, please submit a new request.

If credit is given to another source for the material you requested, permission must be obtained from that source.

TH-1424_09612225

NATURE PUBLISHING GROUP LICENSE TERMS AND CONDITIONS

Feb 27, 2015

This is a License Agreement between md palashuddin sk ("You") and Nature Publishing Group ("Nature Publishing Group") provided by Copyright Clearance Center ("CCC"). The license consists of your order details, the terms and conditions provided by Nature Publishing Group, and the payment terms and conditions.

All payments must be made in full to CCC. For payment instructions, please see information listed at the bottom of this form.

License Number	3577180252959
License date	Feb 27, 2015
Licensed content publisher	Nature Publishing Group
Licensed content publication	Nature Materials
Licensed content title	Quantum dot bioconjugates for imaging, labelling and sensing
Licensed content author	Igor L. Medintz,H. Tetsuo Uyeda,Ellen R. GoldmanandHedi Mattoussi
Licensed content date	Jun 1, 2005
Volume number	4
Issue number	6
Type of Use	reuse in a dissertation / thesis
Requestor type	academic/educational
Format	print and electronic
Portion	figures/tables/illustrations
Number of figures/tables/illustrations	2
High-res required	no
Figures	Figure 1 and 3
Author of this NPG article	no
Your reference number	None
Title of your thesis / dissertation	Versatile Applications of Carbon Nanoparticles
Expected completion date	May 2015
Estimated size (number of pages)	150
Total	0.00 USD
Terms and Conditions	

Terms and Conditions for Permissions

Nature Publishing Group hereby grants you a non-exclusive license to reproduce this material for this purpose, and for no other use,subject to the conditions below:

1. NPG warrants that it has, to the best of its knowledge, the rights to license reuse of this material. However, you should ensure that the material you are requesting is original to